Solar Energy Materials 5 (1981) 229–316
North-Holland Publishing Company

PROPERTIES OF AMORPHOUS HYDROGENATED SILICON, WITH SPECIAL EMPHASIS ON PREPARATION BY SPUTTERING

William PAUL and David A. ANDERSON*
Division of Applied Sciences, Harvard University, Cambridge, MA 02138, USA

Received 15 June 1981

The properties of amorphous hydrogenated silicon are reviewed, with special emphasis placed on results obtained by the method of reactive sputtering in an argon–hydrogen plasma. The subjects treated include characteristics of the sputtering method; structural characterizational methods; determination of the hydrogen bonding configurations and the hydrogen content by several different techniques; trends in optical and electrical properties as a function of the substrate temperature and hydrogen partial pressure used in the preparation; the determination of the density of states in the energy gap by spin resonance, light induced spin resonance, photoemission, field effect, capacitance methods, deep level transient spectroscopy and tunneling spectroscopy; electrical transport, especially as modified by the existence of structural and chemical inhomogeneity; optical absorption near and below the optical absorption edge; photoluminescence as a function of photon energy, temperature, excitation photon energy and intensity; time-domain spectroscopy; and photoconductivity, both steady state and transient. Throughout the discussion an attempt is made to relate the results on a-Si:H prepared by the several methods now current to those of the particular sputtering technique emphasized.

Contents

*Present address: RSRE, St. Andrews Road, Great Malvern, Worcs. WR14 3PS, England.

0165-1633/81/0000–0000/$02.75© 1981 North-Holland

1. Introduction

Early work on the structural, transport and optical properties of thin films of amorphous, tetrahedrally-coordinated semiconductors such as Si and Ge prepared by evaporation or sputtering showed that these materials possessed a large density of structural defects ranging from single dangling bonds to macroscopic voids. There was a corresponding large density of electronic states in the band gap, and these densities were not appreciably reduced by ultra-high vacuum deposition, high substrate temperatures or high temperature annealing [1]. In 1974, however, the group at Harvard University reported [2] that the deliberate addition of H_2 to their Ar sputtering plasma produced films of a-Ge whose spin density and room temperature hopping conductivity were reduced by orders of magnitude, and which showed much reduced absorption at low photon energies and much improved photoconductivity. They interpreted these results in terms of a compensation of dangling bonds and other defects by H, which dismissed states from the band gap deep into the valence band, and thus simulated the effects of defect removal. In the same paper they suggested a similar origin for the well-established "super-annealed" properties [3] of a-Si produced by the glow-discharge (g.d.) decomposition [4] of SiH_4. Without appeal (or need to appeal) to this interpretation [5], Spear and Le Comber demonstrated in 1975 that the g.d. material could be doped n-type or p-type and its conductivity increased by many orders or magnitude [6]. Their success has led to an explosive growth of research as the twin opportunities for basic understanding of an amorphous semiconductor and for technological advance were appreciated [7].

It is now generally accepted that sputtering in Ar–H and g.d. decomposition of SiH_4 both yield a Si:H alloy with up to about 30 at% of H. The properties of the g.d. material, whose device potential has been more developed, have been reviewed recently by Fritzsche [8] and Carlson [9]. While this article will report primarily the basic properties of a-Si:H produced by sputtering of c-Si in an Ar atmosphere [10], our main aim will be to focus on some of the principal current problems of interpretation for *all* a-Si:H, divorced from the details of its fabrication. Thus we shall continuously try to integrate the useful results from the g.d. material in analyzing the data on sputtered material.

Space limitations preclude our writing a comprehensive archival review, which should carefully examine the detailed preparation parameters in different laboratories when reporting the resulting properties [11]. We shall try to isolate the ubiquitous properties of the material while relying heavily on our own results on films whose preparation and characterization we know best. We have also had to forego much discussion of related theory [12a] and of the massive, important subject of doping [12b].

2. Preparation, characterization and property measurement

2.1. Introduction

The ideal program for the study of sputtered a-Si:H would involve co-deposition of films on several different types of substrate under controlled, systematically-varied conditions; characterization of the film structure and chemistry for each set of deposition conditions; measurement of many optical, electrical and magnetic properties; and study of the results to give a coherent model which correlates preparation parameters, on the one hand with the plasma chemistry and physical sputtering processes, and on the other with the structure and chemical composition. Finally, the structure and chemical composition must be correlated with the totality of properties.

The large number of preparation parameters, e.g., argon partial pressure p_{Ar}, hydrogen partial pressure p_H, substrate temperature T_s, sputtering power P_{rf}, substrate bias V_{SB}, system geometry, etc., necessarily limit such a program. We shall concentrate on the results of such a limited program at Harvard, in part because a report drawing predominantly from one program minimizes the influence of unsuspected hidden variables in the nuances of technique of preparation. The principal parameters we have varied are p_{Ar}, p_H, $p_T = p_{Ar} + p_H$, T_s and P_{rf}. Other laboratories have used more extensive ranges of p_{Ar}, p_H, P_{rf}, V_{SB} and geometry, and we can draw on their experience, while noting that the change of a property with a given parameter may not necessarily be the same (even in sign) in different regions of preparation parameter-space. The results for one system must be used as a guide for another, not a rule.

2.2. Preparation

We have used an rf diode sputtering system with $p_{Ar} = 5$–50 mTorr; $p_H = 0$–10 mTorr; $T_s = 25$–450°C; and $P_{rf} = 50$–400 W on 120 cm^2 of polycrystalline Si target. The details of substrate cleaning, base vacuum, target and substrate plasma etching, gas flow control, etc., have been published [37]. Pawlewicz [13] has studied the properties of unhydrogenated a-Si to $p_{Ar} = 150$ mTorr. Jeffrey et al. [14] have studied a-Si:H to $P_{rf} = 4$ W/cm^2 and $p_T = 30$–150 mTorr. Messier [15] has used values of p_T up to 70 mTorr. Others have varied target–substrate spacing [14] or bias applied to the substrate [16].

The nucleation and growth of thin films from vapors has been widely studied [17]. In the case of the reactive sputtering of Si in an Ar–H plasma, both the chemical processes in the plasma and the physics of the sputtering and deposition process must be considered. The chemical constitution of the plasma near the growth surface depends on so many parameters that satisfactory general modelling has not been done [18]. In principle, information might be available from experimental studies of the optical emission spectra of the plasma. However, in contrast to the situation for g.d. plasmas, where SiH (but not SiH_2 or SiH_3 which have no known emission spectra) species are readily identified [19], there is disagreement in two experimental studies [20] on the very occurrence of a Si–H gas phase reaction.

Among the principal parameters in any process of vapor deposition are p_T and T_g, the growth temperature, which may be considerably higher than T_s, the controlled temperature of the substrate. Atoms and ions impinge on the substrate with an energy determined by P_{rf} and p_T (among other parameters). They stick where they land or desorb or diffuse until trapped, depending on their surface mobility, which depends on their incident energy, on T_g, and on the chemical and structural nature of the substrate. Some of them may diffuse in the bulk film in subsequent relaxation processes that minimize the local free energy. Local free energy minimization decides the film composition and structure, with the range of the minimization determined by T_g and the film constitution.

Other parameters specific to the reactive sputtering process can affect the chemical and structural composition of a film. Thus, Ar^+ may become Ar by neutralization at the target and be reflected to the substrate with little loss of energy, there to become implanted, adsorbed or even to resputter the growing film. If, as can happen, the substrate is biased negatively with respect to the plasma, Ar^+ can be attracted to the substrate. Besides leading to Ar incorporation, these processes constitute two of the processes of film bombardment that can be both beneficial and detrimental. Beneficial, in that weakly bound species are swept off the growing surface. Detrimental, in that irremediable damage may be caused. Other such bombardment processes are by sputtered target atoms which reach the substrate with velocities greater than thermal if their mean free paths are much greater than the target–substrate separation (low p_T). Yet another bombardment process, by negative ions formed near the target, by plasma electrons, or even by positive ions, depends on intentional or self-bias of the substrate. Self-bias voltages may be very high in insulating films or conducting films which are electrically insulated. These bombardment processes [21], which distinguish the sputtering from the glow discharge processes by their violence, especially at low p_T, are undoubtedly important for the eventual structure of the film.

As in all film deposition, stable nuclei on the substrate surface grow together and eventually seek to unite. We shall refer to the region of union as connective tissue; its chemical constitution, structure and dimensions – the film microstructure – vitally influence the film properties. We suspect that many of the present problems of interpretation of a-Si:H have sprung from failure to recognize that there may be two "phases", island and tissue, of different chemistry, structure, electronic band structure and intrinsic properties, and that measured film properties are not properly interpretable on a model of homogeneous, although disordered, semiconductor.

2.3. *Structural characterization* [22]

2.3.1. *Continuous random network*

The low electron density of H precludes *precise* determination by X-ray [23] or electron [24] diffraction of the radial distribution function of a-Si:H alloys, although the reduced Si coordination (with Si) is readily apparent. It does not seem to be possible to infer from the present data any clear difference of bond angles or ring statistics between a-Si and a-Si:H deposited by glow discharge at the same temperature. No examinations specifically on sputtered a-Si:H have been reported.

2.3.2. Voids and microstructure

It is known that sputtered unhydrogenated a-Si has electron/atom deficient regions of about 10 Å dimension from measurements of large and small angle X-ray [25] and electron scattering [26]. On the other hand, electron microscope studies of evaporated unhydrogenated a-Si have shown evidence of microstructure on a scale of 100–1000 Å [27]. The results for glow-discharge deposited a-Si:H vary. Thus material deposited on low temperature substrates (as for the pure a-Si studies) by D'Antonio and Konnert [28] showed small angle X-ray scattering similar to the a-Si, which was similarly interpreted in terms of 10 Å dimension voids. Later, the same authors [29], using X-rays, and Leadbetter et al. [30], using neutrons, demonstrated from the absence of small angle scattering that *device-quality* a-Si:H prepared at high T_s was essentially void-free. Postol et al. [30] have studied the small angle neutron scattering from pure, hydrogenated and deuterated a-Si:H prepared by high rate magnetron sputtering, and obtained results consistent with the existence of voids and/or large areas of grain boundary rich in H-content. It seems evident that such measurements are a useful supplement to TEM and SEM studies (see below) where the existence of hetero-structure is suspected.

The more recent close attention to microstructural effects has developed from the electron microscopy studies of Barna et al. [24], Graczyk [24] and Knights and Lujan [31] on g.d. prepared a-Si:H. All of these works found that material, deposited under conditions generally agreed to yield good photoelectronic properties (e.g., high T_s, low power, pure SiH_4), showed no discernible microstructure. On the other hand, Graczyk, and Knights.and Lujan, found that under different deposition conditions (low T_s, high power, Ar dilution), the TEM micrographs revealed islands 100–1000 Å across joined by lower density tissue; evidently in the thickness accessible by TEM columnar islands were preserved throughout the film. Scanning electron microscope studies of the edges of fractured thicker films showed that columns in some film depositions stretched over distances of the order of one micron. The existence of identifiable microstructure depends on the detailed parameters of deposition. It is reported [22, 31] to be emphasized by increased deposition rate, higher Ar/SiH_4 ratio, lower negative substrate bias, lowered substrate temperature and the substitution of large mass and low ionization energy inert gas diluents (Ar, Kr) for lighter mass and higher ionization energy diluents (He, Ne) in the SiH_4 plasma [32]. Further evidence for the chemical and structural differences between islands and tissue comes from etching studies, which preferentially attack the tissue and so modify the electron microscope pictures and the measured infrared absorption properties [33]. While a fully detailed description of the chemical and structural differences between the islands and the connecting tissue has not yet been established, it is generally accepted that the tissue material has lower mass density, higher defect density and a greater multiplicity of different Si–H bonding configurations.

It is natural to attempt to correlate the observation of a two-phase structure in TEM/SEM examinations with other examples of bimodal behavior, such as the occurrence of two different principal frequencies in infrared stretching mode absorption by Si–H entities, the occurrence of two peaks in the spectrum of evolution of

hydrogen as a function of temperature, and most recently, the observation of two differentiable environments for protons in nuclear magnetic resonance. At present, such correlations still need to be treated with caution. The attribution of the infrared peaks (see below) *uniquely* to islands or tissue is almost certainly incorrect, although preferences probably occur; similarly, the low-temperature evolution of hydrogen preferentially from tissue pathways, although plausible, has not been definitively established. The NMR studies [34, 35] found two superposed resonance lines of different temperature-independent widths, present in all samples, whether or not they showed microstructure in electron microscope studies. Here, therefore, it is especially unclear whether the two-phase compositional inhomogeneity responsible bears a one-to-one correspondence to the islands and connecting tissue, and so we shall postpone discussion of these results to section 2.3.3.4. On the other hand, the incidence of *anisotropic* small angle neutron scattering correlates well with the observation of microstructure [30].

Knights and his collaborators have also demonstrated that films with microstructure identifiable in the electron microscope have a larger density of pseudogap states (ESR) and poorer photoelectronic properties (PL). They suggest that films prepared under conditions that lead to better semiconductor properties, suitable for devices, and which display no visible microstructure, nevertheless possess the same underlying island structure with shrunken dimensions for the connective tissue [31]. It is important to realize that this could have profound consequences for transport and recombination processes, a theme which will recur in this review.

The evidence for heterostructure in sputtered a-Si:H is more limited, but is generally confirmatory. As was mentioned in section 2.2, all films deposited from vapors nucleate and knit together in a fashion which involves some degree of connective tissue. The thrust to optimize electronic properties for devices has led to a choice of deposition parameters which automatically tend to minimize the extent of the tissue, which is presumably one reason why it was not observed earlier also in glow discharge a-Si:H.

Messier et al. [36] have made the only extensive study of the occurrence of microstructure in the sputtered material, using the techniques of TEM, SEM, atom probe field ion microscopy and preferential etching. Microstructure is barely visible for $p_T = 5$ and 20 mTorr. However, as p_T is increased to 40 and 70 mTorr, low density regions surrounding higher density columns or islands of about 100 Å dimension become more visible in a-Si, a-Si:H, a-Ge and a-Ge:H. This wide-ranging study is of great value (as is Knights') in helping to delineate by extrapolation the region of preparation-parameter space where films with *no discernible* microstructure and good photoelectronic properties may be found. Although this review will concentrate on such material, the probability is so great of narrow regions of connective tissue, or of a three-dimensional two-phase network not amenable to revelation in either TEM or SEM examination, that indirect evidence of its existence must always be seriously considered.

The ranges of T_s, p_{Ar} and p_H used at Harvard have usually been limited to produce films that are stable to the atmosphere and possess a reasonably low gap state density. Thus we have found no visible microstructure in TEM measurements on films as thin

as 200–300 Å produced at $p_T \leqslant 30$ mTorr. However, there were clear, although indirect, indications of microstructure for a film produced at $p_{Ar} = 30$ mTorr, in that the film displayed poor photoconductivity and photoluminescence, and Si–O vibrational absorption after air exposure [37]. Since the Si–Si distances are unaltered [23], it seems plausible that there was a network of relatively wide pathways to the interior. Nevertheless, there have been no reports for sputtered samples of evidence for porosity from gas uptake [38] such as was found in certain g.d. preparations. In fact, the fractional density reduction on hydrogenation has been reported to be smaller than the included fraction of H [39] (which may, however, be a result of Ar inclusion). Noting also that g.d. a-Si:H has been reported to have substantially less small angle X-ray scattering than a-Si [29, 30], we might conclude that, at least in samples made at low p_T, the H relieves the network of the constraint of four-fold Si coordination and promotes a structure with reduced structural inhomogeneity. Nevertheless, we wish to reiterate our opinion, in agreement with the suggestions of the Knights' group, and the expectations of film deposition models, that a second phase of presently invisible connective tissue very likely permeates our better films and its influence must be considered in the analysis of all property measurements.

Presumably high p_{Ar} reduces, through collisions, the mobility of Si and H ions and atoms on the growth surface and so prevents consolidation into a high density film. Low T_s might have a similar effect. High deposition rate might be expected to lead to burial of atoms before they have found positions of low energy, and so lead to an opener structure. We have argued that the inclusion of H reduces the coordination of Si with Si and so increases the flexibility of the network; it has also been reported to decrease the internal stress in the network [40]; and it might be expected to permit columns to coalesce with minimal stress in the connective tissue. On the other hand, the termination of growth of the network by H forces the network to grow around it, which might be expected to lead to small local defects.

2.3.3. Hydrogen bonding

The local atomic structure near H-sites has been extensively investigated by several techniques, but a satisfactorily complete picture has yet to emerge. In this section we shall discuss the several Si–H entities that have been proposed on the basis of (1) infrared vibrational absorption, (2) H-evolution on heating, (3) photoemission and (4) nuclear magnetic resonance. A definitive interpretation will almost certainly involve resolution of the question of whether there are different predominant Si–H entities in the islands and connective tissue, and what they are. The fact that different sputtering conditions, such as different p_H, can lead to different Si–H configurations, and also different optical and electrical properties, has been repeatedly emphasized [10, 41–47]. Frequent attempts have been made, on the basis of assignment of the different frequencies of infrared absorption to specific H-configurations, to relate their occurrence to the deposition conditions and to the measured properties. Unfortunately, this must still be regarded as somewhat speculative, as we hope to develop below. Some of the configurations (e.g. $(SiH_2)_n$) are often supposed either to lead to, or to coexist with, defects giving pseudogap states. Others have been suggested to give Si–H antibonding

states overlapping the bottom of the a-Si conduction band [48]. Methods for determining the absolute concentration of H, C_H, independent of configuration, will be discussed in section 2.4.

2.3.3.1. Optical studies. The infrared absorption spectra of sputtered [41, 49–51] and g.d. [52–54] produced samples contain essentially the same features, whose intensity depends on the preparation conditions. Modes near 630 cm^{-1} are generally accepted to be due to a mixture of rocking and wagging modes of $\equiv$Si–H and (SiH_n). They cannot be resolved sufficiently to give information about the different configurations. Bending modes occur between 800 and 900 cm^{-1}. The reader is referred to the latest literature [55] for the individual assignments (=Si–H_2, –Si–H_3, (=Si–H_2)$_n$); while these assignments have had a tendency to change, they can be taken at least as clear signatures of the presence of Si atoms with more than one H atom attached.

Stretch modes occur with peaks near 2000, 2090 and 2140 cm^{-1}. The 2000 cm^{-1} absorption has usually been attributed to an isolated $\equiv$Si–H entity, although Shanks et al. [51] have recently suggested that Si–H bonds in clusters of four, pointing towards "the equivalent of a crystalline vacancy" are responsible. We think this unlikely. This configuration (whichever it is) seems to occur both in the islands – since 2000 cm^{-1} absorption can be found in isolation in material showing no visible microstructure – and in the connective tissue – since 2000 cm^{-1} absorption is found in material with identifiable microstructure and preferential annealing of the tissue diminishes it. It would appear that a reasonable consequence of the assignment of 2000 cm^{-1} absorption to isolated $\equiv$Si–H entities would be its dominance in the spectra of samples sputtered at low p_H. Unfortunately this is not the case; other stretch mode frequencies *may* be found for very low H-contents [41], even although there is a tendency for the 2000 cm^{-1} mode to be *relatively* weaker than the 2090 cm^{-1} one at high C_H. The observations for sputtered a-Si:H here differ from a-Ge:H [2, 49] where there is a clear isolation of the $\equiv$Ge–H mode at low H concentrations. Thus, in summary, there are still unresolved questions regarding this mode (also see section 2.4).

The 2090 cm^{-1} absorption was first assigned exclusively to =Si–H_2 [52, 53] and, unfortunately, 2090 cm^{-1} and "dihydride absorption" have sometimes been synonymous in the literature. Observation of the 2090 cm^{-1} mode is usually accompanied by *some* bending mode absorption near 800–900 cm^{-1}, indicating an SiH_n grouping, but the ratio of the integrated absorptions $A(2090)/A(900)$ in sputtered samples as a function of p_H shows considerable scatter. This was evident in the early reports of the Harvard group [41, 49], and has recently received detailed confirmation by Shanks et al. [51]. A complicating circumstance has been the demonstration that the actual magnitudes of the stretching and bending vibrational absorptions depend on the details of the preparatory method [51] and that the ratio of the magnitudes can be changed by He ion bombardment which alters the nearby defect density without changing the H-content [56]. Nevertheless, there seems to be growing acceptance of the view [57] that the mode actually observed at 2090 cm^{-1} may have other contributions than =Si–H_2. Shanks et al. [51] have made the specific suggestion of two Si–H bonds on contiguous atoms, in the vicinity of two dangling bonds; Lucovsky

[58] has calculated that an O–Si–H configuration would serve; and Paul [59], in cataloguing the arguments against the unique $=Si-H_2$ assignment, has discussed a number of entities such as $(=Si-H_2)$, $(\equiv Si-H. . . . H-Si\equiv)$ and $(\equiv Si-H-Si\equiv)$. At the present stage, however, the important fact to be noted by nonaficionados is the possibility of a second single H-environment which has not been previously identified.

It should be noted that both the 2090 cm^{-1} mode and the bending modes seem to be emphasized in samples suspected of having considerable tissue material [31]. The Harvard data on sputtered material indicate that 2090, 890 and 850 cm^{-1} absorptions are emphasized by high p_H, low T_s and any intentional or accidental incorporation of alloying atoms such as Ge, O and F [60]. We have found also that the ratio of 2000 cm^{-1} to 2090 cm^{-1} absorption in any one deposition run depends on where the substrate is placed in the plasma [61]. Researchers from the Ames Laboratory [14], Livermore [62] (magnetron sputtering) and Exxon [63] report the production of sputtered samples with a stretching mode at 2000 cm^{-1} only. In our recent experience [61], there was a clear *inverse* correlation between $A(2000)/A(2090)$ and good photoelectronic properties. Since this is precisely the opposite of the conventional wisdom for g.d. a-Si:H, it should perhaps be reiterated that there is not a unique correlation between the occurrence of 2000 cm^{-1} absorption in isolation and good device properties, nor may it be assumed that dominant 2000 cm^{-1} is synonymous with the production of samples free of microstructural heterogeneity. There are residual mysteries here.

The third, less frequently observed mode at 2140 cm^{-1} has been assigned [52, 53] to $-Si-H_3$ or $(SiH_2)_n$, but this seems questionable (at least as a unique association) in view of the fact that it is seen for sputtered samples only when p_H and C_H are at their lowest values [41].

Finally, it should be mentioned that Knights et al. [32] have reported that the infrared absorption frequencies and magnitudes are affected by the presence of noble gas atoms in the glow discharge plasma. In the case of sputtered material, we have verified [64] that the use of Ne instead of Ar as sputtering gas leads to a narrowing of the 2090 cm^{-1} absorption peak but have not found any shift in frequency. It is not yet clear whether the observed effects are due to a dependence of the network structural disorder on the size of incorporated noble gas atoms, to a change in the microstructural heterogeneity, or to some other cause.

2.3.3.2. Hydrogen evolution. The evolution of H on heating may be studied by inserting a known mass of sample in an evacuated quartz tube of known volume and measuring the increase in pressure as the temperature is raised at a steady rate [65–69]. Two types of information are obtained. The spectrum of pressure rise P versus T gives information about any diversity in the strength of bonding of the H to the network and so implicitly about the Si–H configurations, while the total pressure rise after crystallization may be used to deduce the atomic percentage of H in the sample. We deal with the first type of information here and with the second in section 2.4.4.

An alternative method is to feed the evolved gases continuously to a mass spectrometer, which has the advantage that the gas actually evolved at any T is identified [70, 71]. Provided the throughput of gas to the mass spectrometer is constant with

time, and there are no time lags in registration of signals on the mass spectrometer, the evolution spectrum of H may be found. The absolute amount of H evolved may also be found if the mass spectrometer signals are calibrated as a result of measurement of a sample with H-content separately determined by the nuclear reaction technique.

In the Harvard apparatus, the free sample mass is about 0.5 mg, the quartz tube volume is 255 cm^3, the heating rate is 12°C/min and the total pressure rise is about 0.2 Torr. Fig. 1 illustrates typical P and dP/dT versus T for sputtered samples in this apparatus and fig. 2 representative dP/dT versus T. Samples made at low p_H and moderate T_s show a single peak near 600°C, while those deposited at high p_H also have a second peak centered on 375°C. Glow discharge samples prepared at Argonne [66] and IBM [70], also give two resolved peaks similar to the sputtered material.

Fig. 2 also shows a spectrum for a g.d. sample from Mobil-Tyco measured in our apparatus. It has a "mesa-type" structure, rather than two well-resolved peaks, and resembles spectra on g.d. samples measured at Bell [71] and Xerox [73]. It is evident that, depending on the details of the preparation method, the H is differently distributed in bonding environments. The kinetics of the evolution processes corresponding to the features near 375 and 600°C have been studied by several groups [75]. Here we shall concentrate on the possibility of identification of the responsible Si–H entities.

The occurrence of the large peak at 375°C in sputtered samples, emphasized by low T_s and high p_H, is empirically correlated with poor device parameters. The fact that

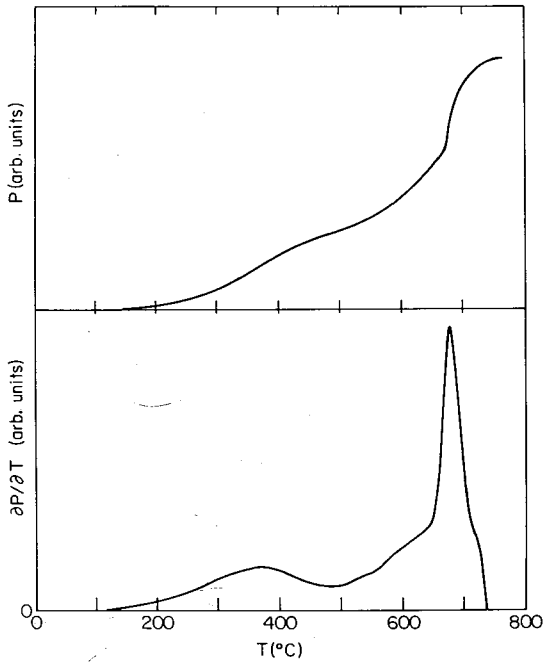

Fig. 1. Typical pressure P versus temperature T and dP/dT versus T for sputtered a-Si:H in the Harvard evolution apparatus [67].

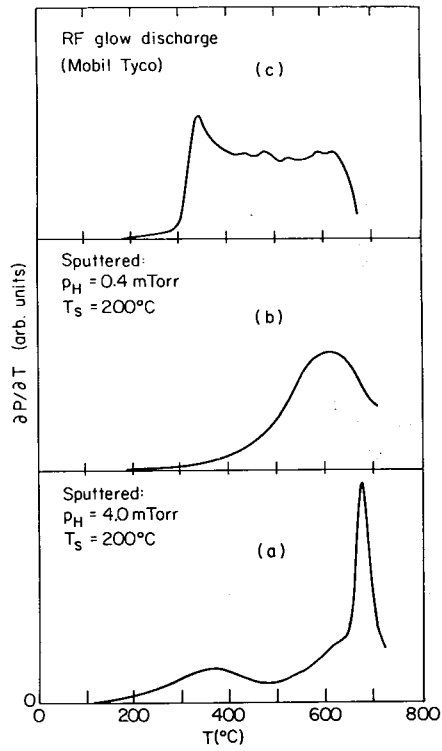

Fig. 2. Evolution spectra, dP/dT versus T, from the Harvard apparatus; (a) sputtered sample, high p_H and low T_s, (b) sputtered sample, low p_H and low T_s, (c) glow-discharge sample from Mobil-Tyco, showing mesa-type structure.

g.d. films, *evolved in the same apparatus*, classify roughly into two categories – mesa or single/double peak – is notable, but its cause is not yet apparent, and no correlation with differences in plasma conditions has yet been done. The different evolution spectra rationalize the observation that annealing has different effects on measured properties. For example, the Xerox group [69] examined the changes in spin resonance, photoluminescence spectra and infrared absorption for samples whose evolution spectrum resemble fig. 2c. Major changes were seen which were interpreted as the result of defect annealing, H-diffusion and H-evolution. An attempt was made to correlate these with different Si–H bonding entities and the microstructure. By contrast [68], the Harvard group studied samples whose evolution spectrum resembled that of the high p_H, low T_s sample of fig. 2. Intermediate temperature anneals led to little change in the infrared spectrum, the absorption edge and electrical transport, but did change the photon energy of the peak photoluminescence. Whether or not the detailed interpretations attempted [68, 69] are correct, they are clearly not directly comparable, since they must involve different evolution processes.

It is tempting to postulate that the 375°C peak be assigned to escape of H from the connective tissue and that the 600°C peak be associated with the breaking of isolated

Si–H bonds. However, experiments correlating evolution with change in observed microstructure (TEM, SEM) have not yet been carried out. Early suggestions that the two peaks be assigned to evolution of $=Si–H_2$ and $\equiv Si–H$, respectively, must be discounted, since remeasurement of the infrared spectrum after partial anneal near 400°C, which removes the H in the first evolution peak (see fig. 2a) does not preferentially diminish any infrared mode [68, 76]; this implies that all of the Si–H configurations occur in both phases of the microstructure. From experiments on many sputtered samples, Oguz [72] has determined that at least 18 at% H may evolve in the peak near 600°C; this does not accord with a model of isolated Si–H bonds in a limit of 3–4 at% as has been inferred from the early NMR studies [34, 35]. Finally, it has been shown that amounts of the order of 5 at% may be evolved in the 375°C peak without much change in the infrared absorption spectrum [68, 72]; unless there are accidentally cancelling increases in oscillator strength of the remaining Si–H entities (unlikely, in our view), this implies the existence of H in configurations (interstitial? H_2?) other than the strongly covalent Si–H entities yielding the bulk of the infrared spectrum [77].

In summary, there are different features in the evolution spectra of differently-prepared films, but their origin is not yet firmly established. Their existence, however, cautions us to be careful in interpreting the results of annealing experiments for various optical and electrical properties.

2.3.3.3. Photoemission. Most of the photoemission work on a-Si:H has been carried out by the Stuttgart group. In the first experiments, von Roedern et al. [78] established that, as the H content of samples sputtered onto a substrate at room temperature was increased, different peaks in the valence band density of states appeared. These were tentatively assigned to different SiH_n configurations largely on the basis of comparisons with similar spectra for H bonded on crystalline Si surfaces. Later several authors [79] calculated the energies expected for the different configurations, enabling a reasonable correlation between theory and experiment, which involved the existence of Si–H, $=Si–H_2$ and $–Si–H_3$ entities. More recently, Ley and Gruntz [80] have examined the valence band and core-photoemission spectra of sputtered a-Si:F and have given convincing evidence (especially from the chemically-shifted Si2p core levels) of the existence of a large fraction of $–Si–F_3$ configurations. Significantly, however, removal of the top surface layers (the photoemission technique probes the first 10–20 Å) reduced the proportion of $–Si–F_3$. If these results can be extrapolated to the earlier data on a-Si:H, it appears likely that, independent of the correctness or otherwise of the correlation of the spectra with different SiH_n entities, the technique must be used with considerable caution in making deductions about Si–H configurations in the sample bulk.

2.3.3.4. Nuclear magnetic resonance. We referred earlier to the observation of two superposed lines in the NMR spectra of all a-Si:H so far examined. The narrower (Gaussian or Lorentzian) line was attributed to monohydride but was dipolar broadened to an extent that suggested clustering of at least some of the monohydride rather than a random distribution [34, 35]. It was reported to contain about 2–4 at% H independent of the total H-content. The broader line contained the rest of the H and

corresponded to densely clustered monohydride or to clustered polyhydride species. Since the line frequencies are only slightly shifted (17 ppm) from those for tetramethylsilane, it was concluded all H was covalently bonded and that there was no molecular or atomic H in "interstitial" sites [22]. Reimer et al. [34] attributed the narrow and broad lines to H incorporated in the islands and tissue, respectively.

These experiments and their interpretation presently are undergoing refinement as more data are accumulated, since several questions are immediately evident. For example, it seems curious that microstructure should be unobservable by electron microscope in some films whose tissue is asserted to contain all but 2–4% of H in films that may have 10–30% H present [81]. Association of the broad line predominantly with polyhydride is not possible. Both Reimer [34] and Jeffrey et al. [82] find both lines in material that shows no infrared bending mode absorption. Jeffrey et al. [82] indicate a larger at% of H in the narrow line (distributed monohydride) than the earlier work.

Carlos et al. [35] have also examined sputtered a-Si:H, and have found striking differences in the dependence of the spin–lattice relaxation time T_1 on temperature: whereas all glow-discharge samples, and sputtered samples prepared at high p_H, show a minimum in T_1 versus T near 40 K (attributed to relaxation via disorder modes), sputtered samples prepared at low p_H show only a weak monotonic decrease of T_1 with increasing T. These films also show no low temperature evolution bump near 375°C, but any connection between the two observations has still to be established.

It is too early to draw definitive conclusions from these experiments, but it is evident that they are rich in information. What is already clear is that, to date, no one-to-one correspondence has been established between the two NMR lines, the doublet infrared spectra and the two phase structural heterogeneity.

2.4. Chemical characterization

This section will concentrate on methods of determining H-content, although the profiles of contaminants will be discussed under 2.4.2. and the Ar and O contents will be briefly discussed under 2.4.5. The average H-content has been estimated by four methods: ^{15}N or ^{19}F nuclear reactions, secondary ion mass spectroscopy (SIMS), infrared vibrational absorption, and thermal evolution.

2.4.1. Nuclear reactions

The nuclear reaction of ^{15}N with H provides the most accurate quantitative method for both depth profiling and H-content [83–85, 70]. The narrow resonance reaction (^{15}N, ^{1}H; $^{12}C^{4}He\ \gamma$) occurs at a depth below the film surface which depends on the energy of the N ions and the density and stopping power of the a-Si sample, which is assumed equal to that of c-Si. The intensity of emitted γ-rays is proportional to the local H-concentration over a depth of the order of 100 Å. It is not possible to study lateral microstructure (islands and columns) since the beam diameter is too large. Since the technique requires access to a reactor, it has often been used to calibrate the

more accessible, but less sure, procedures of infrared absorption and H-evolution on heating.

2.4.2. SIMS

Secondary ion mass spectroscopy permits both depth profiling and content estimation of many "contaminant" elements as well as H. In SIMS [86, 87], samples are bombarded by a beam of ions (for example, Cs) which cause the outermost atom layers to be sputtered off, either as neutral or charged particles. They are then detected and identified in a mass spectrometer. Careful rastering of the bombarding beam erodes a crater in the material, so that a depth profile of the species being examined can be established. The method requires calibration for absolute estimations by measurement of the signal from an ion-implanted Si standard. When the method is used to detect small percentages of contaminants such as C, N and O as well as H, a very high vacuum is required to eliminate false readings from the residual gases. Ref. [86] gives a recent review of results in g.d. produced a-Si:H. In our experience the measured H-profile in sputtered films is very uniform, except near the substrate–film and film–air interfaces. Fig. 3 illustrates the effect. It is uncertain whether the measured spatial *variation* is quantitatively reliable, or may be influenced by sputtering simultaneously from different depths (near the edges of the crater) near a variation in concentration of the examined species.

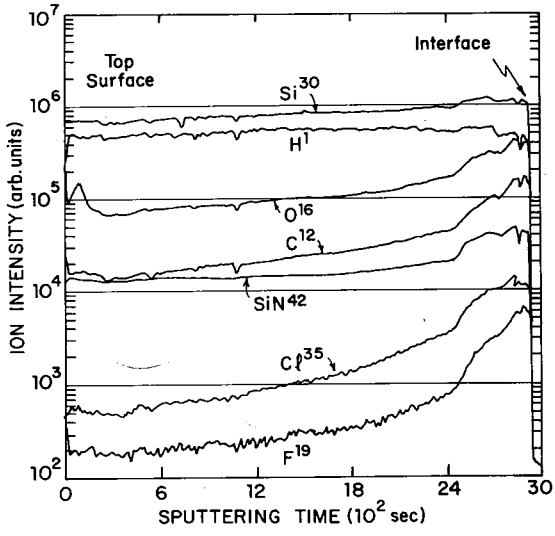

Fig. 3. SIMS profile of H and accidental contaminants in typical (as of 1979) sputtered a-Si:H from Harvard. The figure illustrates the variation with depth (≡sputtering time) of the film constituents. The build-up near the interface and free surface is to be noted. Neither the absolute nor the relative concentration of constituents may be taken from the figure. These require careful calibration of the apparatus variables and this has not been done for this illustration.

2.4.3. Infrared vibrational absorption

Analysis of the integrated intensity of the infrared vibrational absorption provides one of the most widely accessible ways of obtaining the H-content. Connell and Pawlik [49] attempted to use the oscillator strengths of the Ge–H and Si–H wag modes in gaseous GeH_4 and SiH_4, modified by a local field correction for the solid environment. Brodsky, Cardona and Cuomo used a similar approach [50], but applied a different correction which led to a different estimate of H-content. Such methods are less reliable than those which calibrate the oscillator strengths through measurement on the same sample of the H-content, preferably by nuclear reaction [70, 74, 85, 88] or SIMS [86, 87], and less reliably by thermal evolution [41, 51, 70, 74, 89]. Even these calibrations have to be applied with care in view of the experimental [51, 56] and theoretical [55, 58] demonstration that the frequency and magnitude of the absorption are strongly affected by the local environment of defects and impurities. This is perhaps most clearly shown by the demonstration [56] that He ion bombardment which had no effect on C_H altered the integrated infrared absorption, fairly certainly by changing the local environment of defects. There is evidence that modes of roughly the same frequency can occur in different environments of island and tissue, which may vary from preparation to preparation.

Shanks et al. [51, 74] have concluded that the stretch modes appear to be most susceptible, and the wagging modes least susceptible, to impurity and defect effects which vary from preparation to preparation. The insensitivity of the wagging modes in the He ion bombardment experiments [56] confirm this thesis as far as defects are concerned. It would therefore be comforting to report that the oscillator strengths for the wagging modes, determined by calibration of C_H by, say, nuclear reactions, agree between laboratories, but that does not yet appear to be the case. Comparison of calibrations is also rendered more difficult by an inconsistency in definitions of H-content. Thus, Fang et al. [74] and Shanks et al. [51] refer to H-concentrations as the ratio of the density of H atoms, N_H, to Si atoms (equivalent to quoting x in the formula SiH_x) and find $N_H = A_w \int [\alpha(\omega)/\omega]\, d\omega$, with $A_w = 1.6 \times 10^{19}\ cm^{-2}$ for the wagging mode. By contrast, Oguz [90] refers to H-concentrations as $C_H(at\%) = 100 N_H/(N_H + N_{Si})$ (equivalent to quoting x in the formula $Si_{1-x}H_x$) and finds $C_{H,w} = 0.62 K_w$, where $K_w = \int \alpha\, d(\hbar\omega)$ for the wagging mode in eV cm^{-1}. The oscillator strengths for the wagging modes determined on Oguz' sputtered samples were calibrated against C_H established from nuclear reactions by Lanford; they gave agreement within 20% for the C_H of RCA samples measured by IR absorption and by SIMS, and within 10% for the C_H of Sandia samples measured by IR absorption and nuclear reactions. The origin of the discrepancy that appears in estimation of the wagging mode oscillator strength at Stuttgart and Harvard (after correction of the formulae for the different definitions of C_H) is not known at the time of writing.

2.4.4. Hydrogen evolution

As was mentioned in section 2.3.3.2 the total pressure developed in thermal evolution experiments may in principle be used to infer the atomic percentage of H.

Tsai and Fritzsche [65] found that the results for the total of H evolved agreed with those from nuclear reaction measurements. Fang et al. [74] agree that this is so provided the substrates for the a-Si:H are appropriate (c-Si and lime–soda glass). On the other hand, Jones et al. [91] and Oguz, Paul and Lanford [89] found that the evolution method seriously underestimated the C_H determined by ^{15}N nuclear reactions. The latter authors attribute the difference mostly to diffusion of the H into the containing fused quartz of the evolution apparatus, and to a lesser (but finite) extent, to retention of some of the H in the Si after crystallization. Jones et al. [91] found that up to half of the H remained in a Corning 7059 (borosilicate glass) substrate after evolution. It is possible that these different assessments of the utility of the method occur because of different masses of sample and different containing volumes (there is a factor of 25 difference in volume between the Harvard and Chicago apparati) which vary the uptake of H by quartz. The thermal evolution method must therefore be used with caution and may give a lower bound on C_H, always provided a mass spectrometer has been used to verify that H (and not, for example, Ar or O) is the evolving species.

2.4.5. Argon content

The Ar content of Ar-sputtered films has been determined by SIMS and electron microprobe and can rise as high as 6–8 at%. An empirical inverse correlation has been found between C_{Ar} and p_{Ar}, for example Messier [11] reports 7 at% Ar for $p_T = 5$ mTorr and 0.5 at% Ar for $p_T = 70$ mTorr. This may be the result of a dependence on p_{Ar} of the self-bias of the substrate platform with respect to the plasma. A more negative bias is found for low p_{Ar}, and it is argued that Ar^+ ions are thereby attracted to the substrate. On the other hand, low p_{Ar} tends to yield films with very little microstructure or porosity, and this then inhibits the later growth of O-content on exposure of the films to air. The influence of Ar on the plasma chemistry and the ultimate film structure may be significant, but has been insufficiently investigated to this point. In this connection the observation by the Xerox group [32] that admixture of different noble gases to the SiH_4 in glow discharge affected both microstructure and optical properties seems relevant. Tanaka et al. [92] found that up to 8 at% Ar was incorporated for about 8 mTorr Ar plasma pressure. They determined that such films displayed measurably different infrared absorption, specifically, a dominance of 2090 cm^{-1} over 2000 cm^{-1} stretching vibrational absorption, and lower photoconductivity and photoluminescence than g.d. films prepared such that $C_{Ar} \leqslant 1$ at%.

2.4.6. Oxygen content

We have already mentioned the direct measurement of the O-content by SIMS [86]. The O-content, and its effect on properties, is an important subject, since the presence of water vapor in the base vacuum, the gas chamber walls, and the gas lines makes it very difficult to reduce it below, say, 0.1 at% in film a-Si:H. Indeed, various elaborate cleaning, flushing and gettering procedures are being adopted so as to reduce C_0 as far as possible. An unmistakable signature of O at the 1 at% level may be found in Si-O

vibrational absorption near 950 cm^{-1}, and it is probably worth remarking that this absorption band shifts to 1050 cm^{-1} when the O is incorporated on exposure to atmosphere after the film has been made. The possible effect of O on the Si–H vibrational absorption spectrum has been discussed by Lucovsky [55, 58].

The effect of unintended significant levels of O on the optical and electronic properties will not be considered here, because of space limitations, although brief reference will be made to certain aspects of it. The original paper drawing attention to its importance was given by Paesler et al. [93]. Yacobi et al. [94] have measured the effect of small amounts of O and H on the density of states near the band edges and in the pseudogap through measurement of the optical absorption, photoluminescence and photoconductivity. Knights et al. studied the effects of the addition of O to g.d. a-Si:H on the Si-H IR absorption, the absorption edge and the photoluminescence [95] while Griffith's group at Brookhaven [96] has made very extensive studies of the effects of O (and other impurities) on the photoelectronic properties.

2.5. *Trends in electrical and optical property measurements with p_H and T_s*

In this section we shall discuss the changes in structure, chemistry and properties as some of the principal preparation parameters – p_H, p_{Ar}, T_s, P_{rf}, bias, substrate, geometry, gas flow rate – are changed. These may be expected to affect C_H, C_{Ar}, the R.D.F., the void density, the nature of the H-configurations and the microstructure, which in turn determine the optical and electronic properties. We shall concentrate on p_H and T_s, without meaning to play down the importance of the other parameters. We shall also use our own results as illustrations, while noting that limited importance should be attached to the absolute values of p_H and T_s where certain phenomena occur, since these depend intimately on all of the other parameters.

Fig. 4 shows, schematically, the changes in a number of property measurements on samples co-deposited at different p_H, but otherwise fixed preparation conditions. At low p_H (the exact range depends on the other variables), C_H increases with p_H, the spin density N_s associated with uncompensated dangling bonds decreases [97], the absorption edge E^{04} shifts to higher energies [42], the hopping conductivity decreases [98] and the photoconductivity [99] and photoluminescence [100] (1.3 eV peak) magnitudes increase. A satisfactory, self-consistent model for these changes is the obvious one: compensation of dangling bonds and reduction of the occurrence of "reconstructed" weak, or long Si–Si bonds, with the resultant elimination of states from the pseudogap.

The role of H at intermediate and high p_H (the quantitative interpretation of the adjectives depends on the other variables) is evidently far more complex. The content C_H asymptotes, and sometimes even decreases, as p_H is further increased. The IR vibrational absorption spectra show more features attributable to multiple H-bonding. At the highest values of p_H ($\approx$5 mTorr in our system) both the optical absorption edge and the photoconductivity edge show evidence of increased sub-bandgap absorption and a new feature appears in the photoluminescence near 0.9 eV [101]. These results suggest a substantial rise in the state density in the gap. The photoconductivity remains high and shows structure as a function of p_H [99]; the structure is apparently real and very sensitive to the position of the Fermi level.

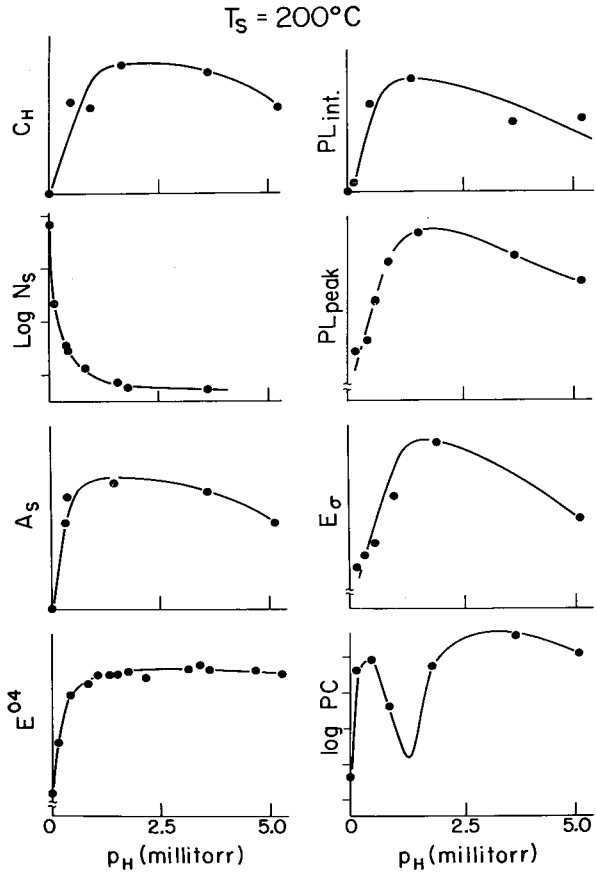

Fig. 4. Schematic illustration of changes in properties for samples co-deposited by sputtering at fixed T_s but systematically varied p_H. A_s is the total integrated area under the IR peak due to stretching vibrations. E_σ is the activation energy for band transport. These are early (circa 1977) data, but later improvements in statistics have not changed the general pattern of behavior.

While the properties so far mentioned all vary smoothly and gradually with p_H, the electrical conductivity [102] shows an abrupt change in magnitude and temperature dependence at approximately the same value of p_H as the 0.9 eV feature in the PL is first observed. Because of their importance in the development of our model we shall discuss these changes in the transport in some detail.

Figs. 5, 6 and 7 show the variation of conductivity σ with T for samples all prepared at the same T_s, but at low (<1 mTorr), intermediate (1–3 mTorr) and high (3–10 mTorr) values of p_H [102]. At low p_H, C_H is increasing uniformly with p_H and $\sigma(T)$ correspondingly decreases. For C_H between 0 and 2 at% the room temperature transport is unactivated and presumably depends on carrier hopping in localized states. It is notable that this persists for H-concentrations much larger than required to compensate the dangling bond density in unhydrogenated samples, a reflection of the fact that the gap states do not just stem from dangling bonds and that the H is not

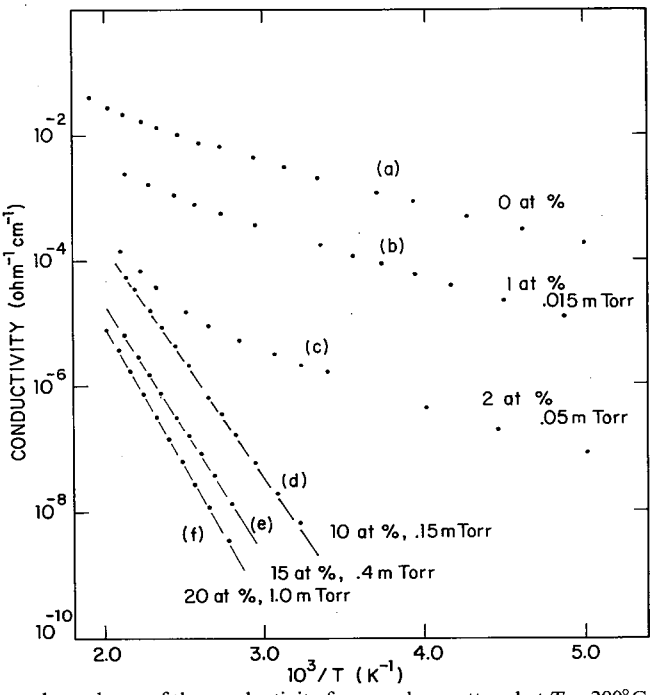

Fig. 5. Temperature dependence of the conductivity for samples sputtered at $T_s = 200°C$ but at p_H between 0 and 1 mTorr [102]. Hydrogen content (at%) and p_H are given on each curve.

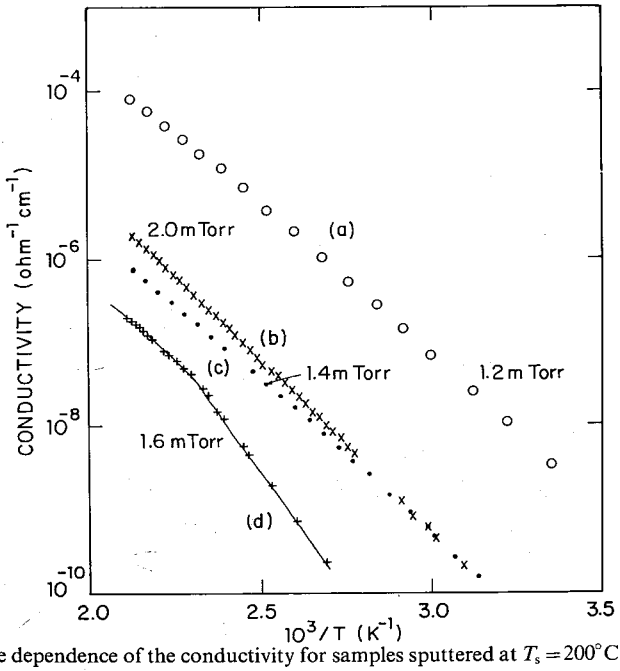

Fig. 6. Temperature dependence of the conductivity for samples sputtered at $T_s = 200°C$ but at p_H between 1 and 3 mTorr [102], as listed on the curves.

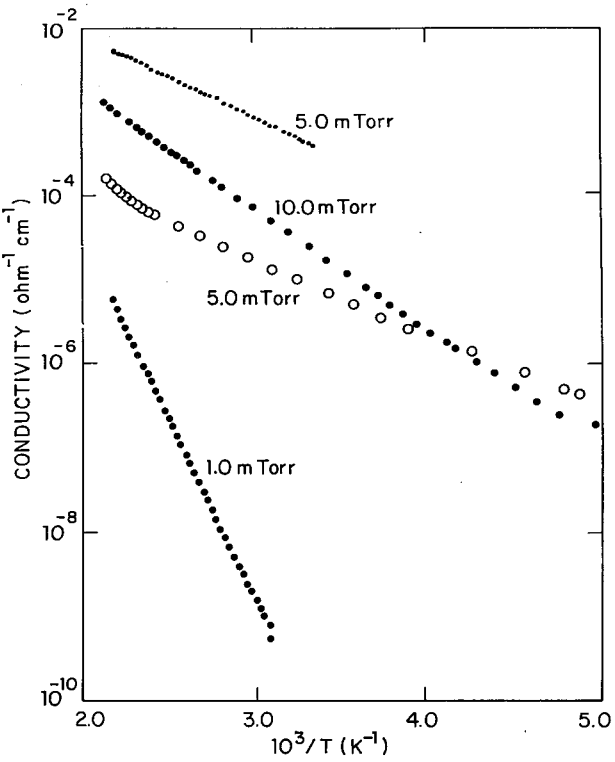

Fig. 7. Temperature dependence of the conductivity for samples sputtered at $T_s = 200°C$ but at a high p_H between 3 and 10 mTorr [102], as listed on the curves.

targeted to eliminate dangling bonds first before it alters other network attachments. For higher C_H the transport is activated.

In the high p_H range (fig. 7), C_H is essentially constant, yet σ is high and unactivated. If we were to examine the thermopower S versus T, we would discover it to be activated for low p_H, but very large and almost constant with T for high p_H [102]. In the intermediate range of p_H(1–3) mTorr), the behavior of σ and S with T is diverse and unpredictable.

We have proposed [102, 103, 170] that the totality of this behavior can be understood on the basis of a model of transport through two mixed phases with different structure, chemistry, electronic band structure and transport parameters. These two phases are postulated to be the islands and connective tissue we have discussed in section 2.3. Their properties are illustrated in fig. 8. The island material is postulated to be a-Si:H with high compensation of defect centers, so that the pseudogap density of states is low and σ and S are both activated with T. The connective tissue is supposed to be rich in H, to present a larger band gap, but also a higher density of defect-related states in it, so σ and S are less dependent on T. We infer from experiment [102] that the importance of the island-connecting tissue is greater for high values of p_H, and note that this is also the regime in which Messier (see section 2.3.2) reports a higher degree

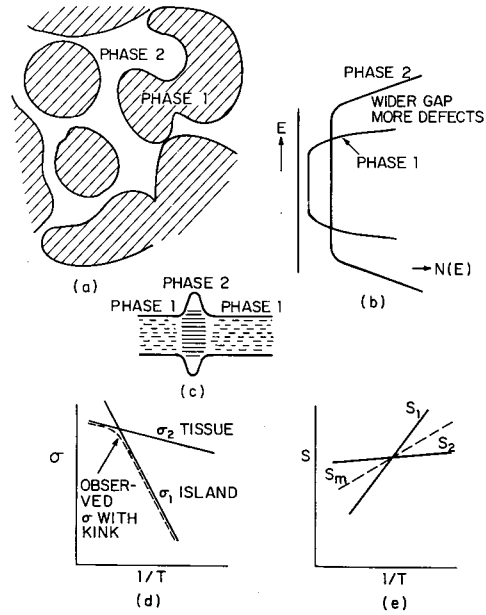

Fig. 8. Model of two-phase microstructure of islands and tissue, with postulated schematic electronic band structure and transport properties. After Paul [17].

of observable microstructure. At low p_H (fig. 5), the transport is dominated by the island material and not until the tissue occupies a considerable fraction of the total volume is its presence clearly seen. Eventually a form of percolation threshold is reached whereupon control of the transport switches abruptly to the tissue regions (fig. 7). In the intermediate p_H of fig. 6 some average of islands and tissue is appropriate. The underlying microstructure of islands and tissue appears to be present in virtually all of the sputtered material we have studied. It also seems to be responsible [103] for a number of wellknown anomalies connected with the transport, such as the fact that the activation energies for σ and S are unequal, that the $1/T=0$ intercept for S is much greater than theory expects and that there occurs a kink in $\ln \sigma$ versus $1/T$ at high T (see section 4). We conclude that studies of the *intrinsic* transport of a-Si:H should be concentrated on films which are the most homogeneous [104].

The changes with p_H of other properties are more gradual since they essentially average over islands and tissue. For example, the optical edge changes its shape: the quantity E^{04} tends to increase slightly with p_H, for fixed C_H, which can be understood as due to increased influence of the wider-gap connective tissue; on the other hand, the absorption at low photon energy increases, which, along with the new PL feature, may be associated with the increased defect density in the gap and tentatively linked to the tissue material.

The model we have proposed has not yet been substantiated through direct observation of microstructure in films made at high p_H. We presume that this is because averaging effects on, say, a 50 Å scale obscure sharp structure delineation in TEM examinations of films at least 200 Å thick. It is notable, however, that the thermal

evolution spectrum of films prepared at high p_H shows an enhanced bump at low T [67, 68], implying that there is an increased amount of lightly bound H, which would be consistent with an increased volume of connective tissue. It is also notable that the one film in which we have observed microstructure, which was prepared at higher p_{Ar} than those for figs. 5, 6 and 7, also showed high σ that was only weakly T-dependent, behavior we have attributed to the connective tissue.

We now turn to the effect of changing T_s, which is comparatively easy to understand. It is known from earlier studies [105] on sputtered unhydrogenated Ge that increased T_s leads to a larger energy gap, lower defect state density and decreased conductivity, all properties consistent with annealing of a continuous random network short of inducing crystallization. Similar changes are observed in unhydrogenated a-Si, but the reduction in defect density for T_s up to 500°C is small. (Even a-Si made by CVD from SiH_4 at $T_s = 650$°C has a very high spin density which suggests that the amount of network healing is still not comparable with the effects of hydrogenation.) T_s does, however, seem to influence the H-incorporation. Thus at fixed low p_H (in the range where we have claimed that the dominant role of H is that of dangling bond compensation) increasing T_s up to roughly 300°C gives results consistent with improved efficiency of H-compensation of defects: the optical edge displaces to higher energies [42], and the hopping conductivity [102] decreases. These results suggest that the tissue regions are less stable at higher T_s, because the islands coalesce more readily, assisted by the increased surface mobility of the depositing atoms. At higher p_H, increase in T_s has little effect on the film properties.

When T_s is increased above about 400°C (recall that the actual growth temperature is not well-established), C_H drops below that necessary to compensate the defects. That C_H decreases may be seen directly in infrared absorption measurements [41] or in the H-evolution experiments [42, 68]. Its effect is seen in a shift of the optical absorption edge to lower energies [42], an increase of σ and conversion to non-activated transport [102], and a decrease in the photoconductivity [99] as the excess carrier recombination time decreases.

Before discussing the effect on properties of other variables such as p_{Ar}, substrate bias, etc., we make an interim summary. It appears that there are two different and opposing influences of H-incorporation. The first is that of dangling bond compensator and continuous random network terminator, which reduces the state density in the gap and at the top of the valence band and creates states with energy deep in the valence band. The second is to catalyse new defect states. These may be in the islands as the network grows around H-terminations. Or, they may be the result of an increase in the relative volume of island-connecting tissue. These two roles of H are played simultaneously and are dominant at low and high p_H, respectively. It follows that, as long as C_H is sufficiently high that the great majority of dangling bonds are compensated, the primary effect of different sputtering conditions (and, indeed, different glow discharge deposition conditions) is that of affecting the degree of heterogeneity. Whether the effect of heterogeneity is visible directly (electron microscope) or is only evident in changes in properties, depends precisely on the width (volume) of the connective tissue. What, then, is the expected effect of deposition parameters on the tissue?

Islands of Si nucleate and grow on the substrate. If the deposition rate is not too high and the substrate temperature not too low, they will grow laterally on the surface and seek to join. In the absence of H, the width of the tissue connecting the islands should not be greater than several interatomic distances. In the presence of H, the rate at which island surfaces are terminated by H depends on p_H. If it is very rapid, then there is apt to be a region between islands which is very sparsely populated. However, there cannot be a width which is larger than the critical diameter of a stable island.

The effect of increasing T_s might then be expected to be to give all atoms more surface mobility, which will tend to eliminate microstructure and promote more homogeneity. Impurity atoms such as Ar may affect the microstructure by reducing the possibility of defect-free union of islands, as well as creating defects in the islands themselves. Bombardment by atoms and ions of Si, H and Ar and by electrons will be affected by the plasma pressure and any substrate bias, whether in a floating substrate or externally-imposed. Low plasma pressures and high P_{rf} will favor bombardment, for example, and possibly cause damage that cannot be annealed. On the other hand, bombardment may have the beneficial effect of sweeping poorly attached atoms off the growing film. Thus, the effects of P_{rf}, bias, p_{Ar}, etc., on the extent of the microstructure would seem to be very complex indeed. Yet it appears that it is in the conceivably delicate balance of the various effects that there lies the possibility of reducing the volume of the connective tissue between islands, which is certainly a necessity for understanding of the intrinsic properties of a-Si:H and probably a necessity for improvement of the device viability of new films.

3. Density of states in the gap

3.1. Introduction

A reliable, direct method of measuring the distribution $N(E)$ of states in the pseudogap would vastly simplify the correlation of properties with preparation conditions. Deductions from transport, phototransport and photoluminescence, described in later chapters, are necessarily indirect. More direct methods include (1) electron spin resonance (ESR) and light induced spin resonance (LESR); (2) low energy optical absorption spectra; (3) certain photoemission spectra; (4) field effect; (5) capacitance–voltage and capacitance–frequency; (6) deep level transient spectroscopy; (7) tunneling spectroscopy. In succeeding sections we shall briefly describe or reference the techniques, and objectively examine their reliability. A review of the situation regarding the density of states in g.d. a-Si:H has been given recently by Fritzsche [8].

Space limitations preclude a long discussion of the origin of the gap states. Those near the band edges are presumed to be caused mostly by the disorder, those further from the band edges by a variety of natural defects and dopants. Among the natural defects are dangling bonds, Si atoms with less than 4-fold coordination and reconstructed long bonds [106–109]. The nature and location of the defects probably depends on the existence of microstructure. At this point the theoretical calculation

of defect energies and stabilities has an uncertain predictive value, and more work on correlation with experiment is needed. Similarly, the results for the DOS of the incorporation of P, As or B may be speculated upon in qualitative terms, but neither the energies for the 4-fold or 3-fold coordinated impurity, or any impurity–defect or impurity–H complex are experimentally or theoretically established. It will be easier to understand these when the gap DOS has been more reliably established from experiment than at present.

3.2. ESR and LESR

ESR measures the total number of unpaired spins and gives a lower limit on the integrated density of states per unit volume in the energy range between E_f and $E_f - U$, where U is the (unknown) correlation energy of the responsible center. From considerations of the g-value (2.0055) the responsible center is almost certainly a Si dangling bond. The spin density in evaporated or sputtered unhydrogenated a-Si is between 10^{19} and 10^{20} cm^{-3}. A summary of the characteristics of ESR in these materials has been given by Stuke (1977) [110].

The early work of Lewis et al. [2] on hydrogenated sputtered a-Ge showed a spin density decrease by about 10^2 as about 6 at% H was added. Continuation of this work by Connell and Pawlik [49] showed several characteristics of a-Ge:H that have carried over, mutatis mutandis, to sputtered a-Si:H: (1) the spin density N_s in unhydrogenated material is much lower than the dangling bond density that would be estimated from the measured mass density or the measured void volume. This suggests that there has been considerable reconstruction of the network involving weak, but diamagnetic, bonds; (2) N_s is decreased by orders of magnitude by hydrogenation, through compensation of dangling bonds by H; (3) far more H atoms are incorporated than would be required simply to compensate the dangling bond density measured by N_s; (4) the line-shape and line-width are a function of both C_H and the temperature. Specifically, the line-width may be written

$$\Delta H_{pp}(T) = \Delta H_{pp}(0) + \delta H_{pp}(T).$$

Then $\Delta H_{pp}(0)$, the width at low T, increases with C_H, and decreases with annealing. On the other hand, $\delta H_{pp}(T)$ increases roughly proportionally to the unactivated hopping conductivity $\sigma_h(T)$. It is deduced that the linewidth cannot be determined wholly by pure dipolar interactions, for then $\Delta H_{pp}(0)$ would decrease with increasing C_H and decreasing N_s.

Pawlik and Paul [111], and Title, Brodsky and Cuomo [112] have further extended this work on a-Si:H. Pawlik finds that about 18 H atoms are incorporated for each spin eliminated, confirming the Ge result that H affects the defect-free network and changes erstwhile diamagnetic entities as well as compensating paramagnetic dangling bonds. The contribution of $\delta H_{pp}(T)$ to the line-width is smaller in a-Si than in a-Ge; presumably the smaller hopping conductivity in the former leads to a longer lifetime for the spins. $\Delta H_{pp}(0)$ again increases with C_H; it is suggested that $\Delta H_{pp}(0)$ in unhydrogenated a-Si is attributable to some combination of exchange narrowing, g-value anisotropy and disorder, such as bond angle variation, in the local environment.

The broadening is then attributed to a decrease in the narrowing mechanism as N_s is decreased.

Pawlik also found that N_s saturated near a few times 10^{16} cm^{-3} at high C_H, but supposed this might simply reflect the density of surface spins. There is, however, no direct evidence to support this, and it is quite possible that it corresponds to a greater bulk defect density to be associated with microstructure.

Two other effects should be mentioned. The first is light induced spin resonance [113], which is possible because there are empty and doubly-occupied states in the gap and because the recombination time for photoexcitation is long. The second is optically detected ESR [114], or a modification of the intensity of photoluminescence when the sample is placed in a pumped microwave cavity, which alters the recombination processes. The first has been studied in both sputtered [111] and g.d. material [113], with quite similar results. Pawlik and Paul reported changes in the line intensity and also the creation of a new resonance line at a higher g-value. Perhaps the most intriguing aspect of their results, which has apparently not been followed up, was the observation of a structured spectral dependence of LESR, extending below the absorption edge, with strong features at 0.8 and 1.4 eV. These energies are close to where special features are also found in the spectra of photoluminescence and photoconductivity.

From the standpoint of the present chapter, the main effect to be noted is a decrease in N_s in a-Si:H sputtered at $p_H = 2 \times 10^{-3}$ Torr and $T_s = 250°C$ to at least 4×10^{16} cm^{-3}. While this is an order of magnitude higher than the lowest value reported by Biegelsen [115, 116], the difference is probably not significant, since the Pawlik examination is 5 years old. Comparison of the Biegelsen value with the field effect density of states (see below) suggests that either U is quite small, or the gap contains many diamagnetic states, or the field effect DOS is unreliable. The lowest Pawlik value tells us that there should be no great difficulty in measuring the bulk DOS in sputtered a-Si:H – which does not turn out to be anywhere close to the facts.

3.3. Low energy optical absorption spectra

Optical absorption below the arbitrarily-defined band gap may be measured directly by standard transmission techniques if it is strong enough; the results for P and B incorporated in sputtered a-Si:H are described in section 5. Another often-used technique is to measure the photocurrent for low photon energy illumination. Crandall [117] has suggested that this is best done using blocking contacts to prevent the complication of secondary photocurrents, which occur when one carrier is trapped and the other may exit and re-enter through injecting contacts thus providing photoconductive gain. Wronski et al. [117], however, have pointed out that such blocking contacts may lead to photoemission from the metal over the barrier to the semiconductor. In fact, these complications may be avoided if sufficient precautions [118] are taken with ohmic contacts and normalization of the deduced absorption coefficient with that determined by a direct measurement is done. Absorption coefficients as low as about 10^{-1} cm^{-1} may be reliably determined [119]. These absorption spectra neither determine the joint density of-states with certainty (unknown matrix

elements) or the single-band density of states, but they are reliable for comparison of samples and they can act as a check on other types of (direct) measurement of the state density.

Fig. 9 illustrates how absorption coefficients from direct transmission measurements and from data on photoconductivity may be overlapped to extend the absorption spectrum [118]. Fig. 10 shows how this extension of the spectra simplifies interpretation of an interesting change that occurs in the photoconductivity spectrum when the p_H of the sputtering plasma is increased to high values. For $p_H \gtrsim 5$ mTorr, and no further increase in C_H, a shoulder or peak grows in the photoconductivity spectra near 1.2 eV [120]. As fig. 10 also shows, a very similar feature appears on introducing PH_3 into the sputtering plasma. Similar shoulders or peaks may be seen in published absorption spectra for undoped g.d. material.

These peaks have been attributed to an optical transition to the conduction band from occupied localized states in the lower half of the band gap [43, 118]. In view of their occurrence in undoped material, they have been associated with an (unspecified) natural defect which may be stabilized or catalyzed by an impurity. It is supposed (see sections 2.5 and 2.4) that p_H in excess of about 1 mTorr in our sputtering plasma leads to increased defect production because of the increase in volume of connective tissue between islands. However, the widespread occurrence of this absorption at close to the same energy in many films suggests that there is a rapid rise in the gap DOS of all films about 1 eV below the conduction band edge. It may be significant that this is just what is inferred from such measurements as field effect (see below). The magnitude of $\alpha(1.2)$ in the sputtered films is typically 10^{-1}–10 cm^{-1}; if we assume that

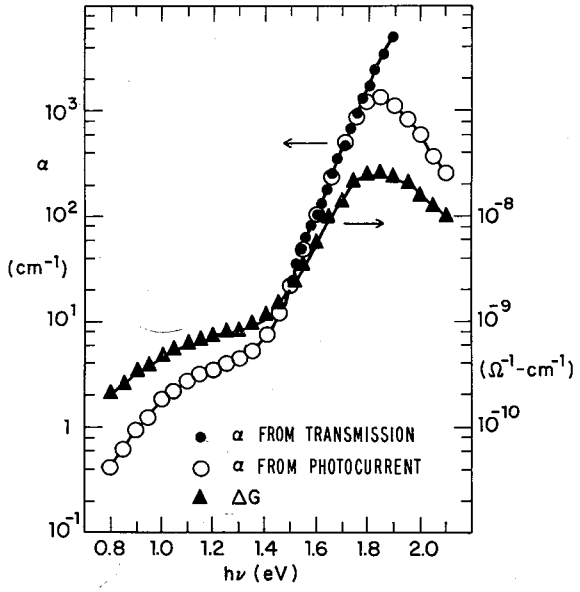

Fig. 9. Extension of absorption spectrum of a typical 10 μm sputtered sample from overlap of $\alpha(h\nu)$ from transmission (●●●) with relative α/α_0 using photoconductivity spectra and fitting to absolute $\alpha(h\nu)$ curve at 1.6 eV (○○○). The triangles (▲▲▲) show the uncorrected photoconductive response [118].

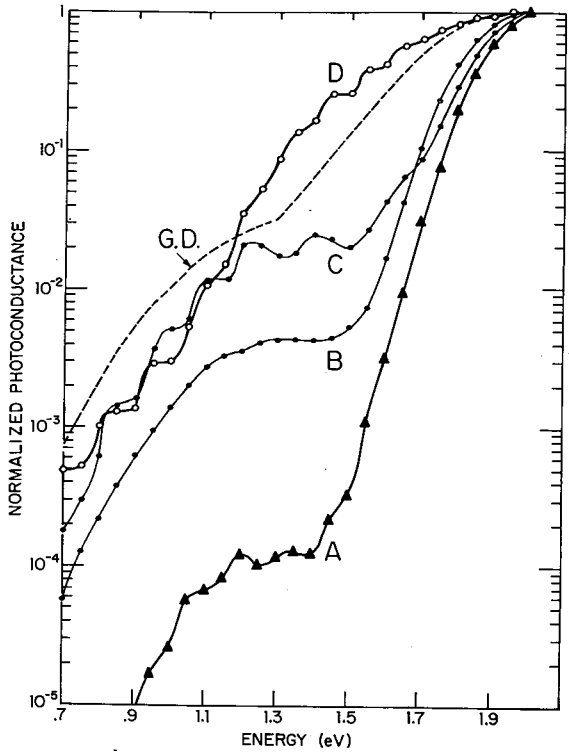

Fig. 10. Spectral dependence of photoconductance [120] for (A) an undoped sample sputtered at low p_H, (B) a lightly P-doped sputtered sample, (C) a more heavily P-doped sputtered sample, and (D) an undoped sample sputtered at high p_H. The curve marked GD is for a glow discharge sample produced and measured at Dundee [200]. The data were normalized at 2.0 eV.

$\alpha = 10^4$ cm^{-1} corresponds to band-to-band transitions, that the state density at the band edge is about 10^{21} cm^{-3}eV^{-1}, and that the optical matrix element is about the same for localized–band as for band–band transitions, then the 1.2 eV peak may be deduced to correspond to a gap DOS of about 10^{17} cm^{-3}eV^{-1}. This is in reasonable agreement with other estimates.

Fig. 11 shows the (schematic) suggested DOS distribution which is supported by the results of a comparison of the photoconductivity with data on photoemission [121]. The magnitude of the 1.2 eV absorption may be correlated with other parameters from measurements on co-deposited samples at different p_H. Thus, as p_H is increased to about 5 mTorr and the peak grows, the room temperature conductivity increases and becomes unactivated, the photoconductivity is greatly increased, and a new, narrow peak appears in the photoluminescence [43, 101]. The magnitude of $\alpha(1.2)$ correlates with the DOS estimated from $C(f)$ measurements, and shows at least qualitative correlation with a decrease in $\mu\tau$ for holes (increased recombination rate) and an increase in $\mu\tau$ for electrons (increased hole trapping leading to increased electron lifetime). Good device performance seems to correlate with a low $\alpha(1.2)$ [122]. We

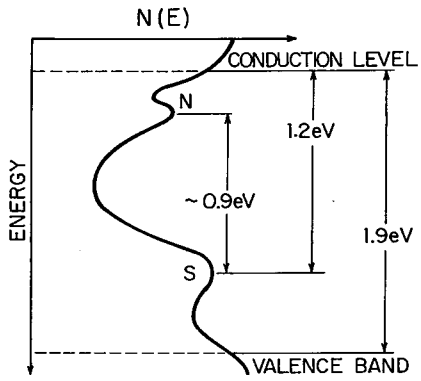

Fig. 11. Schematic model for DOS deduced from data on samples sputtered at high p_H or P-doped at low p_H [120].

conclude that, while this measurement does not give a quantitative estimation, it nevertheless provides very useful semi-quantitative information on the DOS.

More recently, several other types of measurement of low α absorption have emerged: guided wave spectroscopy [123], photoacoustic spectroscopy [124] and photothermal deflection spectroscopy [125]. While it is too early to assess the impact of these techniques, it can be hoped that they may eventually remove any residual uncertainties from the conclusions of photoconductivity studies by checking on various assumptions, such as the independence of the $\mu\tau$ product on photon energy.

3.4. *Photoemission spectra*

We discussed the applicability of the photoemission technique to a-Si:H in section 2.3.3.3. Here we simply draw attention to the fact that von Roedern and Moddel have expanded on earlier work by von Roedern and his co-workers to show that P-doping of a-Si:H leads to a measured increase in the DOS in the lower half of the band gap. This supports, at least qualitatively, the interpretation of the photoconductivity data of section 3.3 which led to fig. 11.

3.5. *Field effect*

3.5.1. *General remarks*

In field effect experiments [126–131], a layer of 0.5–1 μm of a-Si:H is deposited on an insulating substrate of high dielectric strength and very low conductivity. The insulating substrate may be fused silica (we use 175 μm thick SiO_2) or an insulating layer of SiO_2 or Si_3N_4 on a conducting substrate. Source and drain contacts separated by millimeters are deposited on the other surface of the a-Si:H. A voltage applied to the insulator induces charge in the a-Si:H, alters the potential distribution near the insulator–semiconductor interface and changes the carrier density in the a-Si:H. The magnitude of the carrier density change depends on the induced charge and the

density of states near the Fermi level in the a-Si:H. A small potential difference between source and drain contacts is used to measure the conductance of the a-Si:H, which is dominated by the field-induced carrier density change. It is (at least, conceptually) straightforward to work back from the induced current to find the density-of-states at the Fermi level.

Since the field effect was first applied to a-Si:H [126] there have been several analyses of the methods and approximations involved in inverting the induced current characteristic to obtain the DOS [127–130]. Goodman and Fritzsche demonstrated that, in practice, the same field effect response could result from several different DOS, thus placing limits on the magnitude of small features in the DOS that could be appreciated. In particular, they argued that a small peak in the DOS about 0.4 eV below the conduction band edge, deduced by Madan et al., might be an artifact of the analysis. (On the other hand, such small features might well exist and yield no signature in the measured characteristic.)

By carrying out calculations on the DOS determined by the Dundee group [132], Goodman and Fritzsche [127] have shown that the field effect current flows in a narrow channel at the insulator–semiconductor interface about 100 Å wide, and it is therefore much influenced by any interfacial state density. If, as might be the case, the material that close to the surface is different from that in the bulk, then the bulk DOS will not be estimated, whether or not the data reduction is appropriate. It should also be recognized that the deduced DOS includes any surface state density. Thus, surface and interfacial state densities imply that the technique gives at best an upper limit on the bulk $N(E)$.

It should be mentioned that Powell, and Weisfield and Anderson, have devised improved procedures for the data analysis which reduce the labor of computation. These have, however, no effect on the difficulties of experiment or interpretation discussed here.

The field effect technique was used by the Dundee group to obtain the DOS throughout the forbidden gap. In order to extend the deduction over as wide an energy range as possible, n- and p-type doped material was also used [126], it being apparently assumed that the effect of doping was simply to provide carriers that shifted the Fermi level. In view of the low doping efficiency for P, As and B, and the likelihood that non-doping configurations still provide gap states (this is easily argued for 3-fold coordinated B, for example), this seems to be a risky procedure. The more recent evidence that such impurities probably lead to defect-related gap states simply emphasizes the earlier problem and throws doubt on the part of the Dundee DOS derived from doped samples. It should be added immediately that the part that is left spans a considerable range of energy near midgap. In this range of energy it seems reasonable to assume that field effect estimates the DOS in the region of the semiconductor it explores to an accuracy of about a factor of 3. The question which then remains is to what extent this density accurately describes the bulk DOS.

3.5.2. Field effect in sputtered a-Si:H

In g.d. a-Si:H, field effect responses of over four orders of magnitude have been

reported, corresponding to minimum state densities between 10^{16} and 10^{17} cm^{-3} eV^{-1}. However, it had been the experience until recently [133] of all groups studying sputtered a-Si:H that the field effect response was extremely weak and variable. Since the spin density of sputtered a-Si:H is at worst within a factor of 10 of g.d. a-Si:H, and the DOS from $C(f)$ measurement is comparable, this suggests that the sputtered samples are either more heavily defected or impurity-contaminated in the 100 Å near the substrate–semiconductor interface. Since SIMS profiles of both sputtered and g.d. a-Si:H show comparable impurity build-ups at the interface, it seems unlikely that this could be the sole cause of the poor field effect in the sputtered semiconductor. In view of our earlier discussion of microstructure and inhomogeneity, it seems more likely that the coalescence of growth islands in the first 100 Å might be less perfect than in the g.d. material, possibly because of the more violent plasma bombardment.

In a series of experiments to test this hypothesis, Weisfield et al. [134] prepared field effect structures by first depositing 150–200 Å of SiO_x on a fused silica substrate at 300°C by reactive sputtering of c-Si in a plasma containing 5 mTorr Ar and 0.2 mTorr O_2. After ten minutes of deposition, and without extinguishing the plasma, the O_2 flow was cut off, H_2 substituted, and a 1 μm film of a-Si:H deposited on the SiO_x. The SiO_x material has a resistivity $\geqslant 10^{13}$ Ω cm at 200°C, and so the field effect current flows in the a-Si:H overlayer. A typical field effect response at room temperature from this structure is shown in fig. 12. The improvement is spectacular and consistent through several depositions and modifications, which include substitution of SiN_x for the SiO_x. The other electronic properties of the a-Si:H differed little from those of samples with no SiO_x layer. The importance of the interfacial region is very clearly demonstrated here. Even without a full understanding of the precise mechanism of improvement, this technique may be used in devices where field effect responses are desired. In fact, we speculate that the full reasons for improvement may include both better reconstruction in the a-Si:H as it grows on a-Si:O, and the burial of contaminant atoms in the a-Si:O in a density too low to impair its necessary insulating quality.

The DOS extracted [129] from the data of fig. 12 is shown in fig. 13. The value of $N(E_f)$, 10^{17} $cm^{-3}eV^{-1}$, is in very satisfactory agreement with the bulk state density, 6×10^{16} $cm^{-3}eV^{-1}$, deduced from analysis of $C(f)$ measurements (see section 3.6) on co-deposited Schottky diodes. This represents, to our knowledge, perhaps the first direct comparison of the two techniques applied to closely similar samples. The DOS shows evidence of a small peak some 0.2 eV above E_f. This feature, deduced for several of the sputtered samples analyzed so far, bears a good resemblance to the feature reported by Madan et al. [126] for g.d. a-Si:H, about which there has arisen the controversy discussed earlier. It is to be noted, finally, that the minimum state density is as low as that reported for g.d. a-Si:H.

The successful observation of field effect in sputtered a-Si:H, while removing one anomalous difference between the results of two methods of preparation, nevertheless emphasizes the problems of the interface and suggests the possibility that the DOS measured even in g.d. a-Si:H may be affected. To our knowledge, there have been no comparative DOS estimates of co-depositions of that material by several techniques such as field effect, capacitance–frequency and DLTS. Nevertheless, the recent

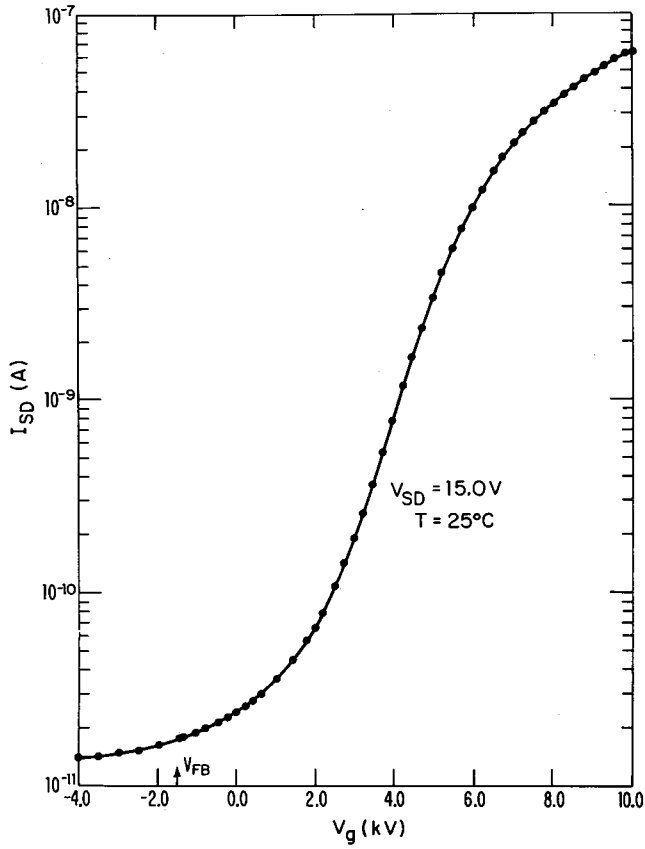

Fig. 12. The field-effect response, source–drain current I_{S-D} versus applied gate voltage (V_g), measured at room temperature for a 1.1 μm thick sputtered sample [134].

demonstration by Goodman and Fritzsche [135] that the field effect characteristic changed with annealing in a manner consistent with an increase in bulk state density caused by H effusion suggests that interface states do not obscure the sought-for bulk DOS.

*3.6. Capacitance–voltage and capacitance–frequency measurements**

Various forms of capacitance–voltage (C–V) and capacitance–frequency (C–f) measurements on a-Si:H Schottky barrier and MIS tunnel diodes have been used in order to discover the distribution of pseudogap state density in glow discharged and sputtered material. These techniques attempt this indirectly by determining the width of the space charge layer electrostatically induced in a diode either through

*Section 3.6 was written by R. L. Weisfield.

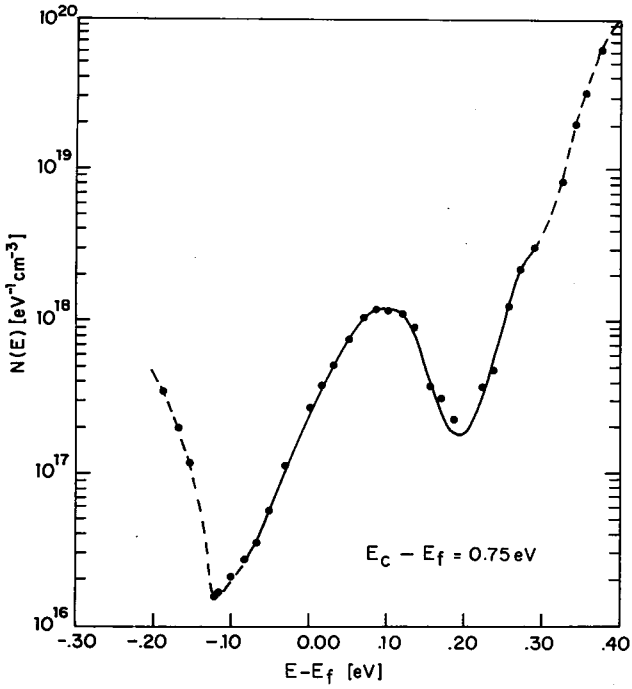

Fig. 13. The density of states derived [129] from the field effect data of fig. 12.

contact to a high work-function metal, in the case of a Schottky diode, or by externally applying bias, in the cases of both Schottky and MIS diodes.

Döhler and Hirose [136] were the first to derive an analytic expression relating the space-charge capacitance as a function of applied dc bias to the DOS distribution. This capacitance is measured by super-imposing a small ac bias whose frequency must be small compared with the thermal emission rate of majority carriers from the deepest gap states involved in the experiment. This is a rather serious constraint, since states at midgap equilibrate at room temperature on a time scale lower than 10^{-3} Hz. This was demonstrated by Beichler et al. [137] who measured the capacitance of a g.d. a-Si:H Schottky diode at 10^{-3} Hz by a quasistatic technique and showed that the capacitance failed to saturate (even at this low frequency). Hirose et al. [131] circumvent this problem by examining P and B doped g.d. material, which equilibrates at much higher frequencies. Using MIS devices, their C–V data give a rather featureless DOS distribution similar in shape but smaller in magnitude to that derived from field effect.

Capacitance measurements on undoped sputtered a-Si:H Pt and Au Schottky diodes were first undertaken by Viktorovitch and Jousse [138]. They proposed a technique combining capacitance–voltage (C–V) and conductance–voltage (G–V) measurements versus frequency for determining the DOS at the Fermi level. This was refined by Viktorovitch and Moddel [139], relying on a general ac equivalent-circuit of resistors and capacitors to model the frequency response of the diode. By consider-

ing the spatial variation of resistivity, response times, and charge density at different depths in the depletion region, assuming a uniform density of states between the bulk and surface Fermi energies, they can derive consistent values for the state density and depletion width from the capacitance and conductance measured at both low and high modulation frequencies, *under* 0 VDC *external bias*. They show that quantitative information about the DOS can be obtained without approaching the zero-frequency limit to measure the capacitance. They argue that unlike the case of c-Si the equilibrium kinetics controlling the filling and emptying of states in the gap are sufficiently fast that the dominant mechanism determining the ability of gap states to respond to ac modulation is the spatially-dependent diffusion of conduction electrons through the depletion region of the diode. Since the transport is argued to be diffusion-limited, the electron quasi-Fermi level will not be flat when the diode is biased, and consequently, the analysis of *CV* data on *Schottky* diodes may not be valid. This point is still open to debate, and so, for example, Tiedje et al. [140] have developed a method of analyzing a-Si:H Schottky diodes which does use dc bias. They have measured sputtered a-Si:H with a midgap DOS as low as 5×10^{14} eV^{-1} cm^{-3}.

Subsequent work by Viktorovitch [141] shows that measuring the conductance and capacitance of both Schottky barrier and MIS tunnel diodes, as a function of frequency and temperature, provides information on the density and kinetics of bulk and surface states in sputtered a-Si:H. He finds that a-Si:H sputtered under various conditions showed DOS ranging from $> 10^{18}$ eV^{-1} cm^{-3} to 10^{15} eV^{-1} cm^{-3}. He demonstrates that surface states are largely screened by the metal in an a-Si:H Schottky diode, but the interposition of an 80 Å, thermally grown oxide on the a-Si:H causes a large density of surface states ($N_{ss} \approx 10^{13}$ eV^{-1} cm^{-2}) to be observable, on previously unoxidized samples whose bulk DOS varies from $< 3 \times 10^{15}$ to $> 10^{16}$ eV^{-1} cm^{-3}. Such surface states problems are avoided when Weisfield et al. [134] sputter a $\approx$150 Å layer of SiO_x on a nichrome coated glass substrate before depositing a-Si:H to produce inverted MIS diodes. The density of interface states is $\leqslant 10^{11}$ eV^{-1} cm^{-2}, so that field effect and the more conventional capacitance–voltage measurements can be compared with $C(f, T)$ and $G(f, T)$ data obtained on codeposited devices. The results confirm the viability of the 0-bias capacitance/conductance technique for analyzing the DOS in a-Si:H.

3.7. Deep level transient spectroscopy, electron tunneling spectroscopy

These two methods are included here for completeness only, since their application to a-Si:H is very recent, and it is too early to assess their usefulness. There have been no reports of measurements on sputtered material.

The DLTS method [142] is claimed to bypass many of the difficulties of the field effect and $C(V)$ methods, primarily in not measuring the surface state density. Indeed, what measurements there are have suggested state densities that are lower – and state density distributions which are different – from those earlier methods. This may be significant, especially in view of the fact that the method usually requires doped samples which are very likely to give *increased* state densities at certain energies in the energy gap.

Tunneling spectroscopy [143] has recently been applied to a-Si:H, having been

tried earlier on unhydrogenated material with puzzling results. The principal conclusion of the new measurements is the identification of a prominent peak in the density of states about 0.45 eV below the conduction band edge, which is identified with a similar peak found in measurement of field effect. However, as for that effect, the measured state density includes both surface and bulk contributions.

3.8. Summary

There are no finally established superior methods of determining the one-electron state densities in amorphous semiconductors. The ESR technique yields, of course, reliable densities per unit volume of only the singly-occupied states in the pseudogap. The LESR is a useful method to explore unoccupied or doubly occupied gap states, especially if studied in conjunction with other more classical techniques such as photoconductivity, but it has not yet been fully exploited. It has the drawback of requiring a considerable mass of sample for measurement. Analysis of low photon energy optical absorption, by ever more ingenious techniques, serves as a useful check on the joint DOS involving the gap states, but cannot, without plausible modelling, be reduced to give a one electron DOS.

The field effect technique itself is well established, and analysis of it has become more elegant and routine. However, it continues to suffer from its ancient malaise: the state density estimated includes surface and interfacial state densities as well as bulk. No doubt the state density variation found for changes in deposition parameters or annealing procedures can be interpreted usefully and even semiquantitatively; however, the application of the detailed $N(E)$ variation to calculate transport properties, especially when these are done on samples other than those actually measured in field effect, seems to be a risky procedure. The recent advances in measuring field effect in sputtered a-Si:H have, if anything, emphasized the potential complications of a contribution of surface/interfacial state densities in *all* a-Si:H, howsoever prepared.

The capacitance methods avoid the surface state problem to some extent, but there still remain questions of physical assumptions which must be resolved before they can be found fully acceptable. Comparison of the results of field effect and capacitance methods, presently being carried out, has not yet reached the stage of decisiveness, and more experimental and theoretical work is needed. Finally, the time has not yet come to adopt the DLTS method over its competitors, despite its apparent advantages in circumventing their troublesome assumptions regarding surface states and sample homogeneity. We repeat our insistence on the need for cautious evaluation of the basic assumptions of the different methods and comparison of their results for the DOS.

4. Electrical transport

4.1. Introduction

In this section we shall deal with only a small, but we believe, central part of the problem of electrical transport. Many measurements on thin films of high resistivity,

related to a low density of states in a band gap of the order of 2 eV, are affected by surface transport which obscures the true bulk properties. Manifestations of this appear in hysteresis effects on heating and cooling, failure of transport to scale properly with sample thickness, and sensitivity to surface adsorbates. There are in addition hysteresis effects more likely to be related to a bulk property. Fritzsche [8] has recently given a comprehensive critique of these aspects of amorphous semiconductor transport. Similar effects are observed in sputtered a-Si:H only when it is prepared under conditions of hydrogenation that lead to low gap DOS. In this limited discussion we shall disregard results on samples that show these "anomalous" effects and shall focus on some other basic problems that appear to be related to the bulk transport. Our thesis will be that an explanation of these problems should be sought in the presence of heterogeneity in the structure and chemistry of the film, but we shall reference, without much discussion, alternative current hypothesized explanations for the sake of completeness.

4.2. Microstructure and anomalies in transport properties

In a recent article Anderson and Paul [102] reported measurements of conductivity and thermopower for sputtered a-Si:H and used the changes in the transport with the preparation variables (T_s and p_H) to develop the microstructural model described in section 2.5. The films are taken to consist of islands of a mostly tetrahedrally coordinated a-Si with hydrogen compensating dangling bonds (phase 1), surrounded and interconnected by a highly defected, hydrogen-rich, spatially non-uniform tissue (phase 2). The growth of the tissue appears to be favored at low T_s and high p_H and, under these conditions, can actually support a separate transport path which bypasses the islands altogether. This we believe to be the origin of the abrupt change seen in conductivity and thermopower at high values of p_H. At the other extreme we can envisage a film made entirely of the island material. Such a film is most likely to be made under conditions of high T_s and low p_H. Most of the transport data in the literature have been obtained on samples prepared somewhere between these two extremes. Although some of the tissue material is undoubtedly present there is not yet enough to either limit the passage of current from island to island or to support a shunting parallel current path. Such samples show an activated conductivity and thermoelectric power with the following characteristics [103]: (a) the conductivity prefactor, σ_0, in $\sigma = \sigma_0 \exp[-E_\sigma/kT]$ is consistently between 10^3 and $10^4\ \Omega^{-1}\ \mathrm{cm}^{-1}$; (b) there is a difference between the activation energies for σ and S, $E_\sigma - E_S \approx 0.15$ eV; (c) the intercept of the thermopower $S = -E_S/|e|T + S_0$ with the $1/T = 0$ axis is higher than simple theory predicts, $S_0 \approx -0.5$ mV/K; and (d) many, but not all, of these samples show a decrease in the slope of $\ln \sigma$ and S versus $1/T$ at a temperature greater than about 440 K.

These observations are not unique to material prepared by rf sputtering. Spear et al. [104] have reported similar kinks in undoped a-Si:H films made by glow discharge and discussed their origin in terms of a mobility edge shifting rapidly with temperature. Beyer and other workers at Marburg [144] suggest movements of the Fermi level with temperature to explain similar observations. The experimental difference

between E_S and E_σ, which has also been observed in glow discharge material, cannot be consistent with extended state transport and has given birth to a number of alternative transport models including small polaron formation [98], localised state hopping in the band tail [145] and conduction distributed over a range of energy levels at the band edge [146]. None of these models, however, can adequately account for all four observations (a)–(d) simultaneously.

Recently, Anderson and Paul [103] demonstrated that in sputtered material prepared under conditions of high T_s and a p_H barely adequate to remove the hopping contribution from the conductivity, the behavior of σ and S versus temperature was much more straightforward. The difference between E_σ and E_s was very much reduced and in some cases dropped to zero within the experimental uncertainty of 0.04 eV, the value of S_0 was very close to zero, and there was no evidence of kinks up to 350°C, the highest temperature of measurement. Figs. 14 and 15 present a comparison between two films which is particularly revealing. The curves labelled type α are representative of a typical lower T_s, moderate p_H film while type β samples are prepared at high T_s and low p_H as described above. The values in the inserts clearly prove some of the points made earlier. But we also see that, below the kink, $(10^3/T \geqslant 2.3)$, the conductivity of the type α film is virtually identical to that of the type β films. The thermo-

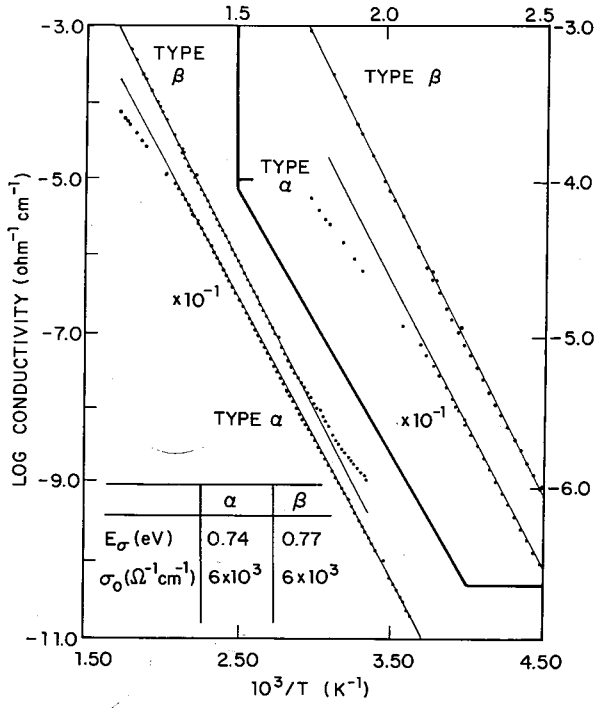

Fig. 14. Temperature dependence of the conductivity for a sputtered sample with high c_H (type α) and with small c_H (type β) [103]. In the expanded high T region of the inset, the data for type α show a clear kink not present for those of type β.

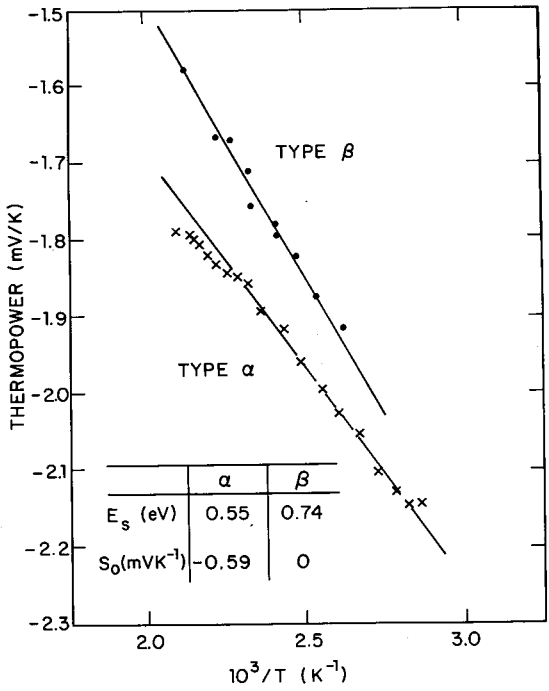

Fig. 15. Temperature dependence of the thermopower for type α and type β samples of fig. 14 [103]. The high T kink is much less well defined here. Comparison of the tables show that $E_s \approx E_\sigma$ for type β, but that there is the (frequently-observed) difference of about 0.2 eV for type α.

power of the type α film is everywhere too high with a slope which is too shallow, extrapolating to an intercept which is anomalously large.

In view of what has been said earlier regarding the existence of microstructure in sputtered films we find these results very suggestive of a link between points (b), (c) and (d) above and the presence of heterogeneity in the film. We would have no hesitation in concluding that the transport in type β films takes place through extended states in the conduction band and that these films are sufficiently homogeneous to observe extended state transport unambiguously.

What then could be the explanation of the anomalies? The model we have proposed assumes that the tissue is continuous through the film yet apparently incapable of supporting a parallel path until present in higher volume. The structural model and the data can be reconciled by assuming, not unreasonably, that the tissue is itself spatially non-uniform and that structural connectivity does not imply electrical connectivity. We therefore have the possibility, over a limited p_H range, of islands of phase 1 cut off from one another by phase 2 with the preferred conduction path passing through both phases in series. In a series combination of resistors, the highest resistor will dominate. If, as a function of temperature, the resistances of the two phases cross, a downward kink will be seen in the conductivity. Anderson and Paul [103] propose this as the explanation of the kink seen experimentally and attach

significance to the fact that the kink is consistently observed in sputtered films prepared in a p_H at the highest end of the range when the transport is activated.

No adequate description exists of the transport in the phase 2 tissue material. However, we may assume that the form of $\sigma(T)$ and $S(T)$ in high p_H sputtered samples, in which phase 2 is believed to dominate the transport, serves as a best approximation. We recall [102] that the conductivity in high p_H samples is high and weakly temperature dependent while the thermopower is large, negative and almost temperature independent. If our suggested explanation for the kinks is correct we expect the conductivity below the kink to be dominated by the island material and that above by the tissue. Fig. 14 clearly shows that below the kink the conductivity is identical to that of the type β, island only, film. Above the kink the temperature range is more limited but the similarity to the high p_H samples is apparent. Fig. 16 compares $\sigma(T)$ for a number of samples which show a similar temperature dependence in the tempera-

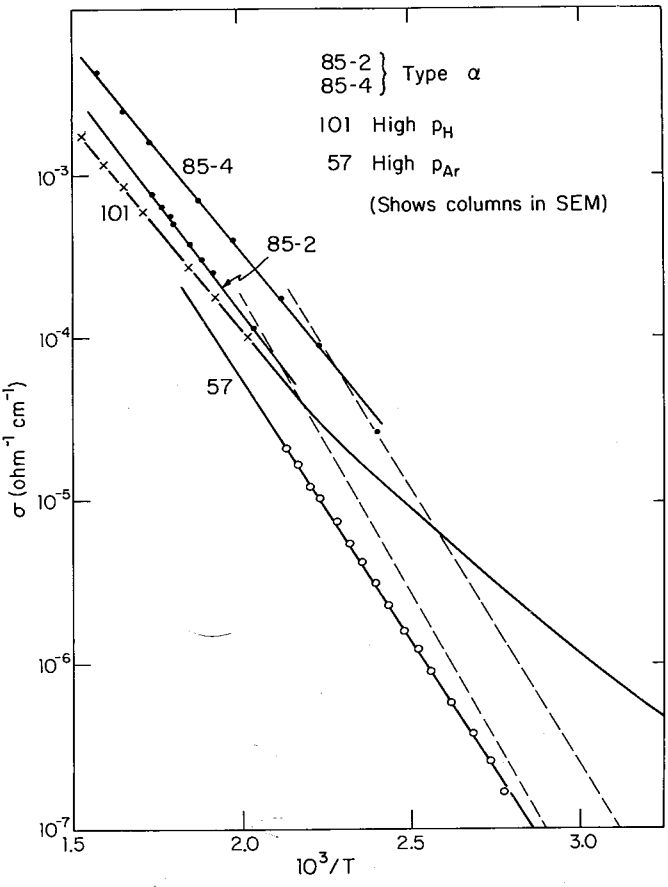

Fig. 16. Comparison of the high temperature conductivity (above the conductivity kink) for two samples, 85–2 and 85–4, which show a kink, and two other samples which show only an "anomalous" transport. Sample 101 was made at high p_H, while sample 57 was made at high p_{Ar}. See text for details.

ture range above the kink. Sample 101 was made at high p_H, sample 57 at high p_{Ar} and samples 85-2 and 85-4 show the kink in σ near $10^3/T=2.2$. Sample 57 showed columnar microstructure in SEM studies.

The analysis of the behavior of the thermoelectric power for the quasi-one-dimensional series circuit we have described is much more complex. However, it is likely that the net thermopower will be some average of the thermopower of the two components. Since S in phase 2 appears to be larger and weakly temperature dependent this averaging will lead to a value which is everywhere larger than that of the island material. The slope will also tend to be shallower and lead naturally to an anomalously larger intercept just as is observed experimentally. Although this simple picture does not necessarily predict a kink in S, it should be pointed out that the thermopower kink is less well defined than that seen in the conductivity and the errors in measurement are sufficient to render a kink indistinguishable from a slow convex curvature with increasing temperature.

4.3. Conductivity prefactor σ_0

Anderson and Paul found values of σ_0 for their sputtered samples consistently between 10^3 and $10^4\ \Omega^{-1}\text{cm}^{-1}$ over the entire range of parameters used; from $T_s=25$ to 400°C, from $p_{Ar}=4$ to 50 mTorr and from $C_H=0$ to 30 at% H. At the same time the activation energy varied between 0.65 and 0.95 eV. Values of E_σ and σ_0 for glow discharge a-Si:H cover a broadly similar range and several authors have drawn attention to an apparent correlation between the two parameters, roughly following $\sigma_0=\sigma_{00}\exp(E_\sigma/E_0)$ [8, 104, 147], with σ_0 ranging from 10 to $10^6\ \Omega^{-1}\text{cm}^{-1}$.

The results of the Dundee group [148] are typical and can be divided into three regions. Values of $E_\sigma \leqslant 0.6$ eV are obtained by phosphorous doping. For these samples σ_0 ranges up to $10^2\ \Omega^{-1}\text{cm}^{-1}$. In some undoped samples having a large E_σ, an extremely large σ_0 is observed, but the majority of the samples have values of σ_0 in the same range as found by Anderson and Paul. It should be remembered that unlike the sputtered material, for which preparation conditions were deliberately varied, the results on undoped glow discharge material represent films prepared under nearly uniform conditions. The statistical distribution is therefore significant.

If all the data on doped and undoped material were plotted as σ_0 versus E_σ then almost identical adherence to the above rule would be observed. However, there is additional evidence from the sputtered material which casts some doubt on the deduced correlation between σ_0 and E_σ.

From a study of conductivity and thermopower of phosphorous doped sputtered a-Si:H, Anderson and Paul [149] have argued that the transport near room temperature in doped films, although activated, does not take place in conduction band extended states. It is not valid therefore to compare the values of σ_0 in doped and undoped material. In fact, they further argue that conduction band transport in these films is seen only at temperatures above 150°C when $\sigma_0 \approx 5\times10^3\ \Omega^{-1}\text{cm}^{-1}$. Thus the lower part of the σ_0–E_σ correlation should be ignored.

Only a handful of sputtered samples have values of σ_0 as high as $10^5\ \Omega^{-1}\text{cm}^{-1}$, most commonly high T_s, low gap state films. We have observed that films made under

these conditions are more likely to exhibit a sensitivity to adsorbed water vapor which is clearly evident in gap cell conductivity measurement. This is seen in fig. 17 in which a typical sample has been heated in a vacuum to 200°C and cooled again. Before heating, the conductivity is high and remains so until about 100–150°C at which point the water vapor is desorbed from the surface. Repeated temperature cycling in vacuum replicates the lower curve but exposure to the atmosphere at room temperature returns the sample to its original high conductivity. We note that had this effect not been suspected and the measurement made only to 100°C the deduced value of σ_0 would be high while the value of E_σ would be virtually unchanged. In this case the slightly high value of σ_0 would not have attracted attention, but fig. 18 shows data from a second sample in which the effect is much larger. This sample, when measured in the usual way to 200°C and back gave $\sigma_0 = 7 \times 10^4\ \Omega^{-1}\text{cm}^{-1}$ with $E_\sigma = 0.82$ eV. If heated to 350°C and cooled the value of σ_0 drops to only $3.9 \times 10^3\ \Omega^{-1}\text{cm}^{-1}$, a value much more consistent with the range quoted by Anderson and Paul. It is puzzling that, once again, the value of E_σ remains unchanged.

The effect of surface adsorbates on conductivity in glow discharge a-Si:H has been studied by Tanielian et al. [150] and is generally found to be stronger than on sputtered material. Other workers [151] have discussed a similar effect at the film–substrate

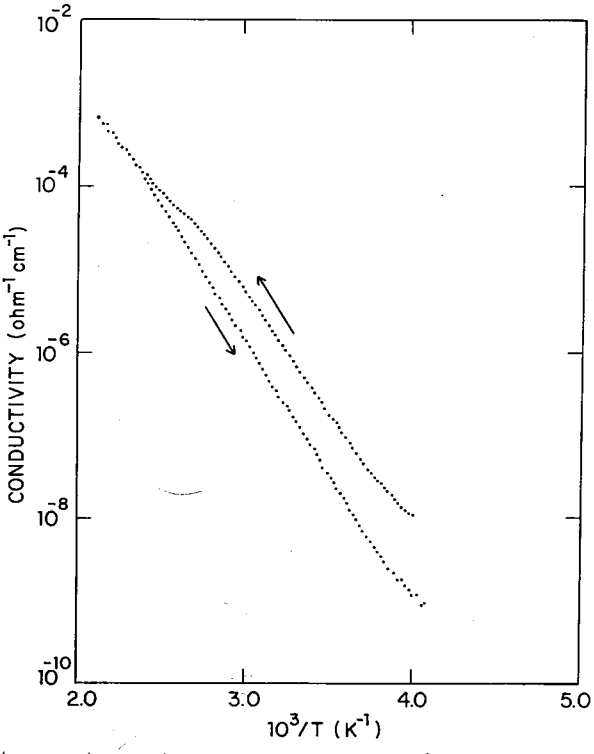

Fig. 17. Conductivity versus temperature measurement on a sample suspected of having surface-adsorbed water vapor. Cycling desorbs water vapor near 100–150°C. Exposure to atmosphere at room temperature leads to upper curve. See text for details.

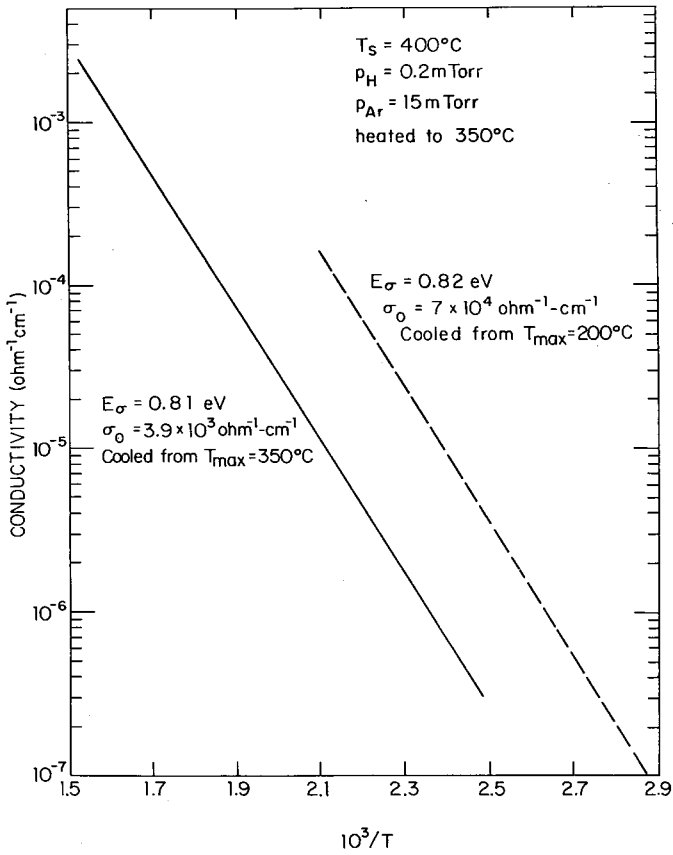

Fig. 18. Conductivity versus temperature measurement on a sample suspected of having surface-adsorbed water vapor. Curve (– – –), whose data points were taken continuously by computer, had been heated only to 200°C, whereas curve (———), whose data points were taken "by hand", had been heated to 350°C. See text for details.

interface where it has been exploited in field effect measurements to estimate the bulk state density. It seems not improbable that given the low bulk state density in the gap and the low surface or interface density, that similarly large anomalous values of σ_0 should be obtained as a result of adsorbed water vapor. If so, the data on sputtered material suggest that the conductivity should be measured after heating to temperatures around 350°C, provided this can be done without causing H-evolution (see fig. 2).

Having provided evidence that both extremes of the range of σ_0 values should be discarded we are left with a range of 10^3 to $10^4\ \Omega^{-1}\text{cm}^{-1}$ in which the vast majority of *all* undoped a-Si:H lie. There is no correlation between σ_0 and E_σ for extended state conduction band transport but there are effects due to surface water vapor which remain unexplained.

4.4. The nature of conduction band transport

The results of the Harvard study of sputtered material clarify the experimental evidence against which various theoretical ideas about the transport process in the band should be judged. It is now evident that conduction is through extended states at a fairly well-defined energy level and that there is no essential difference between sputtered and glow discharge material. Values of σ_0 lie consistently in the range 10^3 to $10^4\ \Omega^{-1}\text{cm}^{-1}$ as indeed they do for almost all amorphous semiconductors.

The prefactor can be written as

$$\sigma_0 = N_c kTe\mu_c \exp(+\gamma/k),$$

where $N_c kT$ is an effective density of conduction band states, μ_c the electron mobility and the exponential allows for any temperature shift of the band edge with respect to the Fermi level, $(E_c - E_f)_T = (E_c - E_f)_0 - \gamma T$. Fig. 19 shows the pairs of values of μ_c and γ which can give $\sigma_0 = 5 \times 10^3\ \Omega^{-1}\ \text{cm}^{-1}$ at 300 K assuming $N_c \approx 10^{21}\ \text{cm}^{-3}\ \text{eV}^{-1}$. For transport at a mobility edge the mobility is often quoted as being expected to lie in the range 1 to 10 $\text{cm}^2\ \text{V}^{-1}\text{s}^{-1}$ although the random phase model used to predict this value [152] is not regarded as a good description of the transport process. We see from fig. 19 that a mobility of 10 $\text{cm}^2/\text{V s}$ requires $\gamma \approx 4.5 \times 10^{-4}$ eV/K. This is slightly higher than the temperature shift of the energy gap for the material ($\approx 4 \times 10^{-4}$ eV/K) and must be regarded as relatively improbable. The possibility of the Fermi level being controlled by extrinsic states in the gap, giving rise to a high temperature coefficient, is also considered unlikely in view of the high values of σ_0 seen in many amorphous semiconductors, both n-type and p-type. We conclude that the mobility is probably larger than 10 $\text{cm}^2\ \text{V}^{-1}\text{s}^{-1}$ and possibly as large as 50 $\text{cm}^2\ \text{V}^{-1}\text{s}^{-1}$.

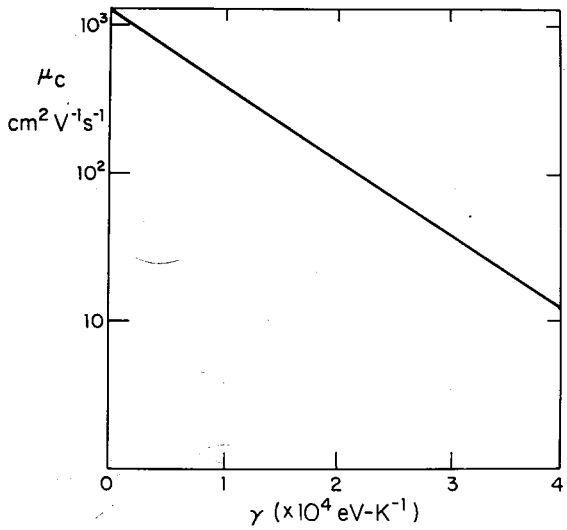

Fig. 19. Parametric relation between μ_c and γ in the formula $\sigma_0 = N_c kTe\mu_c \exp(\gamma/k)$, assuming that $\sigma_0 = 5 \times 10^3\ \Omega^{-1}\text{cm}^{-1}$ at 300 K and $N_c = 10^{21}\ \text{cm}^{-3}\text{eV}^{-1}$.

These data do not resolve the question of the existence of a sharp mobility edge in tetrahedral amorphous solids. The debate may indeed be somewhat academic since it is unlikely that a truly homogeneous thin film can ever be made. Even the most homogeneous glow discharge films show residual rod-like structures of a similar dimension to that of the islands [30] ($\approx$200 Å). The resultant long range potential fluctuations will probably smear out any mobility edge, but may also affect the interpretation of the transport in other ways. Pistoulet et al. [153] have analyzed the drift mobility data for a number of amorphous semiconductors in terms of a potential fluctuation model. They show that the activation energy of the drift mobility, usually interpreted as the extent of the tail of localised states below the mobility edge, can, in their model, be interpreted instead as a measure of the amplitude of the potential fluctuations. If so, the density of states for the "free" and "localised" carriers will be of the same order of magnitude and the band mobility deduced from the data will be considerably larger than the figure of 1–10 $cm^2V^{-1}s^{-1}$ obtained by Le Comber and Spear [154]*.

A band mobility as large as 50 $cm^2V^{-1}s^{-1}$ should be readily detected in Hall measurements but has never been observed in an amorphous semiconductor. In a-Si:H, all the Hall measurements, with the exception of the recent work of Dresner [155] have been performed on phosphorous doped material. All show the sign anomaly – a positive Hall coefficient for electron conduction – and a room temperature mobility of only 0.1 $cm^2\ V^{-1}\ s^{-1}$. From what has been said above, it is clear that more work is required to measure Hall effect, on samples known to be as homogeneous as possible, to establish the true magnitude and sign of the Hall voltage for carriers in the extended states in order to shed more light on the nature of the transport process.

5. Optical absorption [156]

5.1. Optical properties well above the absorption edge

The spectral dependence of the imaginary part of the dielectric constant $\varepsilon_2(h\nu)$ of unhydrogenated a-Si over a photon energy range up to 10 eV [157] has the same overall width and shape as that for c-Si [158], but shows none of the sharp features which can be correlated instructively with the structure of electron energy versus k-vector. See fig. 20. There is a single maximum near 3.5 eV, which indicates that the average (Penn) gap is about the same, in accordance with the measured near-equality (within 20%) of the refractive indices. Measurements of the UV transmission of thin films of undoped and doped g.d. a-Si:H [159], and of the reflectivity of g.d. a-Si:H [160], from which the $\varepsilon_2(h\nu)$ of fig. 20 was deduced, show that the spectra depend critically on preparation conditions such as T_s. The ε_2 peak of the g.d. a-Si:H occurs at a higher energy and reaches a much larger value than in either the evaporated a-Si [157] or

*Very recently, Overhof and Beyer [Phil. Mag. 43 (1981) 433] have discussed the effect of similar long-range fluctuations in the energy of the conduction band edge arising from charged centers distributed at random in the material. Using an assumed density of 5×10^{17} cm^{-3} charged centers, their model can account for the magnitude of $E_\sigma - E_s$ and also estimates σ_0 to be about $10^3\ \Omega^{-1}\ cm^{-1}$ for transport at an unperturbed mobility edge.

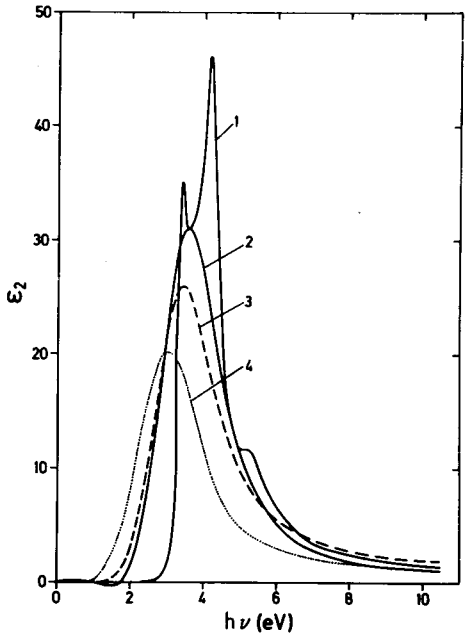

Fig. 20. Spectrum of the imaginary part of the dielectric constant, ε_2, for (1) crystalline Si (2) g.d. a-Si:H, $T_s = 400°C$, (3) CVD a-Si and (4) evaporated a-Si. After Weiser et al. [160].

CVD a-Si:H [161]. These results suggest that the bonding in the amorphous network has been considerably altered by hydrogen incorporation: the lower photon energy of ε_2(max) in evaporated and CVD material suggests a greater incidence of weak bonds, but it is not possible to come to a conclusion about altered transition matrix elements from the variable peak heights without more knowledge about the relative mass densities of the films being compared.

To our knowledge, similar measurements have not been made on sputtered a-Si:H, but with the control of H-content that is possible by this technique, it appears they might be instructive. The refractive index of sputtered a-Si:H has been found to decrease rapidly for the first additions of H and thereafter to decrease more slowly, reaching a value near 3.0 for 20 at% H [42]. Again, although these changes can be rationalized in terms of decreased atomic and electron density and increased average energy gap, a satisfactory quantitative analysis is not possible without more exact knowledge than is generally available of the precise H-content, the density deficit from the crystal, the altered band structure of the hydrogenated alloy and, in the case of sputtered material, the not insignificant percentage of incorporated argon.

In principle, photoemission measurements might also be expected to give information about the valence band density of states distribution in energy. Such measurements [78] on sputtered a-Si:H have already been discussed in section 2.3.3.3. Several narrow peaks develop in the photoemission spectrum, the details depending on T_s. These have been correlated with theoretical calculations of the energy in the valence band of various Si–H bonding configurations, and several possible fits found [78, 79]. Irrespective of the uniqueness of this correlation, there remains some doubt concern-

ing the use of data on the 10–20 Å surface layers of films to characterize the bulk (see section 2.3.3.3). If they could be so used, it might be instructive to correlate the magnitude of the peaks in photoemission with features in the infrared vibrational absorption spectrum, since the identification of some of these is still in question (see section 2.3.3.1). It has also been deduced that the density of states near the top of the valence band, $N_v(E)$, is eroded as C_H is increased [78]. This is consistent with the observed increase of the optical gap but the latter is in fact consistent with both a reduction in the slope of $N_v(E)$ or a displacement to lower energies of the valence band maximum energy. A related question is whether the density of states throughout the whole valence band is uniformly reduced in order to feed the Si–H attributed peaks, or whether there is indeed a preferential shift or erosion at the top of the band. The slope B of the curve of $(\alpha h\nu)^{1/2}$ versus $h\nu$ (see below), which describes the joint conduction band–valence band density of states, has been reported to *increase* with C_H [42]. This appears to be inconsistent with the photoemission result of a decrease of $N_v(E)$ with C_H, unless one speculates on the suggestion [48] that the Si–H antibonding states have energies near the bottom of the conduction band and so augment the joint density of states. There are clearly a number of unresolved questions in the interpretation of the high energy $\varepsilon_2(h\nu)$ and the related state densities.

5.2. The absorption edge

The optical absorption edge [156, 162] is usually described as having three regions: (1) at high energies, and α roughly $>10^4$ cm^{-1}, by $(\alpha h\nu)^{1/2} = B(h\nu - E_o)$. Here B contains an average matrix element, constant with energy, and the joint density of states for the conduction and valence bands. The formula is derived on the basis of a square root dependence of the density of states on energy in both bands. The crystal momentum selection rule is broken by the disorder and so the value of B is much greater than in the crystal. It is this fact that makes these materials viable candidates for thin film solar cells. (2) at intermediate energies, roughly 10^2 cm$^{-1} < \alpha < 10^4$ cm^{-1}, by an exponential variation of α with $h\nu$. This has been variously attributed to exponential tails of states to the valence and conduction bands [163], or to photon-assisted tunneling in the presence of potential fluctuations [164], or a combination of both. (3) at the lowest photon energies and absorption coefficients, by an absorption which is quite variable and is commonly related to defect and impurity states. There is no sharp delineation between these three overlapping regions/processes.

Fig. 21 illustrates a typical edge for g.d. [165] or sputtered [166] a-Si:H. The energy gap in an amorphous material is empirically defined either as the E_0 of region (1) or as E^{03} or E^{04}, the photon energies at which the absorption coefficient is 10^3 or 10^4 cm^{-1}. Roughly speaking, the "intrinsic" part of an edge occurs for $\alpha > 10^4$, and $\alpha \approx 10^4$ marks the demarcation between "intrinsic" edge and a defect/impurity dominated edge. The separation $E^{04} - E^{03}$ is a measure of edge sharpness.

5.2.1. Change of the edge parameter B

Comparison of the absorption edge spectra of unhydrogenated a-Si with those of sputtered samples where C_H is systematically increased [42] shows that the absorption

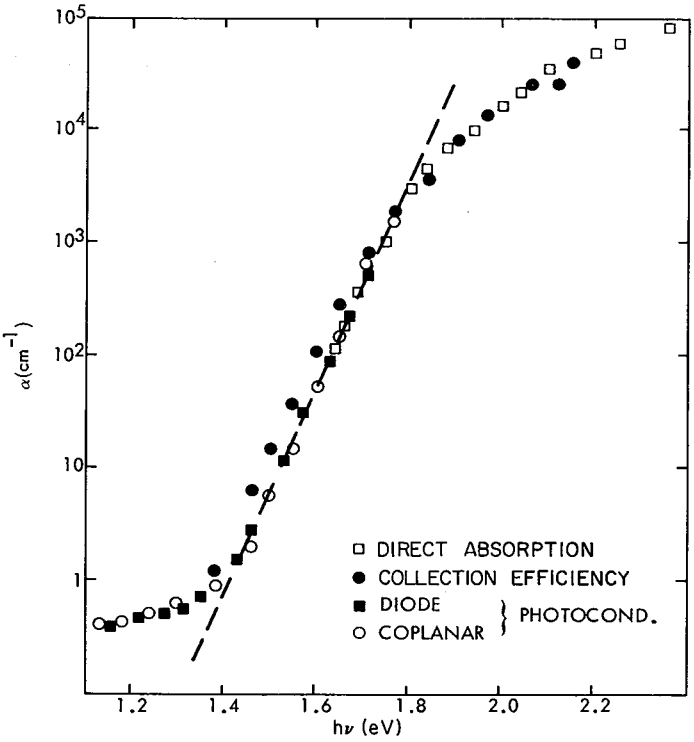

Fig. 21. Absorption edge spectrum of g.d. a-Si:H, determined from direct measurements of optical transmission, form collection efficiency and from photoconductivity. (After B. Abeles, C. R. Wronski, T. Tiedje and G. D. Cody, Solid State Commun. 36 (1980) 537.)

edge sharpens and shifts to higher photon energies. See fig. 22. Care must be exercised to attempt to discriminate between edge sharpening caused by an increase in B (region 1) and that stemming from a decrease in the densities of exponential band tail or gap defect states, or in the magnitude of photon-assisted tunneling (region 2). When the data of fig. 22 are replotted as $(\alpha h\nu)^{1/2}$ versus $h\nu$, they suggest a very mild increase in B of about 20% for 20 at% H. This agrees with an analysis for glow discharge samples that also suggests B increases with E_0 [168]. On the other hand, Freeman [42] finds that annealing a $T_s = 200°C$ sample to 700°C causes the absorption edge between 10^4 and 10^5 cm^{-1} to displace almost rigidly to lower energies. See fig. 23. This is consistent with the evolution of H (above 300°C) *without* an appreciable change in B, but it must be remembered that the effect on α versus $h\nu$ of any decrease in B as C_H is reduced might be offset by the effect of a reduction in photon-assisted tunneling or of the band tail state densities through high temperature thermal relaxation of the network. All things considered, the magnitude of the change of B with C_H – to be related as above to the change in $N_v(E)$ from photoemission – must be regarded as uncertain, although a small increase does seem to be favored.

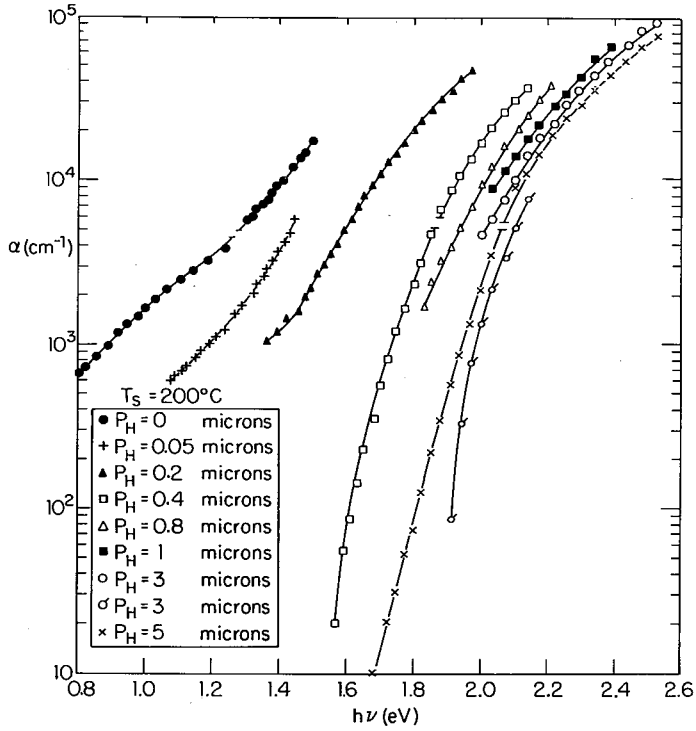

Fig. 22. Shift of the absorption edge of sputtered a-Si:H as p_H is increased from 0 to 5 mTorr at fixed T_s [42].

5.2.2. *Shift of absorption edge with T_s at fixed p_H*

The absorption edge spectra for samples prepared at different T_s and p_H can be analyzed to give changes in the energy gaps E_0, E^{03} and E^{04} and thus in the band and gap densities of states. For samples made at fixed p_H and increasing T_s, the absorption edge first displaces to higher photon energies and then reverses [42]. The first effect is probably related in part to increased relaxation of the network at higher T_s [105] and in part to more efficient defect compensation by the incorporated H, since C_H tends to decrease with increased T_s. The shift reversal stems from the fact that H is not easily incorporated at all at very high T_s. There is no significant residual mystery here.

5.2.3. *Shift of absorption edge with p_H at fixed T_s*

The changes in the absorption edge for sputtered samples prepared at fixed T_s and variable p_H are more complex. Fig. 24 shows, for example, the variation in E^{04} with p_H. The initial increase at very low values of p_H strikingly illustrates the effect of H in eliminating gap defect states and modifying the band tails and band edge states. Inspection of fig. 4 shows that by a p_H of 1 mTorr the C_H has asymptoted. The scatter in E^{04} at high $p_H(C_H)$ is not totally random; closer inspection of E^{04} and E^{03} as a function of C_H suggests [42] that samples of the same C_H have different gaps, and by

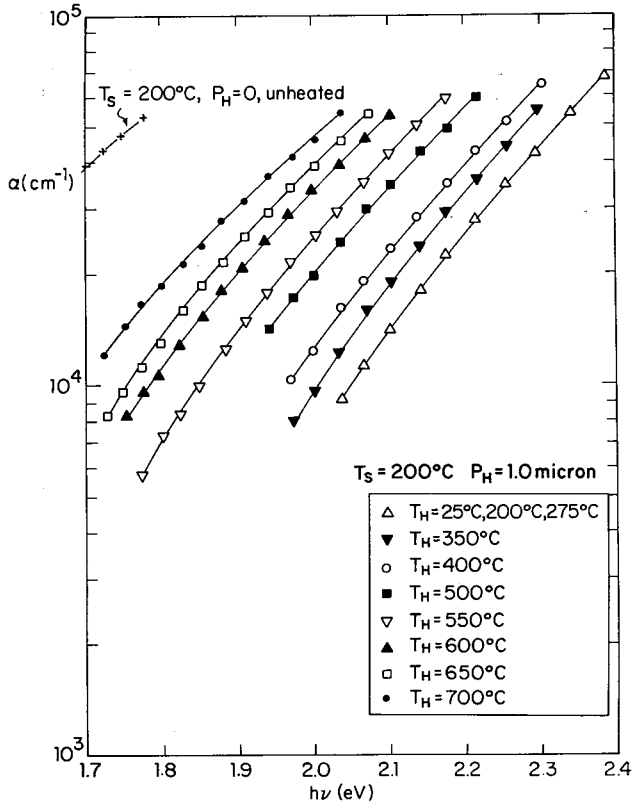

Fig. 23. Shift of the absorption edge of a film sputtered at 200°C with $p_H = 1$ mTorr, when it is successively heated to several temperatures of anneal and then remeasured at room temperature [42]. The shift is consistent with evolution of H above about 300°C. The difference in positions between the asymptoted edge after an anneal at 700°C and the edge for an unhydrogenated film prepared at the same initial T_s (200°C) is attributed to a network healing effect.

inference different gap and band edge DOS, depending on the precise sputtering conditions. It is quite probable that several combinations of the many sputtering parameters lead to the same H-content, but assembled in different Si–H bonding configurations which give different band gap densities of states. It is also likely that the different sputtering parameters lead to different microstructural heterogeneities which again yield different average properties. These ideas form a recurrent theme throughout this review.

5.2.4. Sub-band-gap absorption

For $h\nu \leqslant 1.5$ eV, and $\alpha \leqslant 10^2$ cm^{-1}, shoulders or peaks are found in the absorption [42, 169] and photoconductivity [118] spectra, which depend on the deposition parameters. For example, they are produced by high p_H [101] and during the incorporation of the n-type dopant P [43]. In these cases they are attributed to the creation of

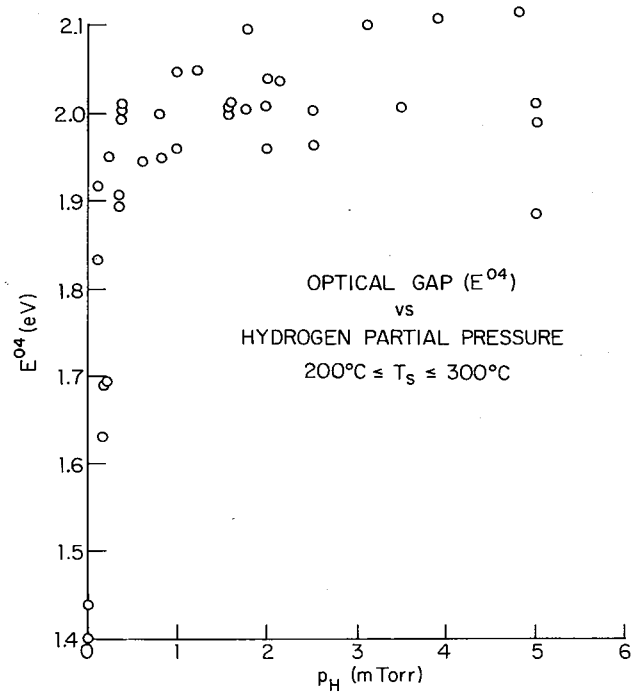

Fig. 24. The optical energy gap E^{04} as a function of p_H. Harvard group, unpublished results.

defect states with energies in the lower half of the band gap, although the precise defect configuration is not known. The magnitude of this absorption, whether related to the presence of defects or undesired contaminants, may lead to an increase in the photoconductivity but cause a deterioration in the performance of devices.

Absorption edge spectra are modified in Si:Ge:H [170] and Si:C:H [171] alloys. As is expected from the behavior of the corresponding crystals the effects of initial Ge and C additions to the Si are to decrease and increase the energy gaps, respectively. There have, however, been no really adequate quantitative analyses of these alloys, since care has not been taken to control or normalize for the H-content. The absorption edges are also modified by dopant-level additions of P and B [42, 169], as well as by alloying compositions. The shifts in the absorption edges are much larger than are expected from hydrogenic impurity energy levels (even when high effective masses are assumed), and are therefore attributed to a combination of new levels from three-fold coordinated P or B and, more tentatively, to dopant-induced defect configurations [42]. See fig. 25.

5.2.5. Shift of absorption edge with pressure and temperature

The shifts with pressure and temperature of the absorption edges have also been

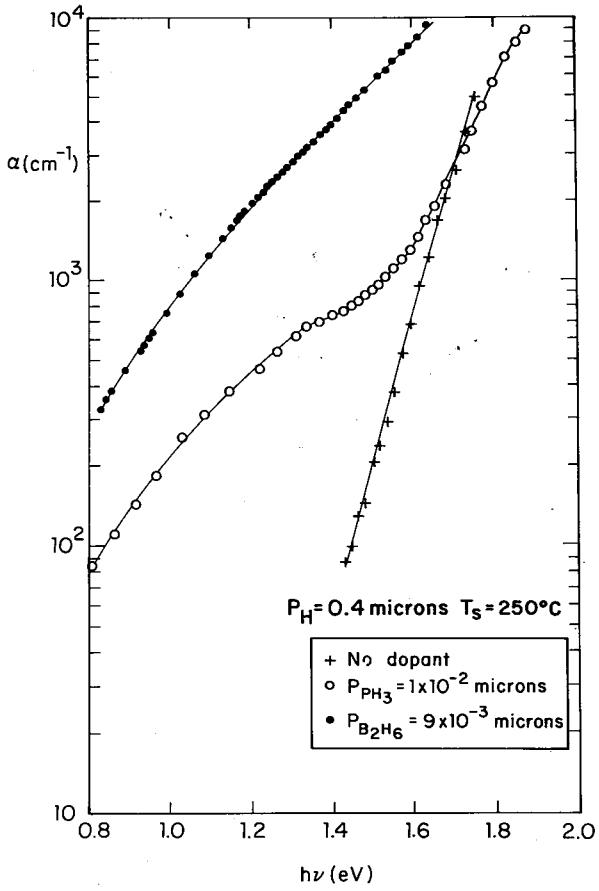

Fig. 25. Influence of P and B dopants on the absorption edge of sputtered a-Si:H [42].

measured. For $C_H=0$, Connell and Paul [172] found a coefficient for a-Si of $(+0.25 \pm 0.5) \times 10^{-6}$ eV bar^{-1} over a pressure range of 10 k bar while Welber and Brodsky [173] found $(-1.0 \pm 0.5) \times 10^{-6}$ eV bar^{-1} for both $C_H=0$ and C_H finite over a much larger range of 60 kbar. These coefficients are both close to the value for the crystal [174] of -1.5×10^{-6} eV bar^{-1}. This is no real surprise, since the states at the bottom of the c-Si conduction band are separated from the next highest extrema by about an eV; thus one might expect the deformation potentials for the valence and conduction band extrema to be about the same in crystal and amorph. The temperature coefficients of E^{03} between 0 and 300 K have been determined for both $C_H=0$ and C_H finite by Freeman [42]. Illustrative data are shown in fig. 26. The quadratic variations with T closely resemble those for the crystal, with about the same parameters. Insignificant differences from studies on glow-discharge produced material occur [168].

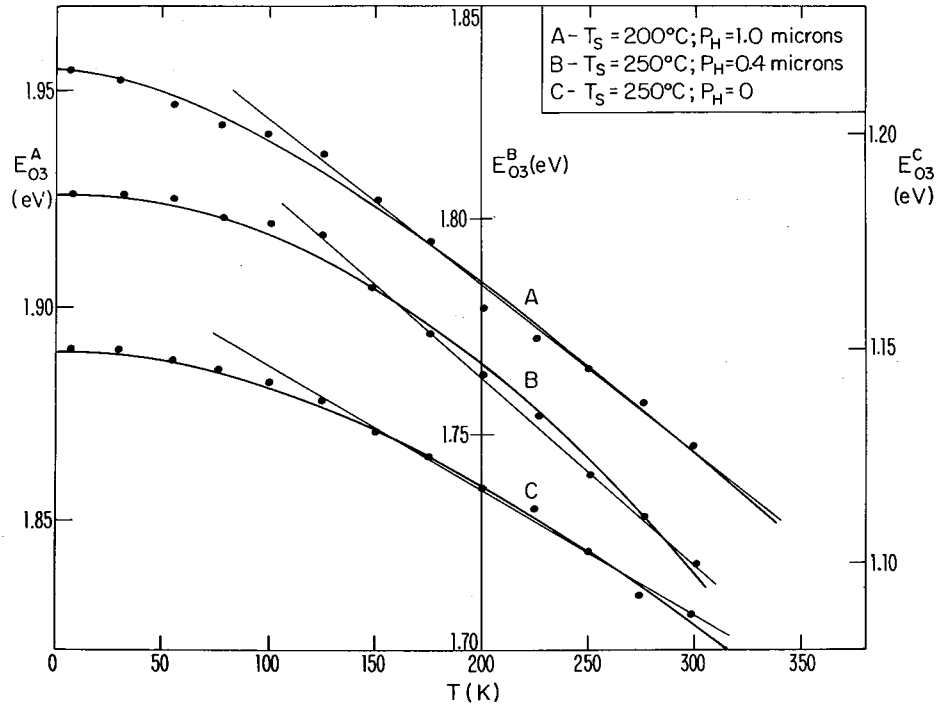

Fig. 26. Temperature dependence of the optical energy gap E^{03} for three samples [42]. With the energy in eV and the temperature in kelvin, the straight line sections are fitted by: $E_A = 1.98\text{–}3.9 \times 10^{-4} T$; $E_B = 1.85\text{–}4.4 \times 10^{-4} T$; $E_c = 1.17\text{–}2.9 \times 10^{-4} T$.

6. Photoluminescence*

6.1. Energy and shape of intrinsic PL spectrum

In this part we shall consider the peak energy and shape of the intrinsic spectrum, leaving to sections 6.2 and 6.3 consideration of its magnitude. Exciting photons of energy much larger than any of the conventional measures of the band gap produce electrons and holes in the conduction and valence bands which thermalize – probably in picoseconds – to the band edges (large gradient in $N(E)$) and then, much more slowly, relax through localized states. The position and width in energy of the PL spectrum should then depend upon (i) the distribution in energy of electrons and holes that recombine radiatively after relaxation through conduction and valence band tail states and through gap states, (ii) the magnitude of any polaronic effect, i.e., movement of the lattice ions in response to either the electron or hole charges, which alters the energy of the electron or hole and therefore also the PL transition energy and the peak width, and (iii) the Coulombic interaction of the electron and hole and the possi-

*This section was written with the expert collaboration of R. Collins.

bility of a distribution in the electron–hole separation, in the event that each is in a localized state which is charged when filled (by an electron or hole, respectively).

Fig. 27 shows some illustrative steady-state photoluminescence (PL) spectra [175], for both sputtered and glow discharge samples, all taken at an excitation photon energy $h\nu_{exc}$ of 2.33 eV, sufficiently low temperature (77 K) that the PL intensity I_{PL} versus T is nearly constant (see below) and sufficiently low excitation intensity I_{exc} that the PL quantum efficiency η is independent of I_{exc}. The differences in spectral position and width are real in the sense that the same optical detection system and deconvolution procedure are used throughout. The characteristics of the samples are given in table 1.

For our sputtered samples, the fwhm depends very little ($\approx 5\%$) on p_H between 0.2 and 5 mTorr, or on C_H between 5 at% and 25 at% (we do not detect PL for $p_H \lesssim 0.1$ mTorr, and do not make samples above $p_H = 5$ mTorr and $C_H = 25$ at%). It also depends very little on T_s between 200 and 400°C. At temperatures T_s below 200°C broadening of the peak tends to occur. The fwhm of our sputtered samples, (0.32 $\pm$0.01) eV, is slightly larger than that for the better glow discharge samples [(0.27 $\pm$0.01) eV]. These results for the fwhm of sputtered and glow discharge samples

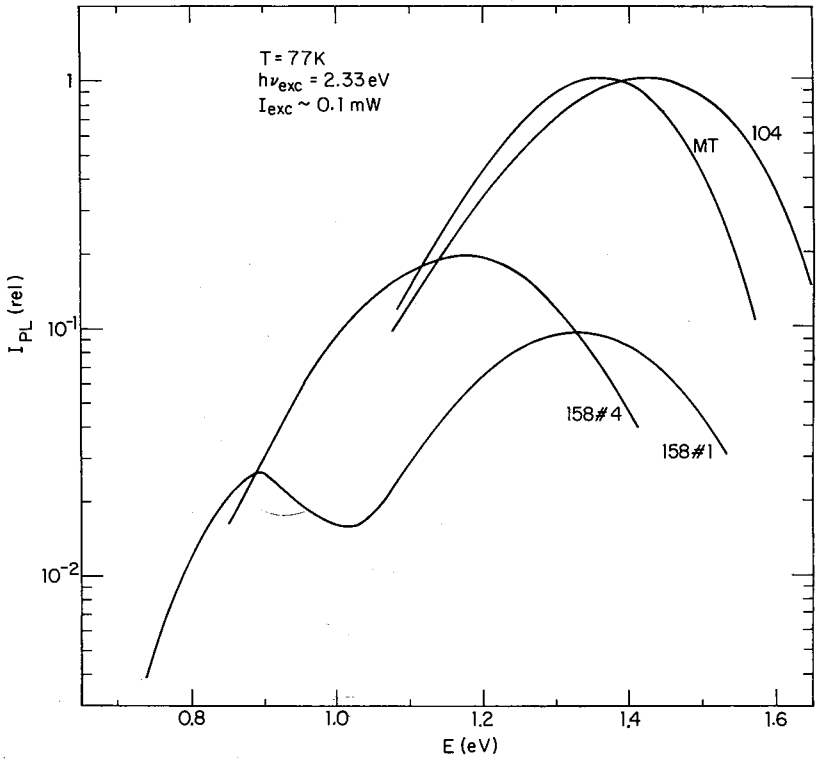

Fig. 27. Steady-state photoluminescence spectra [175] for sputtered and g.d. samples. No. 158–4 was sputtered at low p_H, no. 158–1 at high p_H, and no. 104 at moderate p_H. Sample MT was prepared at Mobil Tyco Laboratories by glow discharge. See table 1 for more details.

Table 1
Characteristics of samples whose photoluminescence is illustrated in fig. 27. Sputtered samples prepared with $p_{Ar} = 5$ mTorr, power = 200 W, deposition rate ≈1 Å/s

Sample	T_s (°C)	p_H (mTorr)	C_H (at%)	E^{03} (eV; 300 K)	E^{04} (eV;300 K)
158#4	400	0.4	8	1.65	1.84
104	200	1.6	25	1.82	≈2.03
158#1	400	5	14	—	—
MT		—	20	1.74	1.92

Sample	η [77]	fwhm (eV)	E_{PL}^{peak} (eV;77 K)	$N(E_f)$ ($cm^{-3}eV^{-1}$)	T_o (K)	Other
158#4	0.1	0.32	1.19	6×10^{17}	26	sp.
104	0.5	0.32	1.43	—	27	sp.
158#1	0.05	0.33	1.32	—		sp.
MT	0.5	0.26	1.35	1×10^{16}	16	g.d.

appear to be general in the literature [176]. Some of the variations are included in fig. 28.

No change of fwhm has been found in annealing of samples which removed some of the H. The fwhm increases slightly (20%) for measurement temperature T above 150 K. It is independent of both $h\nu_{exc}$ and I_{exc}. When 0.2 m Torr of oxygen is substituted for 0.2 m Torr of H in the sputtering plasma, the fwhm increases from 0.32 to 0.64 eV [177]. This is consistent with the results on glow-discharge-produced a-Si:O:H [95] but opposite to our earlier reported result for sputtered a-Si:O:H [93].

Taken overall, these results suggest that both the electrons and holes relax through tail states at the conduction and valence bands whose density and distribution depend very little on the detailed sputtering parameters and the PL quantum efficiency. The distribution is, however, measureably different from g.d. material and material containing O. Even for samples prepared at low p_H, which do not contain sufficient H that all dangling bonds are compensated, and so have low η, the fwhm is little different; this suggests that the more efficient nonradiative recombination channel is not connected with a wider distribution of tail states through which carriers relax and out of which they may ultimately recombine both nonradiatively and radiatively.

The actual contribution to the energy and fwhm of the observed steady-state PL by polaronic effects is not known. The earliest, and largest, estimate of a Stokes shift of 0.5 eV [178] has been frequently contested [179]; nevertheless there is a plausible argument for a more moderate effect if only by extrapolation from experience with deep levels in other materials. Similarly, the evidence for a significant contribution to the *steady-state* spectrum of an e^2/KR (K dielectric constant, R e–h separation) Coulombic term is not settled. We do expect the electrons and holes to charge their respective states, and there is good evidence of an observable contribution from this effect over short times in time-domain spectra to be discussed in section 6.5. It there-

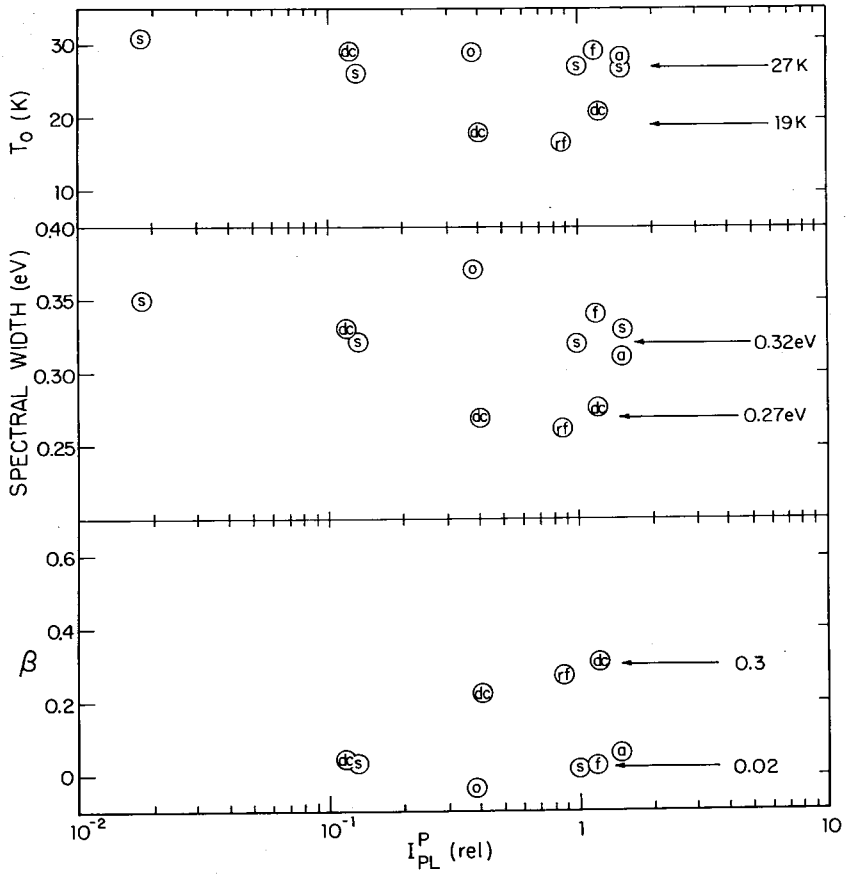

Fig. 28. Variation of T_0 (see text), a quantity β describing the degree of nongeminate radiative recombination, and of the fwhm, as a function of the luminescence efficiency of a group of sputtered and glow discharge produced samples: dc, cathode g.d.; a, anode g.d.; rf, Mobil Tyco g.d.; f, fluorinated g.d.; s, sputtered; o, sputtered in O_2 and H_2.

fore seems reasonable to inquire to what extent the steady-state spectra may be explained *solely* by the tail state density distribution in energy.

From table 1 it appears that $E^{04} - E_{PL}^{peak}$ is about 0.7 eV at 77 K for all of our sputtered samples, but this tells us only that the dominant broadening mechanism – whether band tail extent, polaronic or Coulomb effects – does not change with the preparation variables. The following rough argument may, however, be tried. In section 6.5 we shall find that PL excitation photon energies $\leqslant 2.1$ eV put excited carriers into weakly-localized, rather than extended, states in a sample at 77 K whose E_{PL}^{peak} is about 1.6 eV. We therefore assign 2.1 eV as the band edge separation at 77 K for this sample. We next assume a conduction band localized state tail of 0.2–0.25 eV, which is consistent with frequent estimates in the literature, and is also consistent with activation energies for PL quenching (see section 6.3) and electron mobility activation out of shallow traps. If we were therefore to assume that both electrons and holes

relax by about 0.25 eV before radiative recombination, then E_{PL}^{peak} might be expected to be roughly $(2.1-2\times0.25)$ eV $=1.6$ eV. Since this is, in fact, the observed peak energy, it seems there would be no need to invoke polaronic or Coulomb effects to explain the steady-state PL spectra. Nevertheless, the several assumptions we have had to make prevent any *definitive* estimate of the magnitude of the contribution of polaronic and Coulomb effects.

6.2. *Magnitude of intrinsic PL*

In this part we first consider how the intensity of the intrinsic PL measured under the conditions of fig. 27 depends on the preparation parameters of the samples and the measurement variables.

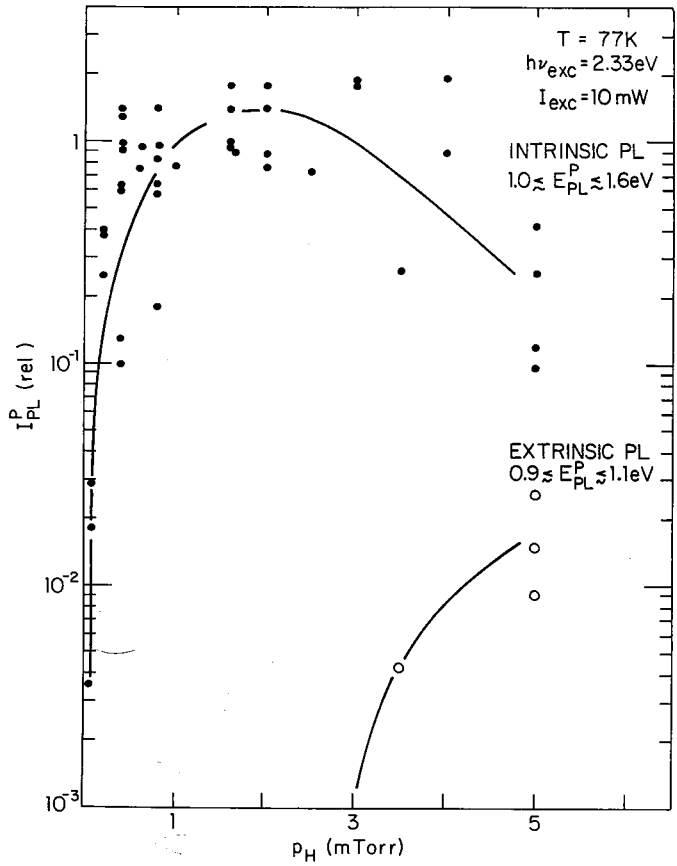

Fig. 29. Dependence of the low T, steady-state PL, measured under fixed conditions, on the partial pressure of H used in the preparation of the sample [175]. Both intrinsic (1.3 eV) and extrinsic (0.9 eV) PL are shown.

In gross terms, the magnitude of the intrinsic PL increases when the deposition parameters are varied in such a way that some measure of the gap state density indicates a decrease: from decreased ESR signal, decreased hopping conductivity or increased field effect response. This gross picture requires refinement, however.

The PL tends to increase with T_s as long as H is not being released (below $T_s \approx 350°C$) in accordance with one's intuition that the defect density and therefore density of nonradiative pathways is being reduced.

In our sputtered samples [175] the PL changes with p_H as depicted in fig. 29. The increase at low p_H clearly parallels the decrease in gap state density as H compensates defect states, but the decrease at high p_H, where C_H (fig. 4) is fairly constant, requires a different explanation. It seems very likely that, following section 2.3, the explanation is connected with the existence of microstructure. The figure suggests that the quantum efficiency η may be modelled by

$$\eta = F(N_o)(1-V)f(T),$$

where N_o is the average density ($eV^{-1}cm^{-3}$) of nonradiative recombination centers throughout most of the material, V is a volume which we suppose contains a very large density of defects which kill any radiative process at any temperature, and $f(T)$ is only weakly sample-dependent, as noted below. We find that the form proposed by Tsang and Street [180] $F(N_o) = \exp(-N_o a^3 \Delta E)$, where ΔE is the energy interval appropriate for the action of the nonradiative cneters and a is a measure of their spatial range, or their distance from either member of an electron–hole pair in order to catalyze recombination, does not work well quantitatively for the sputtered data. Our general identification of V is fitted by a volume of connective tissue between islands which is small, although finite, for $p_H \leqslant 1$ mTorr but increases beyond that so that η eventually decreases (see sections 2.5 and 4).

6.3. Temperature dependence of intrinsic PL

Figs. 30 and 31 display the variation with temperature of the peak intensity I_{PL}^{P} in the steady state $I_{PL}(h\nu)$, for high and low excitation intensities; since the fwhm of the spectrum is a weak function of T (see later), this also represents approximately the variation of the integrated PL intensity with T. At low intensities, the shape of figs. 30 and 31 is very little dependent on the maximum PL quantum efficiency for sputtered samples. The T-dependence for low η glow discharge samples is shallower than that shown in the figures.

The decrease in PL with T above 60 K (fig. 30) has often been plotted as log(PL) versus $1/T$, which leads to two activation energies ≈ 0.05 eV (60 K $< T <$ 125 K) and ≈ 0.2 eV ($T > 150$ K) that are then attributed to electron activation over barriers between localized sites and electron activation to a mobility edge, respectively. Both processes would plausibly lead to nonradiative recombination. Collins et al. [181] have shown, however, that many available data, from both sputtered and g.d. prepara-

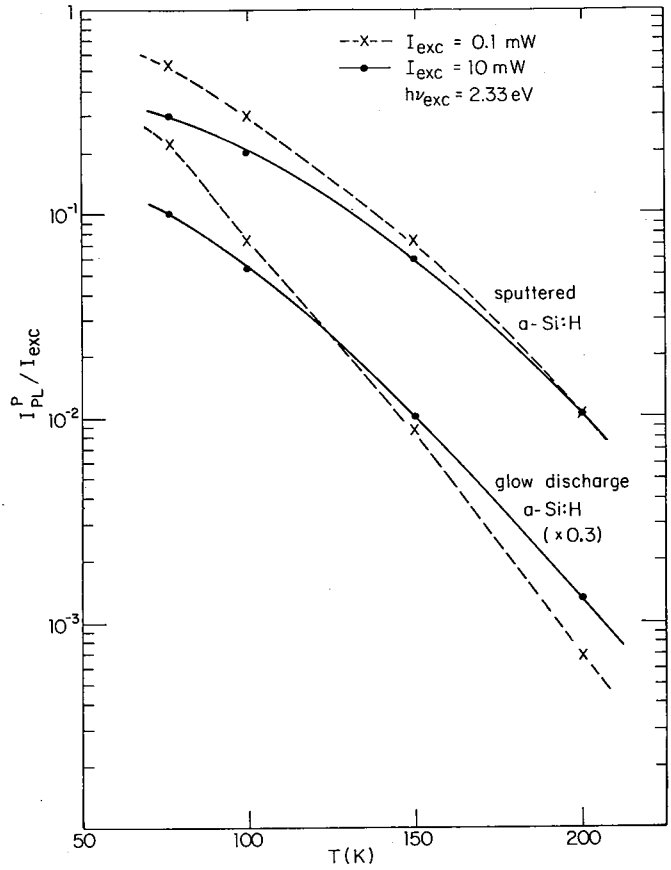

Fig. 30. Dependence on temperature for $T > 77$ K of the ratio of the peak intensity of the steady-state PL($h\nu$) to the excitation intensity, for both sputtered and g.d. samples at high and low excitation intensities [175].

tions, are an excellent fit to a log PL^{-1} versus T law over as many as four orders of magnitude in PL[a]. See fig. 32. We now model this T-dependence [b].

We put

$$\eta \propto f(T) = p_r(T)/[p_r(T) + p_{nr}(T)].$$

[a]Analysis of the T-dependence of PL in much of the early work may be invalidated by the realization that nongeminate recombination gives an excitation intensity dependence to the PL T-dependence. In particular, the data of Street, which were apparently taken at high excitation intensity on samples of high quantum efficiency, were probably affected by nongeminate contributions. Strictly speaking, our suggested rule (or any other) should be tested in the low intensity limit where geminate recombination dominates. The data for the sputtered material of ref. [175] were all taken on samples that had a negligible nongeminate component, independent of low temperature quantum efficiency (see section 6.4).

[b]See Collins and Paul, to be published, for a discussion of approximations made there. The general treatment was much helped by the work of Higashi and Kastner [182], and Gee and Kastner [183].

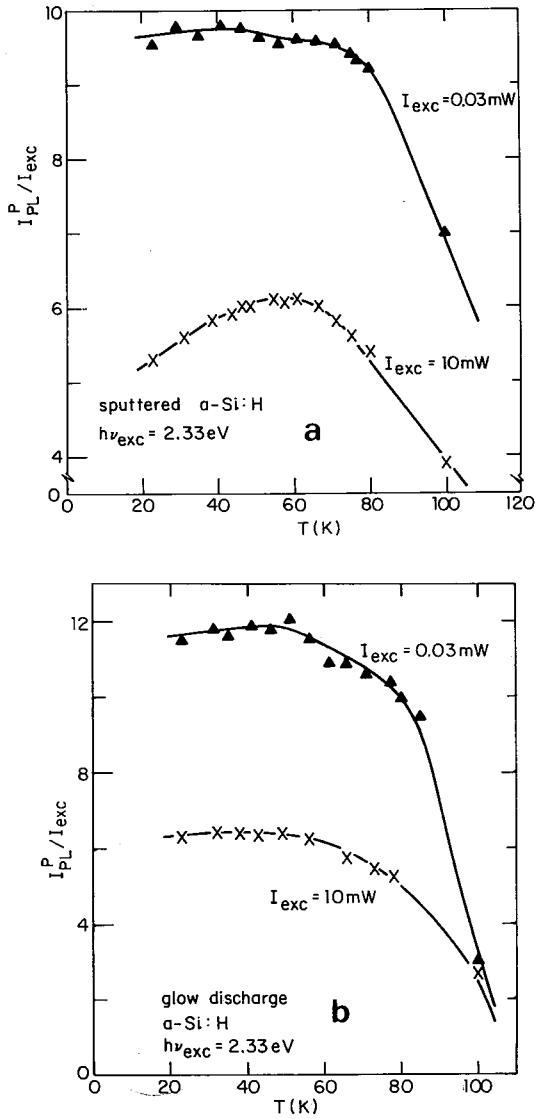

Fig. 31. Dependence on temperature for $T<77$ K of the ratio of the peak intensity of the steady-state PL($h\nu$) to the excitation intensity, for both sputtered (a) and g.d. (b) samples at high and low excitation intensities [175].

We suppose that $p_{nr}(T) = p_0[N_f(\varepsilon)/N_i(\varepsilon)]\exp(-\varepsilon/kT)$ describes the probability that an electron will become delocalized and recombine nonradiatively. Here $p_0 \approx 10^{12}$ s^{-1} and $N_i(\varepsilon)$ and $N_f(\varepsilon)$ are the initial and final state densities involved when an electron is activated to a final state ε above its initial state. Then, if $g(\varepsilon)$ is the probability that an electron will require a minimum energy between ε and $\varepsilon + d\varepsilon$ for delocalization, and if

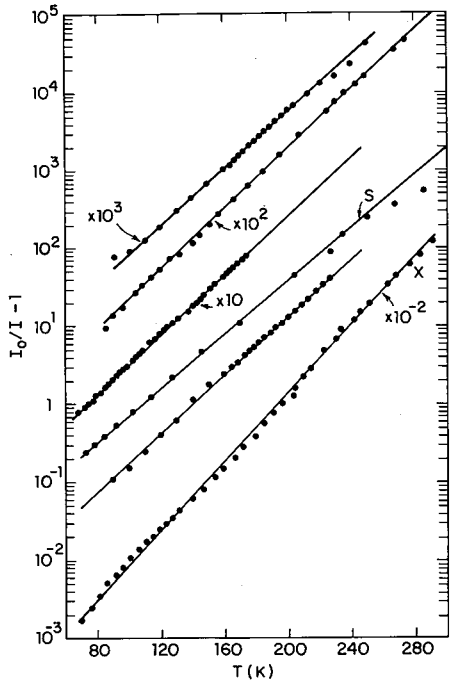

Fig. 32. Dependence on temperature of the steady state PL, plotted as $\log(I_0/I-1)$ versus T [181].

we also suppose that p_r does not depend on T but does depend on ε, then

$$\eta(T)\propto f(T)\propto \int_0^\infty g(\varepsilon)\,\mathrm{d}\varepsilon \Big/ \left(1+\frac{p_0}{p_r(\varepsilon)}\frac{N_f(\varepsilon)}{N_i(\varepsilon)}\exp(-\varepsilon/kT)\right)$$

If we then approximate $p_0N_f(\varepsilon)/p_r(\varepsilon)N_i(\varepsilon)$ by a constant B,

$$\eta(T)\tilde{\propto}\int_{kT\ \ln\ B}^\infty g(\varepsilon)\,\mathrm{d}\varepsilon$$

which can be equated to the experimentally-verified $\eta(T)$

$$\eta(T)\propto[A\exp(T/T_0)+1]^{-1}$$

to yield:

$$g(\varepsilon)\propto\exp(-\varepsilon/\varepsilon_0)/(\exp(-\varepsilon/\varepsilon_0)+A)^2,$$

where $\varepsilon_0=kT_0\ln B$.

Thus $g(\varepsilon)$ has a maximum at $\varepsilon_{max}=-kT_0\ln A\ln B$ with an fwhm of $\Delta\varepsilon\approx 3.5kT_0\ln B$. Then $(\varepsilon_{max}/\Delta\varepsilon)=(-\ln A/3.5)$.

Since, for our sputtered samples, $A=1\times10^{-2}$ (determined experimentally from PL versus T), then $\varepsilon_{max}/\Delta\varepsilon=1.3$. We next propose that ε_{max} should be approximated by the activation energy for drift mobility determined from photoconductivity, which is $\approx$0.25 eV. Thus $\Delta\varepsilon\approx$0.2 eV. Considering that there may be other contributions

to the PL spectral width, the derived $\Delta\varepsilon$ is reasonably close to the observed fwhm of 0.32 eV.

Assuming $\varepsilon_{max}=0.25$ eV, ln $B=27$ and $\varepsilon_0=0.054$ eV, we numerically integrate

$$\eta(T)\propto\int_{-\infty}^{+\infty}\left\{\frac{1}{1+Be^{-\varepsilon/kT}}\right\}\left\{\frac{e^{-\varepsilon/\varepsilon_0}}{(e^{-\varepsilon/\varepsilon_0}+A)^2}\right\}d\varepsilon$$

and compare this with the experimental results for a typical sputtered sample in fig. 33.

The asymptote in PL versus T (fig. 31) for the samples of highest η has sometimes been claimed to be close to 1, but in our samples, careful measurements usually indicate values between 0.1 and 1 (best 0.5), depending on the preparation conditions. It is generally supposed that under the conditions of the asymptote the radiative recombination is geminate. The asymptote in η less than 1 then may represent the fraction of photo-produced pairs produced near, and certain to recombine nonradiatively in, a highly-defected partial volume such as that we have identified as the connective tissue between growth islands.

The T_0's observed are significantly different depending on the method of sample preparation. Thus the T_0's for glow discharge material of high quantum efficiency are about 10 K smaller than for the best sputtered material at the lowest excitation intensities measurable. The data suggest that the glow discharge material (lowest T_0) has the least extensive conduction band tail of states, that the tail is somewhat larger in sputtered a-Si:H and a-$Si_{1-x}Ge_x$:H alloys, and much larger and deeper ($T_0\approx 70$ K) in a-Si:O. The T_0's correlate quantitatively with the fwhm of the PL, as is suggested by the model described giving $\Delta\varepsilon=3.5\,kT_0$ ln B.

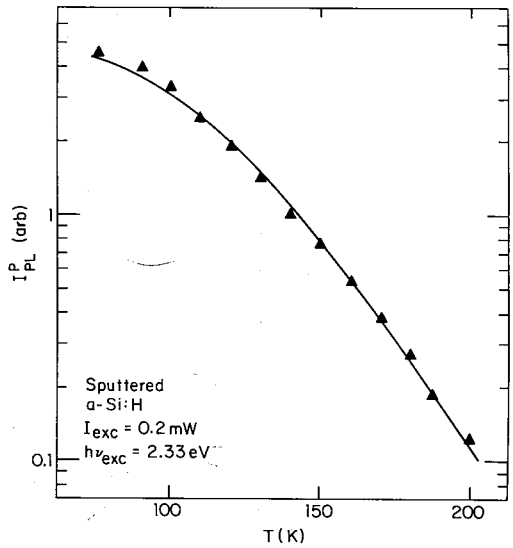

Fig. 33. Comparison of the observed I_{PL}^{peak} (▲▲▲) with that obtained from numerical integration of the formula for $\eta(T)$ of section 6.3 [175].

6.4. Nongeminate PL

We consider next the increase in η with I_{exc} shown in figs. 34 and 35, which has been attributed to nongeminate radiative recombination of the high density of photo-produced electrons and holes [184]. We note the following (i) there is no such effect for any sputtered or glow-discharge samples at the temperatures of the asymptote in η of fig. 31. This is probably caused by the fact that there is very little ionization of electron–hole pairs at low T, in which case the fact that $\eta < 1$ must imply that geminate recombination at low T may also be nonradiative. Alternatively, it is possible that all pairs produced in one subvolume (islands?) recombine radiatively, while other pairs produced in a second subvolume (tissue?) are certain to recombine nonradiatively. (ii) there is no such effect for samples for which η is very low (<0.1), say produced by sputtering at quite low p_H or by glow discharge incorporating Ge, indicating that the high density of nonradiative recombination centers prevents any nongeminate effects. (iii) the nongeminate effect is at most 10% in the best sputtered samples, much lower than the increase for glow-discharge samples of comparable low $T-\eta$. Compare, for example, sample 104 of fig. 34 with sample MT of fig. 35. The magnitude of the different effects is not explained by the easier ionization with T of electron–hole pairs in g–d material (lower T_0). Nor is it explained by differences in the gap state densities (possible nonradiative recombination centers) which are comparable from $C(f)$ and spin density estimates. Despite the lack of a detailed explanation, we can conclude that one

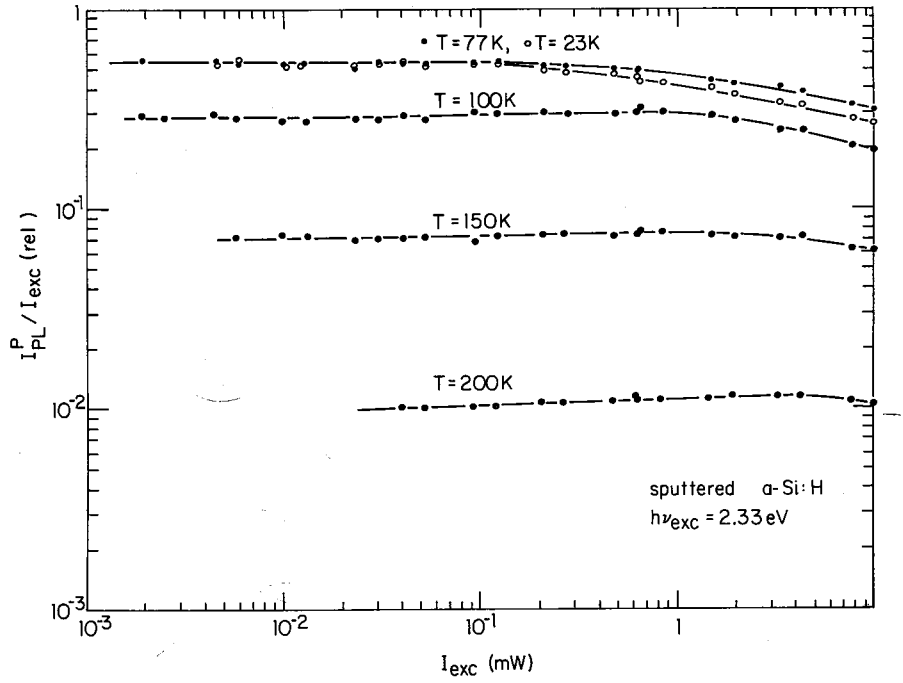

Fig. 34. Variation of PL relative efficiency $\eta \equiv I_{PL}^{peak}/I_{exc}$ with I_{exc} for sputtered sample 104 (see table 1) at several temperatures [175].

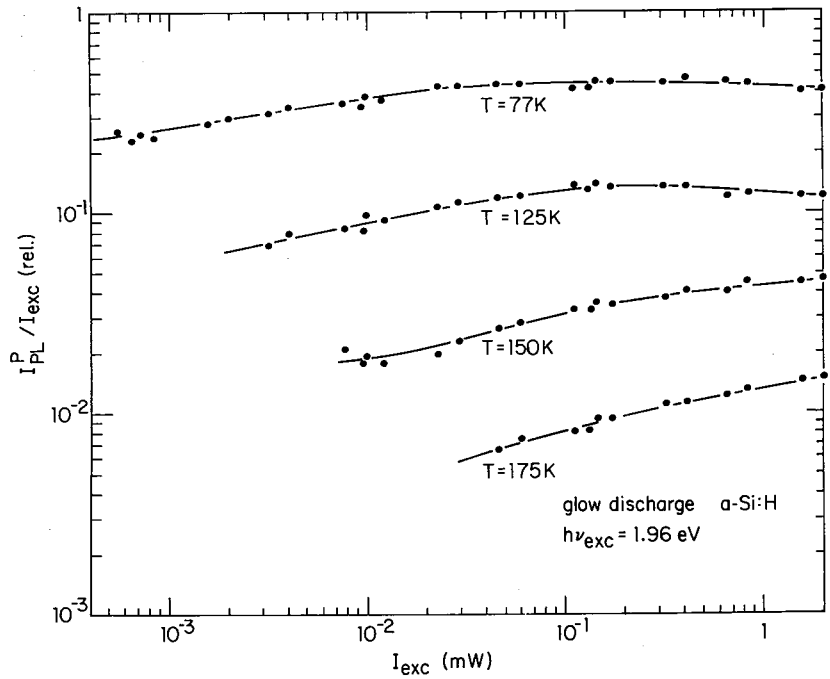

Fig. 35. Variation of PL relative efficiency $\eta \equiv I_{PL}^{peak}/I_{exc}$ with I_{exc} for g.d. sample MT (see table 1) at several temperatures [175].

cannot uniquely link a high η at low T with a large nongeminate radiative recombination, as has been done [184]. This is confirmed by the result of the Mobil Tyco sample [175] of fig. 35 which combines a quite modest low $T-\eta$ with as large a nongeminate effect as has been seen. Significantly, this sample also had the lowest T_0 of any measured, and the narrowest PL fwhm. This suggests the smallest tail of conduction band states and possibly the least quantitative disorder.

The fall-off in η at the highest I_{exc} for all T, as well as the reduction in η with T decreasing below 60 K for moderate I_{exc}, has been attributed by Street [184] to Auger recombination. The fact that the fall-off in I_{PL}/I_{exc} occurs at high intensity at a lower I_{exc}, the lower the temperature (see figs. 34 and 35) is consistent with the decrease in PL intensity as T is lowered below 60 K at a fixed high excitation intensity. Thus some of the early data were not taken under conditions of I_{exc} sufficiently low to ensure only geminate recombination. As is also illustrated in fig. 31 a decrease in I_{exc} eliminates the PL decrease with T.

6.5. Time-domain PL

Time-domain PL spectra [185] have shown that the photo-produced pairs recombine up to milliseconds after their creation. The model proposed for this is that a geminate pair can increase its separation either during the thermalization process to the band edges or by diffusion after thermal excitation out of relatively shallow

localized states, and that this leads to a spectrum of times for radiative recombination involving tunneling of

$$\tau = \tau_0 \exp(2R/R_0).$$

Here $\tau_0 \approx 10^{-8}$ s, R is the pair separation and R_0^{-1} the localization parameter for the less localized partner. Fig. 36 shows the shift in E_{PL}^{peak} with time after cessation of a very short excitation pulse, for different $h\nu_{exc}$; results for the Harvard sputtered material [186] and Street's glow discharge material are shown. There are several differences: (i) an initial faster decrease in E_{PL}^{peak} ($t < 20$ ns) is found for sputtered material and has been modelled in ref. [186]. (ii) a striking inversion of E_{PL}^{peak} with time is found for 50 ns $< t < 1$ μs suggesting that pairs recombining at times in the minimum may have a large Coulomb energy of interaction contribution to their transition energies. This is basically Street's explanation [187] for an increase in E_{PL}^{peak} with time for g.d. samples with heavy O incorporation. A small number of preliminary results for sputtered material suggests that the depth of the valley increases as the energy gap increases.

Fig. 36 also illustrates a new effect when the photon energy $h\nu_{exc}$ is changed. For $h\nu_{exc} \gtrsim 2.2$ eV, the shift of E_{PL}^{peak} with time is independent of $h\nu_{exc}$, which suggests that the different extents of thermalization have little affect on the R-distribution of pairs. When $h\nu_{exc}$ is decreased to 2.0 eV, however, for the sample illustrated, there is a striking shift of E_{PL}^{peak} to lower energy at a fixed time after pair excitation. This strongly suggests that carriers are being produced in more localized states and thus separate less, and have a larger Coulomb contribution upon radiative recombination. If this is

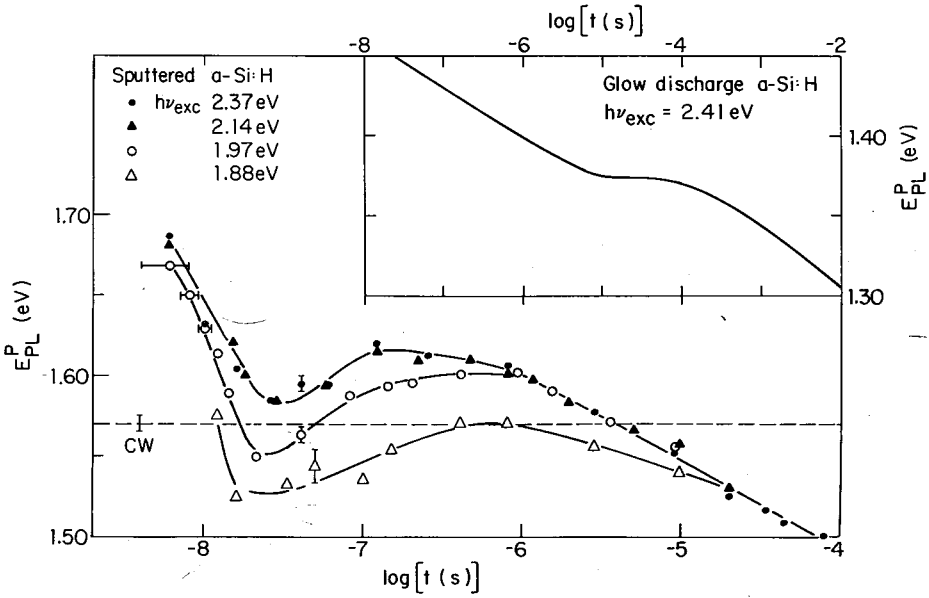

Fig. 36. Time decay of the photon energy of the peak PL intensity, E_{PL}^{peak}, for several $h\nu_{exc}$, for a sputtered sample of high C_H [186]. The inset shows similar results from ref. [180].

indeed a signature for the energetic separation at which localized states begin, it will be useful to correlate it with other optical and electrical properties of the sample.

6.6. Extrinsic PL

A new extrinsic PL peak at 0.95 eV, with a small fwhm of (0.20 ± 0.02) eV, and $\eta_{max} \approx 0.01$, was reported by Anderson et al. [101] in undoped samples sputtered at high p_H. The variation in the intensity of this peak with p_H is included in fig. 29. Later, Anderson et al. [43] and Collins et al. [188] attributed the PL process to a transition between two features in the gap DOS 0.3 and 1.2 eV below the conduction band, respectively. Among several possible models they favored one of states produced by an intrinsic defect in a-Si catalyzed or stabilized by the high p_H preparation conditions. Anderson et al. [43] also demonstrated certain similarities between this PL peak and one caused by P doping, although the PL peak in the latter case had a much larger fwhm. Among the details of the study by Collins et al. was the information that the 0.95 eV peak in high p_H material was more efficiently excited by subband gap radiation at least down to 1.6 eV.

An extrinsic peak was also reported at Leningrad [189] on undoped, glow-discharge samples, and more recently, on n and p-type doped g.d. material. Because the T-dependences and PL peak widths are different in detail [188–190], it is not yet established whether these are due to one and the same defect as in the sputtered Si, although we tend to favor the possibility. Street et al. [190] have presented a detailed model for the transition in glow-discharge material, which correlates its occurrence with a simultaneous increase in the intensity of the (dark) spin resonance normally associated with dangling bonds. In their picture, without giving the details, the starting state for the electron whose recombination gives the extrinsic PL is the doubly-occupied (negatively-charged) dangling bond site. Fig. 29 illustrates a difficulty in applying Street's model to try to explain the peak in sputtered samples: the dangling bond density is highest at low values of p_H, but no extrinsic effect is seen; indeed, the extrinsic effect correlates better with the range of p_H where our transport data suggest the existence of microstructure.

Apparently more work is needed to clarify the nature of the transition giving the extrinsic photoluminescence.

7. Photoconductivity

7.1. Introduction

The study of photoconductivity is important for many devices, and is also likely to give basic information about gap state densities, transport mechanisms and trapping and recombination processes. Several reviews are available [191]. The discussion here is intended only to outline the present understanding of the phenomenon in a-Si:H, which we believe to be incomplete in several respects.

First, it is necessary to note that the photoconductivity of the bulk of a-Si:H may be

obscured by surface effects: band bending, surface space charge layers, surface recombination centers and surface traps [8]. These can lead to results that depend on the sample thickness [192], on the history of its surface treatment, and the nature of any surface adsorbates [193]. Second, the photoconductivity may vary with light-induced changes in the bulk [194], the creation of traps and recombination centers by light, which may be reversed by anneal at high temperature. These surface and light-induced bulk effects are important, but we shall not discuss them further here, at least in part because, for the majority of samples produced by sputtering, such effects seem to be sufficiently small that they may be neglected in a first discussion [195]. This is possibly, but not necessarily, linked to the fact that many sputtered samples contain a higher density of gap states than do those prepared by glow discharge [196]. Third, analysis of photoconductivity has yet to consider the possible influence of a two-phase microstructure on the results. As will develop, an analysis based on the supposition that one is examining bulk photoconductivity of a homogeneous phase already faces formidable difficulties, so that it is appropriate to postpone such complications.

We are usually concerned with photocurrents measured using nonblocking contacts, so that carrier injection may occur to replace carriers that have completed their transit, in the circumstance that one of the carriers suffers long-time trapping. This photoconductive gain is important for devices relying on high photoresponse, but may be misleading if not recognized, when the material parameters are being sought. In this connection it is well to recognize that the magnitude of the photoconductivity is an uncertain indicator of the "cleanliness" of the energy gap: both a low density of recombination centers and a high density of minority carrier traps can lead to good majority carrier photoconductivity. For applications such as solar cells [197], efficient minority carrier transport is essential and experiments (surface photovoltage, carrier collection in Schottky structures) yielding the diffusion length or Schubweg of the minority carrier should be conducted in parallel with those on the majority carrier.

7.2. Illustrative results

The steady state electron photoconductivity* is given by

$$\Delta\sigma = en_c\mu_c = eG\tau\mu_c,$$

where n_c is the photocarrier density, μ_c the microscopic mobility in the conduction band, G the volume generation rate of carriers and τ the free electron lifetime. The volume generation rate is given by

$$G = F\eta f(R)(1-e^{-\alpha d})/d,$$

where F is the density per unit area of incident photons, η the quantum efficiency for

*We assume, as is usually done, that the hole contribution is smaller, but we emphasize that this is because the hole trapping is very probably more severe (deeper trap energies) and not because the hole microscopic mobility is small. Indeed our evidence is that the hole microscopic mobility is comparable to that of the electron.

generation of free carriers, α the absorption coefficient, $f(R)$ an appropriate correction factor for reflectivity [198], and d the sample thickness. In the event that the electron suffers capture in and release from shallow traps before final recombination, it is appropriate to write the expression for $\Delta\sigma$ as

$$\Delta\sigma = eG\mu_d\tau_r,$$

where μ_d is a trap-limited drift mobility and τ_r describes the initial rate of decay of $\Delta\sigma$ after the removal of an excitation pulse. (Strictly, $\tau_r^{-1} = \lim_{t\to 0} \Delta\sigma(d\Delta\sigma/dt)^{-1}$.)

Fig. 37 shows the variations of $\Delta\sigma$ with $1/T$ for representative sputtered and glow discharge samples from the Harvard laboratory [199], which are quite similar to those for g.d. a-Si:H already published [200] from other sources. Fig. 38 gives their τ_r versus $1/T$ and fig. 39 the deduced μ_d versus $1/T$. Table 2 lists the activation energies (slope of

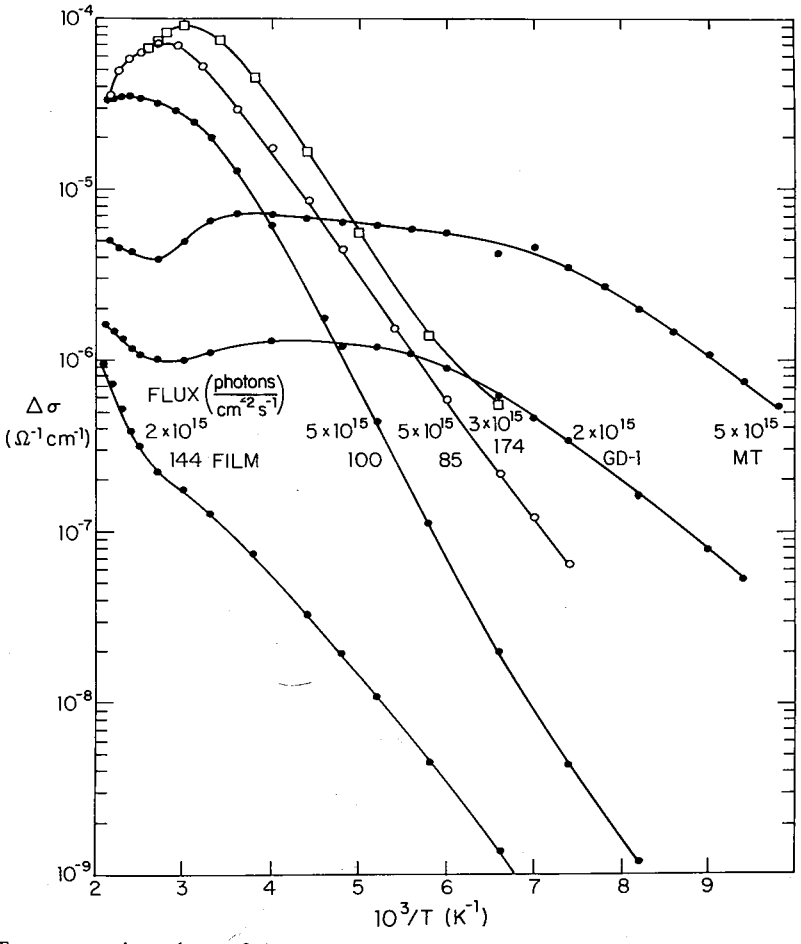

Fig. 37. Temperature dependence of photoconductivity $\Delta\sigma$, for representative sputtered and glow discharge samples. Films 144, 100 and 85 were sputtered in hydrogen, film 174 in hydrogen plus PH_3, while GD-1 and GD-MT were prepared by glow discharge. Further details are given in table 2.

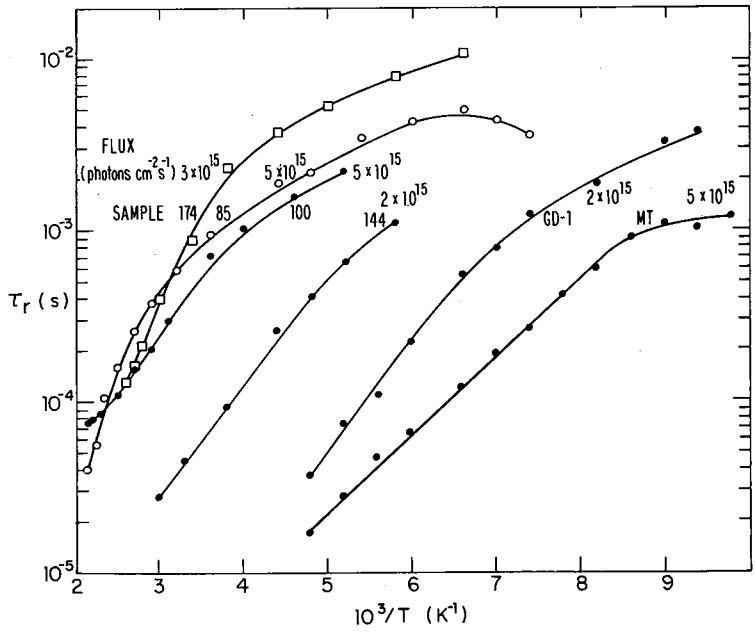

Fig. 38. Temperature dependence of the initial slope τ_r of the decay of photoconductivity after illumination is terminated, for the samples of fig. 37.

Table 2a
Approximate (because of the range of the parameters) activation energies for phototransport of the samples of figs. 37, 38 and 39

Sample	Preparation	E_σ (eV)	Activation energy (eV) and (range in $10^3/T$ (K^{-1}))		
			$\Delta\sigma$	$(\tau_r)^{-1}$	μ_d
144	sp.	0.9	0.12	0.12	0.22(3.3–5.8)
100	sp.	0.7	0.2	0.05	0.23(4–6)
85	sp.	0.6	0.15	0.06	0.20(3.2–6)
174	sp.+PH_3	0.3	0.15	0.04	0.24(3.8–5.8)
GD-1	g.d.	0.9	≈0	0.13	0.15(4.8–6.6)
GD-MT	g.d.	0.9	≈0	0.09	0.12(4.8–7.8)

ln (quantity) versus $1/T$) for $\Delta\sigma$, τ_r and μ_d, where these can be legitimately estimated from the figures, and also other relevant quantities. In addition to the data depicted in figs. 37 to 39 the dependence of the photocurrent on the illumination intensity, $I_p \propto F^\beta$, has been used as an indicator of whether the recombination is mono- or bimolecular [201]. Fig. 40 shows the variation of β with T for the samples of figs. 37 to 39.

Fig. 41 shows the variation of the room temperature photoconductivity, measured under standard conditions, for samples produced at nearly the same T_s, but with p_H systematically varied. For p_H less than 1 mTorr, the photoconductivity increases

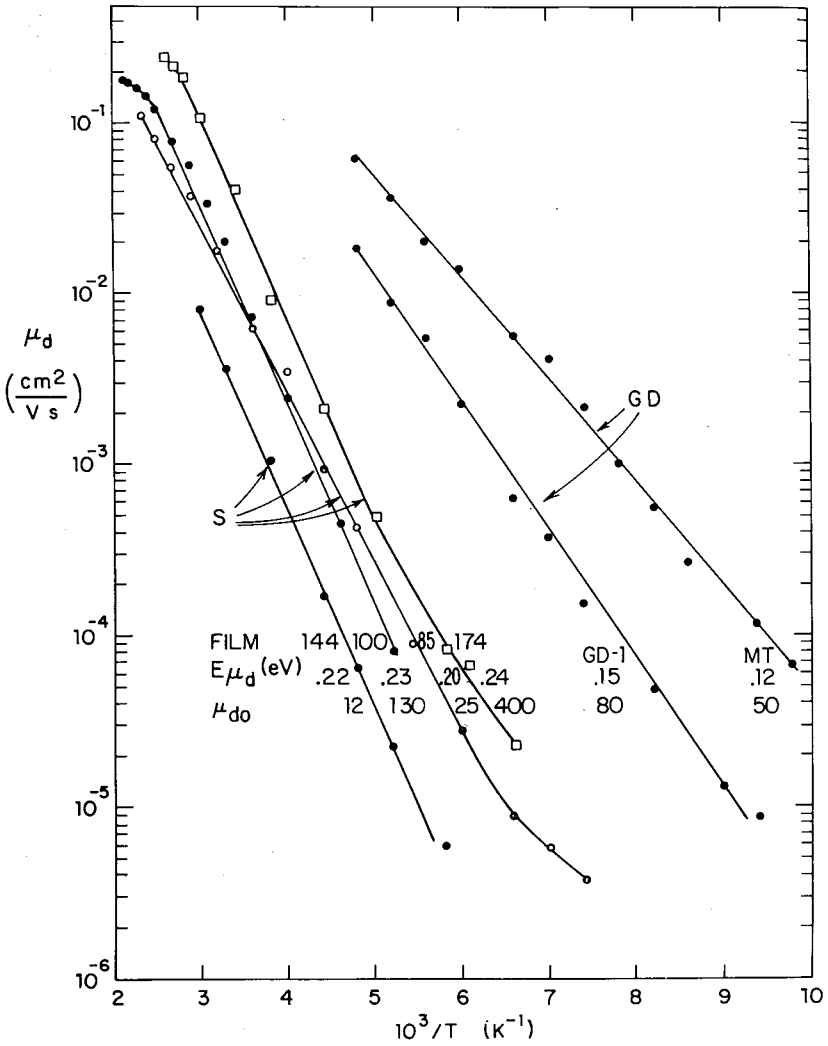

Fig. 39. Temperature dependence of the drift mobilities of the samples of fig. 37, deduced from the data of figs. 37 and 38.

monotonically. Beyond 1 mTorr there is much scatter, but some degree of order is restored when the photoconductivity is plotted against the activation energy for the dark conductivity, shown in fig. 42.

7.3. Recombination models

It is immediately clear, from the complexity of the curves shown, that different processes of transport and/or recombination are likely to be operative, quite possibly simultaneously. As later sections of this chapter will indicate, several new types of

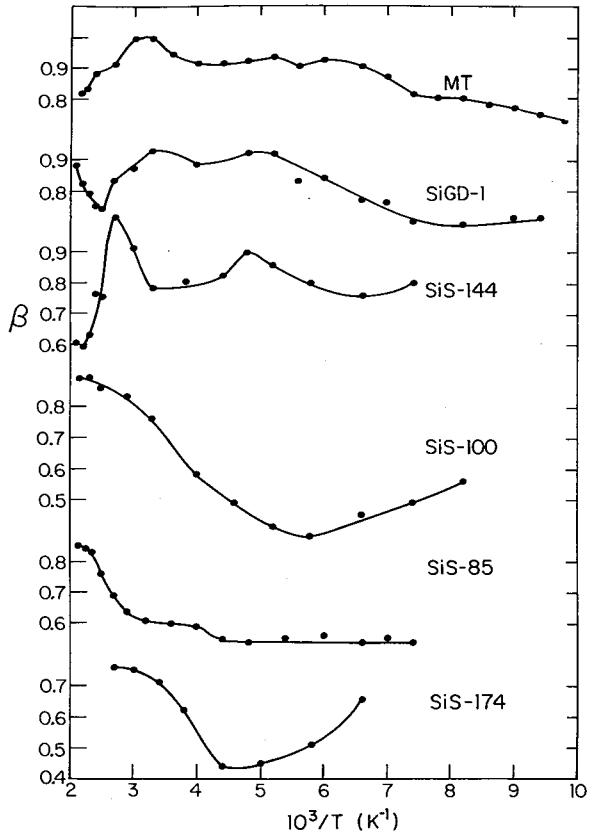

Fig. 40. Temperature dependence of the parameter β in $I_p \propto F^{\beta}$, for the samples of fig. 37.

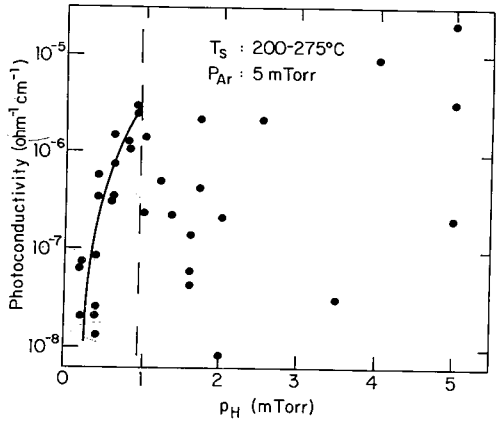

Fig. 41. Variation of the room temperature photoconductivity, measured under standard conditions, for samples produced at the same T_s but varied p_H (Moddel [199].

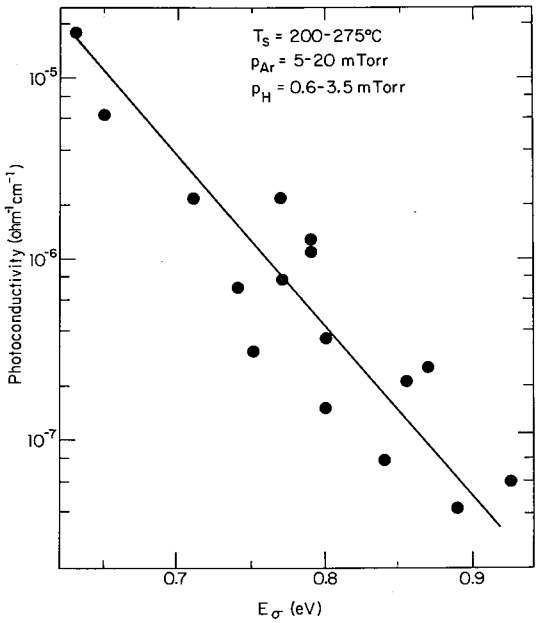

Fig. 42. Test of correlation between the magnitude of the photoconductivity (fig. 41) and the corresponding activation energy for dark transport (Moddel [199].

experiment – for example short time domain responses – may shortly clarify the picture. They are unquestionably necessary, for the interpretations given without them have either been seriously flawed by oversimplification, or so impenetrable in their unsimplified generality as to be unusable for extrapolation in physical terms.

One example of the over-simplified type concerns the assumption that a recombination path can be guessed and the steady state carrier distribution versus T derived. Let us take as an example film 174 of fig. 37 whose broad maximum as a function of T appears to be typical of pure or lightly-doped n-type samples, glow discharge or

Table 2b
Activation energies for $\Delta\sigma$, τ_r^{-1} and μ_d, assuming the single recombination paths of fig. 43. It is possible to match up these activation energies with the experimental observations of table 2a to identify, for example, the transitions for 144 with path 1 and those for GD-1 with path 4. See, however, the cautions in the text

Transition (fig. 43)	Activation energies (fig. 43)		
	$\Delta\sigma$	$(\tau_r)^{-1}$	μ_d
1	$\frac{1}{2}(E_c - E_A)$	$\frac{1}{2}(E_c - E_A)$	$E_c - E_A$
2	$E_c - E_A$	0	$E_c - E_A$
3	$E_c - E_A$	0	$E_c - E_A$
4	0	$E_c - E_A$	$E_c - E_A$

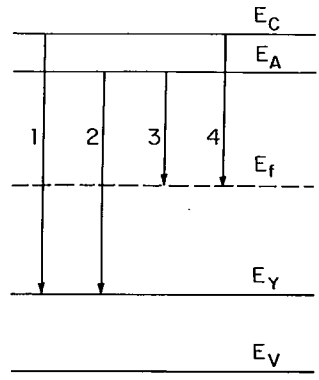

Fig. 43. Single recombination paths for photo-electrons and holes, for modelling purposes. The corresponding activation energies for $\Delta\sigma$, τ_r and μ_d are given in table 2.

sputtered [199, 200]. The range of $\Delta\sigma$ for T below the peak has been modelled as electronic transport by carriers activated out of states at energy E_a, below the conduction band transport level at E_c. If the principal recombination path is from E_a into a lower level at E_y whose hole density is proportional to the total hole density, then it is easy to show that

$$\Delta\sigma \propto \exp[-(E_c - E_a)/kT].$$

Thus $\Delta\sigma$ is activated and the intensity dependence of $\Delta\sigma$ is bimolecular. The activation energies for τ_r and μ_d may be derived similarly. Without giving the detailed derivations, we list in table 2 the activation energies for $\Delta\sigma$, τ_r and μ_d, under the assumption that it is legitimate to adopt the single principal recombination path for all T shown in fig. 43. We have restricted the listing to the case where $\Delta\sigma \gg \sigma$ (dark), but have included cases where recombination is bimolecular ($\beta = 1/2$) and monomolecular ($\beta = 1$). It then appears from the correlation of experimentally observed with modelled activation energies that a plausible description can been identified. This conclusion must be treated with great caution, for such modelling ignores many complexities: simplicity of physical description has been bought at too dear a price.

An attempt to set the subject on a more rigorous footing has been made by Anderson and Spear, who recognized the strong dependence of the recombination path on the shifts of the quasi-Fermi levels for electrons and holes, which themselves depended strongly on the temperature and excitation flux. Their approach, however, depended on the adoption of the density of states distribution established at Dundee by field effect measurements and its use for all the undoped and doped samples studied. As we discussed in section 3, the correctness of this state density distribution has been repeatedly challenged. Whether or not it is correct, it now seems clear that it is wrong to assume, as Anderson and Spear did, that the distribution is unaltered by doping; or to be more specific, that the distribution of states near the Fermi and quasi-Fermi levels stays unaltered when doping by P or B is carried out.

We can make additional qualitative analyses with some confidence. Thus, the

quenching of $\Delta\sigma$ in certain regions as T is increased may be explained by the activation of trapped holes to extended states or to recombination centers of larger capture cross section for electrons than the trap states. The slow variations at low T may involve conduction by hopping in localized states rather than activation to a band. The increase in $\Delta\sigma$ at the highest T of fig. 37 (sample 144) may be attributed to contributions from hole transport in a sample of low density of recombination centers. In general, however, there is a dangerous lack of unique explanations for the various features. It is our view that very little is presently settled and that reliable explanations still lie ahead.

The dependence of $\Delta\sigma$ on p_H is relatively straightforward. Thus in fig. 41, the increase in $\Delta\sigma$ as p_H is increased below 1 mTorr corresponds to the elimination of dangling bond and other recombination centers by H-compensation. Above 1 mTorr, the correlation between $\Delta\sigma$ and E_σ confirms a relation first pointed out by Anderson and Spear [200]. They, however, interpreted the relation as an increased electron lifetime when recombination centers near mid-gap were filled as the Fermi level rose. Whether or not this effect exists, it seems significant that the increased $\Delta\sigma$ and decreased activation energy often correlate also with a decreased $\mu\tau$ product for holes. This suggests that the main operative effect is increased minority carrier trapping, as the Fermi level rises, which in turn leads to an increased electron lifetime.

7.4. Additional experimental techniques

7.4.1. Two-beam photoconductivity

Dependences of $\Delta\sigma$ on $1/T$ similar to those in fig. 37 have been reported by Vanier and Griffith [202] and by Persans [202]. Vanier and Griffith interpret their results on a wide variety of doped and undoped glow-discharge samples in terms of three sets of trap states of different electron capture cross section. The occupancy of these states depends on the Fermi level position (doping) and on temperature. Thus the quenching of $\Delta\sigma$ (decrease of $\Delta\sigma$ as T is increased) is explained by the thermal excitation of holes from traps of low electron capture cross section to recombination centers of higher cross section. This may also be accomplished by infrared radiation of suitable energy, and therefore the spectrum of increase or decrease of the steady-state $\Delta\sigma$ as a second monochromatic infrared beam illuminates the sample can provide information about the recombination and trapping kinetics and the energetic position of the participating states. Such experiments are valuable in reducing the number of viable recombination models, although it is too early to say whether they will be sufficient in themselves to provide unique mechanisms and densities of states for a-Si:H [203]. These two-beam photoconductivity experiments form part of a class of experiments which includes combinations of light-induced spin resonance and photoconductivity. This latter combination, which would simultaneously explore the lifecycles of trapped and free carriers, does not seem to have been tried as much as seems warranted. Nor have experiments which explore the influence of infrared light, which quenches photoconductivity, on the phototransport ($\mu\tau$ product) of the minority holes. It seems evident that a more complete picture of the kinetics of recombination processes, particu-

larly the influence of trapped holes, would be afforded by a judicious combination of experiments that probe the lifecycle of *both* carriers.

7.4.2. Short time-domain photoconductivity and time-dependent mobilities

Much attention is now being focused on phototransport at very short times (from picoseconds on) after photo-excitation. Although there are as yet insufficient results to give a definitive picture (for both glow discharge and sputtered samples) one can nevertheless perceive the lines of investigation which must come together. They are photoinduced absorption [204] and photoconductivity in the picosecond regime [205]; photoluminescence spectra in the nanosecond and microsecond regime as a function of temperature and excitation energy (see Section 6); drift mobility by the time-of-flight technique, which separates the electron–hole pairs [206]; and photoconductivity in the nanosecond regime after an exciting pulse is terminated [207]. An even more complete picture might be possible if one could add light-induced spin resonance.

The experiments on photoinduced absorption indicate that photocarriers thermalize to the valence and conduction band edges inside a picosecond, which presently prevents any estimate of variation of carrier mobility with energy in the band, and very likely eliminates any high energy band-to-band photoluminescence. The thermalization is more than 5 times faster in unhydrogenated a-Si than in a-Si:H. An explanation based on carrier interaction only with polar phonons in the latter has been offered [208].

Drift mobility experiments are often interpreted in terms of dispersive transport [209], which occurs when carriers may be temporarily immobilized for times of the same order as the time of the experiment (say, the time for transit across the sample by a carrier that is not immobilized). The immobilization could, in principle, be in localized states out of which the carrier eventually hops to another localized state [210], or in shallow traps, out of which it is excited to a (higher energy) transport level [211]. It has been shown that the current may be written

$$I(t) \propto t^{-(1-\alpha)}, \quad t < t_T$$

for times t less than a (carefully defined) transit time, and

$$I(t) \propto t^{-(1+\alpha)}, \quad t > t_T$$

for longer times. A fiduciary mark corresponding to the transit time therefore appears when a current trace is displayed as $\log I$ versus $\log t$. This behavior of the current may be understood in terms of a distribution of event (hop or excitation) times

$$\psi(t) = \text{const}\ t^{-(1+\alpha)}; \quad 0 < \alpha < 1.$$

Recently, Tiedje and Rose [212], and Orenstein and Kastner [213], elaborating on earlier treatments [214], have shown that the formal results may be derived on the basis of a model which supposes that photoinjected carriers relax into an exponential (in energy) distribution of shallow traps. The traps are supposed to have equal capture cross sections, but release times that depend on their depth (in energy) and the temper-

ature. Thus the occupancy of the shallowest of them is described by a Boltzmann function, while the occupancy of the deepest is proportional to the trap density in energy. The demarcation level between these two distribution functions moves lower in energy with time. The final result for the drift mobility experiment is a transient photoconductive response which decreases with time (before carriers reach the receiving contact) as the constant total density of carriers spends a smaller and smaller fraction of time in the conducting bands.

We now refer very briefly to two aspects of this transport: first, the present observations of dispersive transport in sputtered material and second, the possible implications of a time-dependent mobility for the usual photoconductivity experiments.

7.4.2.1. Dispersive transport. The data on glow discharge produced a-Si:H have been widely discussed [215]. Tiedje et al. [216] have reported results on both g.d. and sputtered material. Both nondispersive and dispersive transients are observed in differently-prepared g.d. samples. Later work reported a change-over from nondispersive to dispersive behavior as the temperature was reduced [217]. Preliminary illustrative results from the Harvard laboratory [218] are presented in figs. 44 and 45. Fig. 44 shows the transient plotted linearly and also as log I versus log t, when the clear break-point gives a transit time, which may be used to define a drift mobility. Fig. 45 illustrates the occurrence of dispersive transients of this sort at low T, changing to nondispersive behaviour – a constant current with a sharply defined "corner" – at high T. The break-point in the dispersive transients in voltage-dependent, creating an uncertainty in the estimated transit time. For the nondispersive transient, a transit time may also be defined, either from the "corner" time or the time at which the current has fallen to half its constant value. Adopting the second definition we arrive

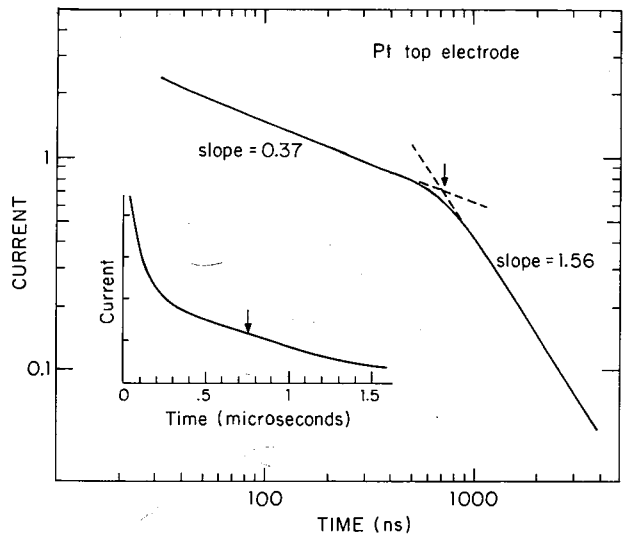

Fig. 44. Current transient for dispersive transport from a drift mobility experiment, plotted both linearly and on a log I versus log t graph, in order to show a break-point defining a transit time [218].

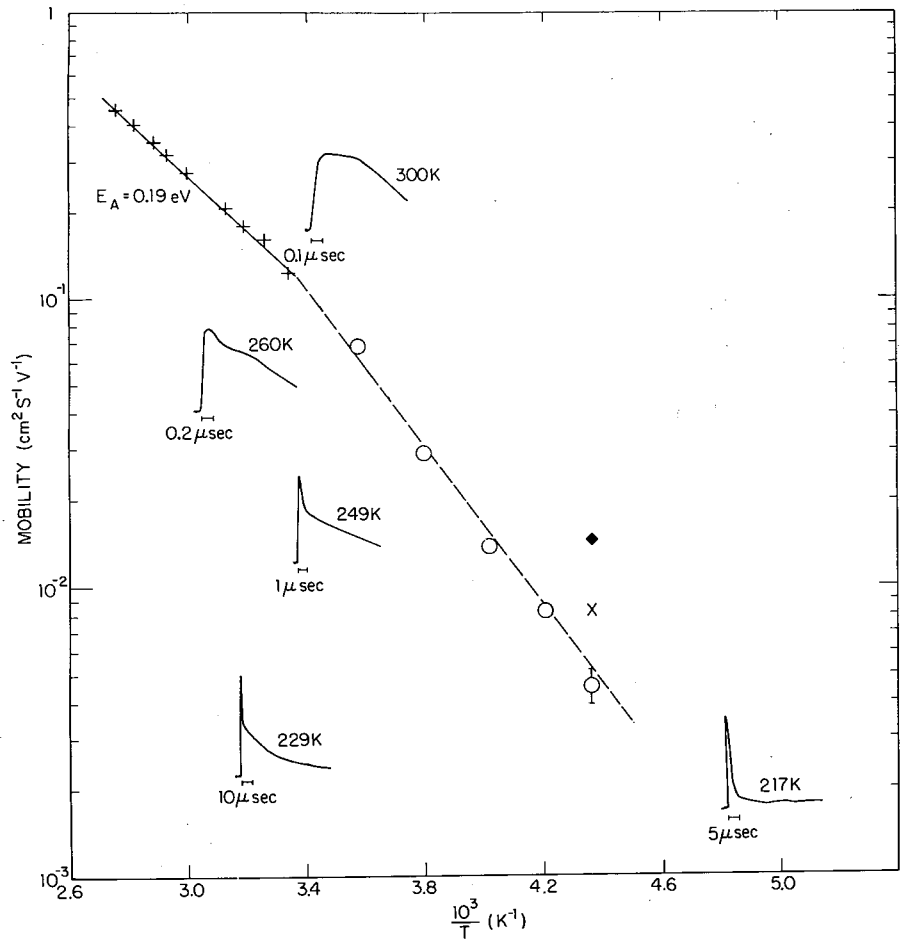

Fig. 45. Mobility versus temperature for a sample displaying nondispersive transport at high temperatures and dispersive transport at low temperatures [218].

at the dependence of mobility on temperature shown in fig. 45. Its activation energy is 0.2 eV, which is close to the values found from photoconductivity experiments (see fig. 39), and also to the activation energy for nonradiative recombination (see section 6). There are many details of such measurements which we omit in this brief account, but two quite general points may be made. First, the same features are found in time-of-flight experiments on sputtered as on glow-discharge samples [216–218] – whether understood fully or not – and second, a model of shallow trapping and release seems to be viable, with only quantitative differences in trap distributions between the two types of sample.

7.4.2.2. Analysis of photoconductivity experiments. Time-dependent mobilities – or more precisely, a continuously decreasing contribution over time to the photocon-

ductivity per carrier by photocarriers which remain unrecombined – may affect the interpretation of both transient and steady-state photoconductivity experiments. Street [219] has formally analyzed the consequences of a mobility with time dependence $\mu(t)=\mu_0 t^{-(1-\alpha)}$ on (1) the magnitude of photoconductivity at time T after the start of a constant illumination pulse, when $T \ll$ the recombination time τ (2) the decay of photoconductivity after termination of an exciting pulse of finite time duration, again on a time scale $t \ll \tau$ (3) the magnitude of the steady state photoconductivity in the presence of both a time-dependent mobility and a single recombination time. From experiments on glow discharge produced samples, he has used his analysis to obtain information on $\mu(t)$ over many decades of time. It is too early to assess the significance of his results on steady state photoconductivity, except to make the point that his analysis asserts that some conventional interpretations (of β in $I_p \propto F^{\beta}$, for example) must be modified.

Transient photoconductivity experiments have also been carried out by Hvam and Brodsky [220] on glow discharge a-Si:H and by Kirby [218] on sputtered material. The latter are illustrated in fig. 46 for both an undoped and a doped sample. It is to be noted that there is a sharp initial decrease of photoconductivity in the purer sample [221]. We link this with an anomaly in the mobility deductions of fig. 39. If we write $\mu_d = \mu_{do} \exp(-E_{\mu d}/kT)$, then μ_{do} should vary as $N_c kT/N_t$ where N_t is the density of shallow traps at some average depth $E_{\mu d}$. The μ_{do}'s for the several samples of fig. 39 are shown on the figure. If we could make the tentative (unproven) assumption that the corresponding density N_t of shallow traps is proportional to the level density near E_f, or to the magnitude of low photon energy absorption $\alpha(1.2)$, then high μ_{do} should correspond to low $N(E_f)$ or low $\alpha(1.2)$. Yet, precisely the opposite relation holds for these samples.

Figs. 39 and 46 suggest that for the undoped samples either the mobility decreases faster with time (without recombination) or that some recombination occurs at very short times. The time-of-flight experiments on the same undoped samples, however, show no evidence either of recombination or of particularly fast mobility decay. In

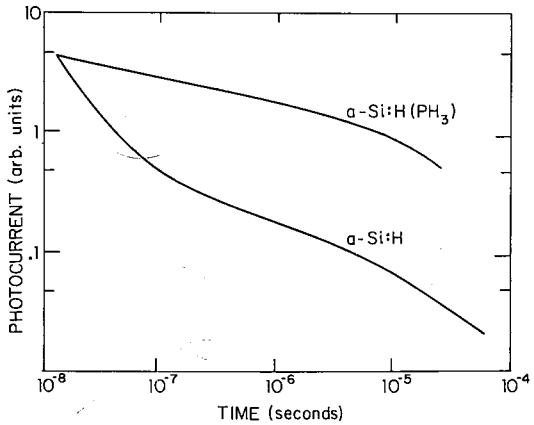

Fig. 46. Transient photoconductivity for an undoped and a doped sputtered sample, showing a faster fall-off for the former [218].

these experiments, however, the minority holes are immediately separated by a high field from the electrons; it therefore appears possible that the photoholes in undoped samples are able to induce very fast recombination. In doped samples, on the other hand, immediate hole trapping might prevent such an occurrence. We emphasize that these are speculations on current experiments and more data are needed. Nevertheless, they illustrate the complexity of the problem, for rapid (partial) carrier recombination obviously affects the quantitative interpretation of experiments designed to study time-dependent mobilities.

7.5. Present situation

The study of photoconductivity in amorphous semiconductors [222] is in a new developing phase, so that this review will probably soon be out dated. Time-domain experiments will probably provide the bulk of the new information, but we might also expect informative input from quench spectra [202, 203], experiments on the collection efficiency of Schottky devices [223], on the diffusion length or Schubweg of the holes [224], and geminate recombination and xerography [225].

8. Conclusion

Ten years ago, in surveying the properties of unhydrogenated semiconductors [226], one of the authors found it appropriate to refer to the advice in the introduction to Shockley's classic text. Paraphrased, it suggested the experimenter find out which atoms he was dealing with, how they got to be where they were, and what the consequences of their position were for the properties. Unfortunately, the fact that amorphous semiconductors produced as thin films may be structurally and chemically inhomogeneous, and that the heterogeneity may render difficult a property analysis constructed for a homogeneous substance, has been too often ignored. It is essential it be remembered.

Acknowledgements

This review was much improved by the elimination of errors, inaccuracies and inconsistencies by the present Harvard postdoctoral fellows and graduate students: Robert Collins, Paul Kirby, Jalil Lachter, Garret Moddel, Suha Oguz, Dilip Paul, Bolko von Roedern, Richard Weisfield and Ben Yacobi. In the immediately prior period their research was augmented by the work of Jay Blake and Pierre Viktorovitch, which also built on the earlier fine work of another generation of members of this group. To all of these men and women go our grateful appreciation. We acknowledge also the contributions of Philip Ketchian and David MacLeod and the financial support of the DOE through a S.E.R.I. grant, of the Joint Services Electronics Project at Harvard, of the NSF-DMR-MRL program, and of a continuing NSF-DMR grant to William Paul.

References

[1] Accounts of the early work may be found in the Proc. Conf. on Amorphous and Liquid Semiconductors, at Ann Arbor, 1971, J. Non-Crystalline Solids 8–10 (1972); and at Garmisch-Partenkirchen, 1973, eds. J. Stuke and W. Brenig (Taylor and Francis, London 1974).
Other general reviews include: D. Adler, CRC Critical Rev. Solid State Sci. 2 (1971) 317, which includes over 1000 references; papers in Amorphous and Liquid Semiconductors, ed. J. Tauc (Plenum, New York, 1974); papers in Electronic and Structural Properties of Amorphous Solids, eds. P. G. LeComber and J. Mort (Academic Press, London, 1973); W. Paul, in: Proc. 11th Semiconductor Conf., Warsaw, 1972 (Polish Academy of Sciences, Warsaw, 1972).
A very detailed account of the properties of unhydrogenated a-Ge which probably represents current understanding of this material is to be found in three articles by W. Paul, G. A. N. Connell and R. J. Temkin, Advan. Phys. 22 (1973) 529.

[2] A. J. Lewis, Jr., G. A. N. Connell, W. Paul, J. R. Pawlik and R. J. Temkin, Intern. Conf. on Tetrahedrally-Bonded Amorphous Semiconductors, AIP Conf. Proc. 20 (1974) 27.

[3] W. E. Spear, in: Proc. Fifth Intern. Conf. on Amorphous and Liquid Semiconductors, Garmisch-Partenkirchen (1973) p. 1.

[4] H. F. Sterling and R. C. G. Swann, Solid State Electron. 8 (1965) 653. R. C. Chittick, J. H. Alexander R. C. Chittick, J. H. Alexander and H. F. Sterling, J. Electrochem. Soc. 116 (1969) 77.

[5] It had been speculated earlier (M. H. Brodsky, R. S. Title, K. Weiser and G. D. Pettit, Phys. Rev. B1 (1970) 2632) that the differences between sputtered and g.d. a-Si might be caused by "hydrogen contamination".

[6] W. E. Spear and P. G. LeComber, Solid State Commun. 17 (1975) 1193; Phil. Mag. 33 (1976) 935.

[7] See, for example, the Proceedings of recent conferences: Seventh Conf. on Amorphous and Liquid Semiconductors, Edinburgh, 1977, ed. W. E. Spear (CICL, University of Edinburgh, 1977); Eighth Conf. on Amorphous and Liquid Semiconductors, Cambridge, 1979, eds. W. Paul and M. Kastner, J. Non-Crystalline Solid 35/36 (1980); Photovoltaic Material and Device Measurements Workshop, San Diego, 1980, ed. J. L. Stone, Solar Cells 2 (3, 4) (1980); Fundamental Physics of Amorphous Semiconductors, Proc. 1980 Kyoto Summer Institute, ed. F. Yonezawa (Springer Verlag, Berlin. 1981); Intern. Conf. on Tetrahedrally Bonded Amorphous Semiconductors, Carefree, Arizona, March 1981, eds. R. A. Street, D. K. Biegelsen and J. C. Knights (AIP Conf. Ser. No. 73, New York, 1981). Also see Amorphous Semiconductors, ed. M. H. Brodsky, Topics in Applied Physics, Vol. 36 (Springer Verlag, New York, 1979); J. C. Knights and G. Lucovsky, CRC Critical Rev. Solid State Mater. Sci. 9 (3) (1980); W. E. Spear, Advan. Phys. 26 (1977) 811; H. Fritzsche, C. C. Tsai and P. Persans, Solid State Tech. (1978) 55.

[9] D. E. Carlson, Solar Energy Mater. 3 (1980) 503.

[10] The early work was reported in: W. Paul, A. J. Lewis, Jr., G. A. N. Connell and T. D. Moustakas, Solid State Commun. 20 (1976) 969; T. D. Moustakas, D. A. Anderson and W. Paul, Solid State Commun. 23 (1977) 155; D. A. Anderson, T. D. Moustakas and W. Paul, first of ref. [7], p. 334. For a general review, see T. D. Moustakas, J. Electron. Mater. 8 (1979) 391.

[11] (Sheffield) M. J. Thompson, M. Alkaisi and J. Allison, Rev. de Phys. Appl. 13 (1978) 625; I. G. Austin, K. Richards, T. M. Searle, M. J. Thompson, M. Alkaisi, I. P. Thomas and J. Allison, Intern. Phys. Conf. Ser. 43 (1979) 1155; J. Allison, M. J. Thompson, D. P. Turner and I. P. Thomas, Proc. 3rd European Photovoltaic Conf., Cannes, 1980.
(Penn. State) R. Messier and I. S. T. Tsong, Final Report to the D. O. E. on Contract No. DE–AC03–79ET23038 (May 1980); R. Ross and R. Messier, J. Appl. Phys., in press.
(Argonne) J. A. McMillan and E. M. Peterson, J. Appl. Phys. 50 (1979) 5238.
(Iowa State) Ref. [14].
(IBM) M. H. Brodsky, M. Cardona and J. J. Cuomo, Phys. Rev. B16 (1977) 3556.
(Stuttgart) C. J. Fang, K. J. Gruntz, L. Ley, M. Cardona, F. J. Demond, G. Müller and S. Kalbitzer, J. Non-Crystalline. Solids 35/36 (1980) 255.
(Exxon) J. P. de Neufville, T. D. Moustakas, A. F. Ruppert and W. A. Lanford, J. Non-Crystalline. Solids 35/36 (1980) 481.

(Grenoble) J. C. Bruyère, A. Deneuville, A. Mini, J. Fontenille and R. Danielou, J. Appl. Phys. 51 (1980) 2199.
(ETL) K. Tanaka, S. Yamasaki, K. Nakagawa, A. Matsuda, H. Okushi, M. Matsumura and S. Iizima, J. Non-Crystalline. Solids 35/36 (1980) 475.
(Pacific Northwest) P. M. Martin and W. T. Pawlewicz, J. Non-Crystalline. Solids, 45 (1981) 15.
[12](a) See, for example, B. Kramer and D. Weaire, in: Amorphous Semiconductors, ed. M. H. Brodsky, Topics in Applied Physics, Vol. 36 (Springer Verlag, New York, 1979); D. Adler, in: Fundamental Physics of Amorphous Semiconductors, Proc. 1980 Kyoto Summer Institute, ed. F. Yonezawa (Springer Verlag, Berlin, 1981); review papers in ref. [7]; and J. D. Joannopoulos and D. C. Allan, to be published.
(b) See, for example, P. G. LeComber and W. E. Spear, in: Amorphous Semiconductors, ed. M. H. Brodsky, Topics in Applied Physics, Vol. 36 (Springer Verlag, New York, 1979); D. A. Anderson and W. Paul, ref. [102].
[13] W. T. Pawlewicz, J. Appl. Phys. 49 (1978) 5595.
[14] F. R. Jeffrey, H. R. Shanks and G. C. Danielson, J. Appl. Phys. 50 (1979) 7034; J. Non-Crystalline. Solids 35/36 (1980) 261.
[15] See ref. [11].
[16] See Messier and Tsong, ref. [11]. R. E. Jones, C. L. Standley and L. I. Maissel, J. Appl. Phys. 38 (1967) 4656.
[17] See, for example: J. A. Thornton, Ann. Rev. Mater. Sci. 7 (1977) 239; J. Vac. Sci. Technol. 11 (1974) 666.
[18] See, however, discussion and references in Messier and Tsong, and in Ross and Messier, ref. [11].
[19] For a recent review, see, for example, F. J. Kampas and R. W. Griffith, Solar Cells 2 (1980) 385. See also F. J. Kampas and R. J. Griffith, and M. Hirose, T. Hamasaki, Y. Mishima, H. Kurata and Y. Osaka, in: Proc. Intern. Conf. on Tetrahedrally Bonded Amorphous Semiconductors, Carefree, Arizona, March 1981, eds. R. A. Street, D. K. Biegelsen and J. C. Knights (AIP Conf. Series No. 73, New York 1981) p. 10.
[20] M. A. Paesler, T. Okumura and W. Paul, J. Vac. Sci. and Technol. 17 (1980) 1332:
A. Matsuda, K. Nakagawa, K. Tanaka, M. Matsumura, S. Yamasaki, H. Okushi and S. Iizima, J. Non-Crystalline. Solids 35/36 (1980) 183.
[21] See Allison et al., ref. [11].
D. P. Turner, I. P. Thomas, J. Allison, M. J. Thompson, I. G. Austin and T. M. Searle, Intern. Conf on Tetrahedrally Bonded Amorphous Semiconductors, Carefree, Arizona, March 1981, eds. R. A. Street, D. K. Biegelsen and J. C. Knights (AIP Conf. Series No. 73, New York, 1981) p. 47.
R. Ross and R. Messier, Intern. Conf. on Tetrahedrally Bonded Amorphous Semiconductors, Carefree, Arizona, March 1981, ed. R. A. Street, to be published.
[22] An excellent brief review of structural studies on a-Si:H, primarily from glow discharge, has been given by J. C. Knights, Solar Cells 2 (1980) 409.
[23] R. Mosseri, J. C. Malaurent, C. Stella and J. Dixmier, J. Non-Crystalline. Solids 35/36 (1980) 507.
[24] A. Barna, P. B. Barna, G. Radnoczi, L. Toth and P. Thomas, Phys. Stat. Sol. (a) 41 (1977) 81.
J. F. Graczyk, Phys. Stat. Sol. (a) 55 (1979) 231.
[25] N. J. Shevchik and W. Paul, J. Non-Crystalline. Solids 8–10 (1972) 381, 13 (1974) 1, 16 (1974) 55.
W. Paul, G. A. N. Connell and R. J. Temkin, Advan. Phys. 22 (1973) 529.
R. J. Temkin, W. Paul and G. A. N. Connell, Advan. Phys. 22 (1973) 581.
[26] S. C. Moss and J. F. Graczyk, Phys. Rev. Lett. 23 (1969) 1167.
[27] T. M. Donovan and K. Heinemann, Phys. Rev. Lett. 27 (1971) 1794.
[28] P. D'Antonio and J. H. Konnert, Phys. Rev. Lett. 43 (1979) 1161.
[29] P. D'Antonio and J. H. Konnert, Intern. Conf. on Tetrahedrally Bonded Amorphous Semiconductors, Carefree, Arizona, March 1981, eds. R. A. Street, D. K. Biegelsen and J. C. Knights (AIP Conf. Series No. 73, New York, 1981) p. 117.
[30] A. J. Leadbetter, A. A. M. Rashid, R. M. Richardson, A. F. Wright and J. C. Knights, Solid State Commun. 33 (1980) 973.
T. A. Postol, C. M. Falco, R. Kampwirth, I. Schuller and W. B. Yelon, Phys. Rev. Lett. 45 (1980) 648.
[31] J. C. Knights and R. A. Lujan, Appl. Phys. Lett. 35 (1979) 244.
J. C. Knights, J. Non-Crystalline. Solids 35/36 (1980) 159; Japan. J. Appl. Phys. 18 (1979) 101.

[32] J. C. Knights, R. A. Lujan, M. P. Rosenblum, R. A. Street, D. K. Biegelson and J. A. Reimer, to be published.
[33] R. J. Nemanich, D. K. Biegelsen and M. P. Rosenblum. Proc. 15th Intern. Conf. Physics of Semiconductors, Kyoto, 1980; J. Phys. Soc. Japan, 49, Supp. A (1980) 1189.
[34] J. A. Reimer, R. W. Vaughan and J. C. Knights, Phys. Rev. Lett. 44 (1980) 193.
J. A. Reimer and J. C. Knights, Intern. Conf. on Tetrahedrally Bonded Amorphous Semiconductors, Carefree, Arizona, March 1981, eds. R. A. Street, D. K. Biegelsen and J. C. Knights (AIP Conf. Ser. No. 73, New York, 1981) p. 78.
[35] W. E. Carlos and P. C. Taylor, Phys. Rev. Lett. 45 (1980) 358.
W. E. Carlos, P. C. Taylor, S. Oguz and W. Paul, Intern. Conf. on Tetrahedrally Bonded Amorphous Semiconductors, Carefree, Arizona, March 1981, eds. R. A. Street, D. K. Biegelsen and J. C. Knights (AIP Conf. Ser. No. 73, New York, 1981) p. 67.
[36] See the references to Messier and Tsong, and Ross and Messier, under ref. [11].
[37] D. A. Anderson, G. Moddel, M. A. Paesler and W. Paul, J. Vac. Sci. Technol. 16 (1979) 906.
[38] H. Fritzsche and C. C. Tsai, Solar Energy Mater. 1 (1979) 471.
[39] E. C. Freeman, Thesis, Harvard (1980) unpublished. E. C. Freeman and W. Paul, ref. [42].
[40] F. Cocks, L. Dimmey, P. L. Jones and A. Korhonen, J. Appl. Phys. (in press).
[41] E. C. Freeman and W. Paul, Phys. Rev. B18 (1978) 4288.
[42] E. C. Freeman and W. Paul, Phys. Rev. B20 (1979) 716.
[43] D. A. Anderson, G. Moddel and W. Paul, J. Non-Crystalline. Solids 35/36 (1980) 345
[44] D. A. Anderson and W. Paul, Phil. Mag. (1981) (in press).
[45] T. D. Moustakas, C. R. Wronski and D. L. Morel, J. Non-Crystalline. Solids 35/36 (1980) 719.
[46] J. C. Bruyère, A. Deneuville, A. Mini, J. Fontenille and R. Danielou, J. Appl. Phys. 51 (1980) 2199.
[47] A. Deneuville, J. C. Bruyère, A. Mini, H. Kahil, R. Danielou and E. Ligeon, J. Non-Crystalline Solids 35/36 (1980) 469.
[48] T. D. Moustakas, D. A. Anderson and W. Paul, Solid State Commun. 23 (1977) 155.
W. Y. Ching, D. J. Lam and C. C. Lin, Phys. Rev. Lett. 42 (1979) 805.
R. Fisch and D. C. Licciardello, Phys. Rev. Lett. 41 (1978) 889.
[49] G. A. N. Connell and J. R. Pawlik, Phys. Rev. B13 (1976) 787.
[50] M. H. Brodsky, M. Cardona and J. J. Cuomo, Phys. Rev. B16 (1977) 3556.
[51] H. Shanks, C. J. Fang, L. Ley, M. Cardona, F. J. Demond and S. Kalbitzer, Phys. Stat. Sol. (b) 100 (1980) 43.
[52] M. H. Brodsky, M. Cardona and J. J. Cuomo, Phys. Rev. B16 (1977) 3556.
[53] J. C. Knights, G. Lucovsky and R. J. Nemanich, Phil. Mag. B37 (1978) 467.
G. Lucovsky, R. J. Nemanich and J. C. Knights, Phys. Rev. B19 (1979) 2064
J. C. Knights, G. Lucovsky and R. J. Nemanich, J. Non-Crystalline. Solids 33 (1979) 373.
[54] P. J. Zanzucci, C. R. Wronski and D. E. Carlson, J. Appl. Phys. 48 (1977) 5227.
[55] For recent comprehensive reviews, see G. Lucovsky, Fundamental Physics of Amorphous Semiconductors, Proc. 1980 Kyoto Summer Institute, ed. F. Yonezawa (Springer Verlag, Berlin, 1981) p. 87; and in: Solar Cells 2 (1980) 431.
[56] S. Oguz, D. A. Anderson, W. Paul and H. J. Stein, Phys. Rev. B22 (1980) 880.
[57] See, for example, refs. [41, 49, 51, 55, 58, 59].
[58] G. Lucovsky, Solid State Commun. 29 (1979) 571.
[59] W. Paul, Solid State Commun. 34 (1980) 283.
[60] Ref. [41]. Also unpublished material.
[61] S. Oguz, D. K. Paul, J. Blake, R. Collins, A. Lachter, B. G. Yacobi and W. Paul, Proc. Ninth Intern. Conf. on Amorphous and Liquid Semiconductors, Grenoble, 1981, to be published.
[62] Private communication.
[63] Private communication.
[64] S. Oguz and B. Yacobi, private communication.
[65] H. Fritzsche, M. Tanielian, C. C. Tsai and P. J. Gaczi, J. Appl. Phys. 50 (1979) 3366.
[66] J. A. McMillan and E. M. Peterson, J. Appl. Phys. 50 (1979) 5328.
[67] S. Oguz and M. A. Paesler, Phys. Rev. B22 (1980) 6213.
[68] S. Oguz, R. W. Collins, M. A. Paesler and W. Paul, J. Non-Crystalline. Solids 35/36 (1980) 231.

[69] D. K. Biegelsen, R. A. Street, C. C. Tsai and J. C. Knights, Phys. Rev. B20 (1979) 4839.
[70] M. F. Brodsky, M. A. Frisch, J. F. Ziegler and W. A. Lanford, Appl. Phys. Lett. 30 (1977) 561.
[71] K. J. Matysik, C. J. Mogab and B. G. Bagley, J. Vac. Sci. Technol. 15 (1978) 302.
[72] S. Oguz, Thesis, Harvard University (1981) unpublished.
[73] Ref. [69]. Also see Biegelsen, Street, Tsai and Knights, J. Non-Crystalline. Solids 35/36 (1980) 285.
[74] C. J. Fang, K. J. Gruntz, L. Ley, M. Cardona, F. J. Demond, G. Müller and S. Kalbitzer, J. Non-Crystalline. Solids 35/36 (1980) 255.
[75] Refs. [66, 67, 70, 73]. Also see K. Zellama, P. Germain, S. Squelard, J. Monge and E. Ligeon, J. Non-Crystalline. Solids 35/36 (1980) 225.
[76] P. John, M. Odeh, M. J. K. Thomas, M. J. Tricker, J. McGill, A. Wallace and J. I. B. Wilson, J. Non-Crystalline. Solids 35/36 (1980) 237.
[77] For supporting evidence, see J. C. Bruyère, A. Deneuville, A. Mini, J. Fontenille and R. Danielou, J. Appl. Phys. 51 (1980) 2199; K. Zellama, P. Germain, S. Squelard, B. Bourdon, J. Fontenille and R. Danielou, Phys. Rev. (submitted).
[78] B. von Roedern, L. Ley and M. Cardona, Phys. Rev. Lett. 39 (1980) 1576.
B. von Roedern, L. Ley, M. Cardona and F. W. Smith, Phil. Mag. B40 (1979) 433.
B. von Roedern and G. Moddel, Solid State Commun. 35 (1980) 467.
[79] W. Y. Ching, D. Lam and C. C. Lin, Phys. Rev. Lett. 42 (1979) 805
J. D. Joannopoulos, J. Non-Crystalline. Solids 32 (1979) 241.
D. C. Allan and J. D. Joannopoulos, Phys. Rev. Lett. 44 (1980) 43.
W. Y. Ching, D. Lam and C. C. Lin, Phys. Rev. B21 (1980) 2378.
[80] L. Ley and K. J. Gruntz, Intern. Conf. on Tetrahedrally Bonded Amorphous Semiconductors, Carefree, Arizona, March 1981, eds. R. A. Street, D. K. Biegelsen and J. C. Knights (AIP Conf. Ser. No. 73, New York, 1981) p. 161.
[81] However, one should not discount the possibility that the highly clustered form is concentrated on the inner surfaces of small voids, or in tissue material so distributed that it would elude observation even in thin TEM samples.
[82] F. R. Jeffrey, M. E. Lowry, M. L. S. Garcia, R. G. Barnes and D. E. Torgeson, Intern. Conf. on Tetrahedrally Bonded Amorphous Semiconductors, Carefree, Arizona, March 1981, eds. R. A. Street, D. K. Biegelsen and J. C. Knights (AIP Conf. Ser. No. 73, New York, 1981) p. 83. Second reference under [35].
[83] See W. A. Lanford, Solar Cells 2 (1980) 351 for a detailed description of method, further references and results.
[84] W. A. Lanford, H. P. Trautvetter, J. F. Zeigler and J. Keller, Appl. Phys. Lett. 30 (1977) 566.
[85] M. Milleville, W. Fuhs, F. J. Demond, H. Mannsperger, G. Müller and S. Kalbitzer, Appl. Phys. Lett. 34 (1979) 173.
[86] C. W. Magee and D. E. Carlson, Solar Cells 2 (1980) 365.
[87] G. J. Clark, C. W. White, D. D. Allred, B. R. Appleton, C. W. Magee and D. E. Carlson, Appl. Phys. Lett. 31 (1977) 582.
[88] J. C. Bruyère, A. Deneuville, A. Mini, J. Fontenille and R. Danielou, J. Appl. Phys. 51 (1980) 2199.
[89] S. Oguz, W. Paul and W. A. Lanford, unpublished collaboration. See ref. [83].
[90] S. Oguz, unpublished Harvard results.
[91] D. I. Jones, R. A. Gibson, P. G. LeComber and W. E. Spear, Solar Energy Mater. 2 (1979) 93.
[92] K. Tanaka, S. Yamasaki, K. Nakagawa, A. Matsuda, H. Okushi, M. Matsumura and S. Iizima, J. Non-Crystalline. Solids 35/36 (1980) 475.
[93] M. A. Paesler, D. A. Anderson, E. C. Freeman, G. Moddel and W. Paul, Phys. Rev. Lett. 41 (1978) 1492.
[94] B. G. Yacobi et al., to be published from the Harvard Laboratory.
[95] J. C. Knights, R. A. Street and G. Lucovsky, J. Non-Crystalline. Solids 35/36 (1980) 279.
[96] See, for example, R. W. Griffith, F. J. Kampas, P. E. Vanier and M. D. Hirsch, J. Non-Crystalline. Solids 35/36 (1980) 391; P. E. Vanier, A. E. Delahoy and R. W. Griffith, submitted for publication. R. W. Griffith, Solar Materials Science, ed. L. E. Murr (Academic Press, New York, 1980) ch. 19.
[97] J. R. Pawlik, Thesis, Harvard (1979) unpublished.
J. R. Pawlik and W. Paul, ref. [111].
[98] D. A. Anderson, T. D. Moustakas and W. Paul, Proc. 7th Intern. Conf. on Amorphous and Liquid

Semiconductors, Edinburgh, 1977, ed. W. E. Spear (CICL, University of Edinburgh, 1977) p. 334.
[99] T. D. Moustakas, D. A. Anderson and W. Paul, Solid State Commun. 23 (1977) 155.
[100] T. D. Moustakas and W. Paul, unpublished Harvard results (1977). M. A. Paesler and W. Paul, Phil. Mag. B41 (1980) 393.
[101] D. A. Anderson, G. Moddel, R. W. Collins and W. Paul, Solid State Commun. 31 (1979) 677.
[102] D. A. Anderson and W. Paul, Phil. Mag. (to be published).
[103] D. A. Anderson and W. Paul, Proc. 15th Intern. Conf. Physics of Semiconductors, Kyoto (1980); J. Phys. Soc. Japan 49, Suppl. A (1980) 1197.
[104] It should be remarked that there have been other suggestions made to explain these anomalies. See, for example, W. E. Spear, D. Allan, P. G. LeComber and A. Ghaith, J. Non-Crystalline. Solids 35/36 (1980) 357; G. H. Döhler, J. Non-Crystalline Solids 35/36 (1980) 363; and H. Overhof and W. Beyer, J. Non-Crystalline. Solids 35/36 (1980) 375.
[105] W. Paul, G. A. N. Connell and R. J. Temkin, Advan. Phys. 22 (1973) 529.
[106] For a qualitative discussion in physical terms see: W. Paul, in: Amorphous Semiconductors, Proc. Third Intern. Summer College on Physics and Contemporary Needs, Nathiagali, Pakisan, 1978 (Plenum, New York, 1979).
[107] For a general discussion of defects in tetrahedrally-bonded and chalcogenide semiconductors, see the review by J. C. Knights and G. Lucovsky, ref. [7], p. 242.
[108] J. C. Phillips, Phys. Rev. Lett. 42 (1979) 1151.
[109] For a more quantitative treatment than ref. [106], see: D. Adler, Phys. Rev. Lett. 41 (1978) 1755; J. Non-Crystalline. Solids 35/36 (1980) 819; Solar Cells 2 (1980) 199.
S. R. Elliott, Phil. Mag. B38 (1978) 325.
J. Joannopoulos, J. Non-Crystalline. Solids 35/36 (1980) 781.
[110] J. Stuke, Proc. 7th Intern. Conf. on Amorphous and Liquid Semiconductors, Edinburgh, 1977, ed. W. E. Spear (CICL, University of Edinburgh, 1977) p. 406.
[111] J. R. Pawlik and W. Paul, Proc. 7th Intern. Conf. on Amorphous and Liquid Semiconductors, Edinburgh, 1977, ed. W. E. Spear (CICL, University of Edinburgh, 1977) p. 437.
[112] R. S. Title, M. H. Brodsky and J. J. Cuomo, Proc. 7th Intern. Conf. on Amorphous and Liquid Semiconductors, Edinburgh, 1977, ed. W. E. Spear (CICL, University of Edinburgh, 1977) p. 424.
[113] J. R. Pawlik and W. Paul, ref. [111]. D. K. Biegelsen and J. C. Knights, Proc. 7th Intern. Conf. on Amorphous and Liquid Semiconductors, Edinburgh, 1977, ed. W. E. Spear (CICL University of Edinburgh, 1977) p. 429.
J. C. Knights, D. K. Biegelsen and I. Solomon, Solid State Commun. 22 (1977) 133.
A. Friederich and D. Kaplan, J. Electron. Mater. 7 (1978) 253.
R. A. Street and D. K. Biegelsen, J. Non-Crystalline. Solids 35/36 (1980) 651.
[114] D. K. Biegelsen, J. C. Knights, R. A. Street, C. Tsang and R. M. White, Phil. Mag. B37 (1978) 477.
K. Morigaki, D. J. Dunstan, B. C. Cavenett, P. Dawson, J. E. Nichols, S. Nitta and K. Shinakawa, Solid State Commun. 26 (1978) 981.
K. Morigaki, B. C. Cavenett, P. Dawson, S. Nitta and K. Shinakawa, J. Non-Crystalline Solids 35/36 (1980) 633.
[115] D. K. Biegelsen, Solar Cells 2 (1980) 421.
[116] Other general references on e.s.r. in g.d. a-Si:H:
M. H. Brodsky and R. S. Title, Structure and Excitations in Amorphous Solids, A.I.P. Vol. 31 (1976) p. 97.
U. Voget-Grote, J. Stuke and H. Wagner, Q.I.P. Conf. Proc. 31 (1976) 91.
R. A. Street, J. C. Knights and D. K. Biegelsen, Phys. Rev. B18 (1978) 1880.
H. Fritzsche, C. C. Tsai and P. D. Persans, Solid State Technol. 21 (1978) 55.
[117] R. S. Crandall, Solar Cells 2 (1980) 319; J. Non-Crystalline Solids 35/36 (1980) 381.
C. R. Wronski, B. Abeles, G. D. Cody and T. Tiedje, Appl. Phys. Lett. 37 (1980) 96.
[118] The paper by G. Moddel, D. A. Anderson and W. Paul, Phys. Rev. B22 (1980) 1918 examines the necessary assumptions in detail.
[119] P. G. LeComber, A. Madan and W. E. Spear, in: Electronic and Structural Properties of Amorphous Semiconductors, eds. P. G. LeComber and J. Mort (Academic Press, New York, 1973) p. 373.
D. A. Anderson, G. Moddel, R. W. Collins and W. Paul, ref. [101].

D. A. Anderson, G. Moddel and W. Paul, ref. [43].
J. I. Pankove, F. J. Pollack and C. Schnabolk, J. Non-Crystalline Solids 35/36 (1980) 459.
T. D. Moustakas, Solid State Commun. 35 (1980) 745.
G. D. Cody, C. R. Wronski, B. Abeles, R. B. Stephens and B. Brooks, Solar Cells 2 (1980) 227.
[120] Ref. [43], and T. D. Moustakas, ref. [119].
[121] B. von Roedern and G. Moddel, ref. [78].
[122] Harvard group results, to be published.
[123] M. Olivier, J. C. Peuzin and A. Chenevas-Paule, J. Phys. Soc. Japan 49 (1980) Suppl. A, 1201.
[124] S. Yamasaki, K. Nakagawa, H. Yamamoto, A. Matsuda, H. Okushi and K. Tanaka, Proc. Conf. on Tetrahedrally-Bonded Amorphous Semiconductors, Carefree, Arizona, March 1981, eds. R. A. Street, D. K. Biegelsen and J. C. Knights (AIP Conf. Ser. No. 73, New York, 1981) p. 258.
[125] W. Jackson and N. M. Amer. Proc. Conf. on Tetrahedrally-Bonded Amorphous Semiconductors, Carefree, Arizona, March 1981, eds. R. A. Street, D. K. Biegelsen and J. C. Knights (AIP Conf. Ser. No. 73, New York, 1981) p. 263.
[126] W. E. Spear and P. G. LeComber, J. Non-Crystalline Solids 8–10 (1972) 727.
W. E. Spear and P. G. LeComber, Phil. Mag. 33 (1976) 935.
A. Madan, P. G. LeComber and W. E. Spear, J. Non-Crystalline Solids 20 (1976) 239.
A. Madan and P. G. LeComber, Proc. 7th Intern. Conf. on Amorphous and Liquid Semiconductors, Edinburgh, 1977, ed. W. E. Spear (CICL, Edinburgh, 1977) p. 377.
[127] N. B. Goodman, H. Fritzsche and H. Ozaki, J. Non-Crystalline Solids 35/36 (1980) 599.
N. B. Goodman and H. Fritzsche,Phil. Mag. B42 (1980) 149.
[128] M. Powell, Phil. Mag. 43 (1981) 93.
[129] R. Weisfield and D. A. Anderson, Phil. Mag. B44 (1981) 83.
[130] M. Grünewald, P. Thomas and D. Würtz, Phys. Stat. Sol. (b) 100 (1980) K139.
[131] M. Hirose, T. Suzuki and G. H. Döhler, Appl. Phys. Lett. 34 (1979) 234.
[132] W. E. Spear, P. G. LeComber and A. J. Snell, Phil. Mag. B38 (1978) 303.
[133] Discussions at a Summer School in Trieste, Italy (1980).
[134] R. L. Weisfield, P. Viktorovitch, D. A. Anderson and W. Paul, Appl. Phys. Lett. 39 (1981) 263.
[135] N. B. Goodman and H. Fritzsche, Proc. Intern. Conf. on Tetrahedrally-Bonded Amorphous Semiconductors, Carefree, Arizona, March 1981, eds. R. A. Street, D. K. Biegelsen and J. C. Knights (AIP Conf. Ser. No. 73, New York, 1981) p. 176.
[136] G. H. Döhler and M. Hirose, Proc. 7th Intern. Conf. on Amorphous and Liquid semiconductors, Edinburgh, 1977, ed. W. E. Spear (CICL, Edinburgh, 1977) p. 372.
[137] J. Beichler, W. Fuhs, H. Mell and H. M. Welsch, J. Non-Crystalline Solids 35/36 (1980) 587.
[138] P. Viktorovitch, D. Jousse, A. Chenevas-Paule and L. Vieux-Rochas, Rev. Phys. Appl. 14 (1979) 201.
P. Viktorovitch and D. Jousse, J. Non-Crystalline Solids 35/36 (1980) 569.
[139] P. Viktorovitch and G. Moddel, J. Appl. Phys. 51 (1980) 4847.
[140] T. Tiedje, C. R. Wronski and J. M. Cebulka, J. Non-Crystalline Solids 35/36 (1980) 740.
T. Tiedje, C. R. Wronski, B. Abeles and J. M. Cebulka, Solar Cells 2 (1980) 301.
[141] P. Viktorovitch, J. Appl. Phys. 52 (1981) 1392.
[142] D. V. Lang, J. Appl. Phys. 45 (1974) 3032.
J. D. Cohen, D. V. Lang, J. P. Harbison and J. C. Bean, Solar Cells 2 (1980) 331.
J. D. Cohen, D. V. Lang and J. P. Harbison, Proc. Intern. Conf. on Tetrahedrally Bonded Amorphous Semiconductors, Carefree, Arizona, March 1981, eds. R. A. Street, D. K. Biegelsen and J. C. Knights (AIP Conf. Ser. No. 73, New York, 1981) p. 217.
[143] I. Balberg and D. E. Carlson, Phys. Rev. Lett. 43 (1979) 58. I. Balberg, Phys. Rev. B22 (1980) 3853.
[144] W. Rehm, R. Fischer, J. Stuke and H. Wagner, Phys. Stat. Sol. (b) 79 (1977) 539.
W. Beyer, R. Fischer and H. Overhof, Phil. Mag. B49 (1979) 205.
W. Beyer and H. Overhof, Solid State Commun. 31 (1979) 1.
[145] M. Grünewald and P. Thomas, Phys. Stat. Sol. (b) 94 (1979) 125.
[146] G. H. Döhler, Phys. Rev. B19 (1979) 2083.
[147] D. E. Carlson and C. R. Wronski, in: Amorphous Semiconductors, ed. M. H. Brodsky, Topics in Applied Physics, Vol. 36 (Springer Verlag, New York, 1979) p. 287.

[148] W. E. Spear, D. Allan, P. G. LeComber and A. Ghaith, J. Non-Crystalline Solids 35/36 (1980) 357, fig. 2.
[149] D. A. Anderson and W. Paul, Phil. Mag. to be published.
[150] M. Tanielian, M. Chatani, H. Fritzsche, V. Smid and P. D. Persans, J. Non-Crystalline Solids 35/36 (1980) 575.
[151] I. Solomon, J. Perrin and B. Bourdon, Proc. 14th Intern. Conf. on Physics of Semiconductors, Institute of Physics Conf. Series No. 43 (1979) p. 689.
[152] N. K. Hindley, J. Non-Crystalline. Solids 5 (1970) 17.
[153] B. Pistoulet, J. L. Robert, J. M. Dusseau and L. Ensuque, J. Non-Crystalline. Solids 29 (1978) 29.
[154] P. G. LeComber, A. Madan and W. E. Spear, J. Non-Crystalline. Solids 11 (1972) 219.
[155] J. Dresner, Appl. Phys. Lett. 37 (1980) 742.
[156] For a recent general review, see G. A. N. Connell, in: Topics in Applied Physics: Amorphous Semiconductors, ed. M. H. Brodsky, Vol. 36 (Springer Verlag, New York, 1979) p. 73.
For an earlier review, see M. L. Theye, in: Physics of Structurally Disordered Solids, ed. S. S. Mitra (Plenum Press, New York, 1976) p. 111; this NATO Advanced Study Institute Series volume also contains useful early reviews on the physics of many phenomena examined in the present article.
For a recent review specifically on a-Si:H, see G. D. Cody, C. R. Wronski, B. Abeles, R. B. Stephens and B. Brooks, Solar Cells 2 (1980) 227.
[157] D. T. Pierce and W. E. Spicer, Phys. Rev. B5 (1972) 3017.
[158] H. R. Philipp and H. Ehrenreich, Phys. Rev. 129 (1963) 1550.
[159] I. Haller and M. H. Brodsky, Proc. 14th Intern. Conf. Phys., Edinburgh (1978) p. 1147.
[160] G. Weiser, D. Ewald and M. Milleville, Phil. Mag. B40 (1979) 291; J. Non-Crystalline Solids 35/36 (1980) 447.
[161] M. Janai, D. D. Allred, D. E. Booth and B. O. Seraphin, Solar Energy Mater. 1 (1979) 11.
[162] J. Tauc, in: Amorphous and Liquid Semiconductors (Plenum Press, New York, 1974).
[163] D. L. Wood and J. Tauc, Phys. Rev. B5 (1972) 3144.
[164] J. Tauc, Mater. Res. Bull. 5 (1970) 721.
J. D. Dow and D. Redfield, Phys. Rev. B5 (1972) 594.
[165] R. J. Loveland, W. E. Spear and A. Al-Sharbaty, J. Non-Crystalline. Solids 13 (1973/4) 55.
P. J. Zanzucchi, C. R. Wronski and D. E. Carlson, J. Appl. Phys. 48 (1977) 5227.
J. C. Knights, A. I. P. Conf. Proc. 31 (1976) 296.
J. I. Pankove, F. H. Pollak and C. Schnabolk, J. Non-Crystalline. Solids 35/36 (1980) 459.
[166] Ref. [42], A. Deneuville, J. C. Bruyere, A. Mini, H. Kahil, R. Danielou and E. Ligeon, J. Non-Crystalline. Solids 35/36 (1980) 469.
J. P. de Neufville, T. D. Moustakas, A. F. Ruppert and W. A. Lanford, J. Non-Crystalline Solids 35/36 (1980) 481.
[167] B. Abeles, Solid State Commun. 36 (1980) 537.
[168] See Cody et al., ref. [156].
[169] J. C. Knights, in: Structure and Excitations of Amorphous Solids, eds. G. Lucovsky and F. Galeener, A.I.P. Conf. Proc. No. 31 (A.I.P., New York, 1976) p. 296.
[170] J. Chevallier, H. Wieder, A. Onton and C. R. Guarnieri, Solid State Commun. 24 (1977) 867.
W. Paul, in: Fundamental Physics of Amorphous Semiconductors, ref. [7]. D. K. Paul et al., to be published.
[171] D. A. Anderson and W. E. Spear, Phil. Mag. 35 (1977) 1.
T. Shimada, Y. Katayama and K. F. Komatsubara, J. Appl. Phys. 50 (1979) 5530.
[172] G. A. N. Connell and W. Paul, High Temp.–High Pressures 6 (1974) 85; J. Non-Crystalline Solids 8–10 (1972) 215.
[173] B. Welber and M. H. Brodsky, Phys. Rev. B16 (1977) 3660.
[174] W. Paul and G. L. Pearson, Phys. Rev. 98 (1955) 1755.
[175] R. W. Collins, data to be published.
[176] I. G. Austin, K. Richards, T. M. Searle, M. J. Thompson, M. Alkaisi, I. P. Thomas and J. Allison, 14th Intern. Conf. on Physics of Semiconductors, ed. B. L. H. Wilson (Inst. Phys., London, 1978) p. 115. Narrower widths were observed for sputtered samples measured by M. H. Brodsky, J. J.

Cuomo and F. Evangelisti, Proc. 7th Intern. Conf. on Amorphous and Liquid Semiconductors, Edinburgh, 1977, ed. W. E. Spear (CICL, Edinburgh, 1977) p. 402.
More general reviews of PL in g.d. produced a-Si:H are to be found in the following references: R. Fischer, in: Amorphous Semiconductors, ed. M. H. Brodsky, Topics in Applied Physics, Vol. 36 (Springer Verlag, New York, 1979).
H. Fritzsche, ref. [8].

[177] R. W. Collins, See B. G. Yacobi et al., ref. [94].

[178] R. A. Street, Phil. Mag. B37 (1978) 35.

[179] See M. A. Paesler and W. Paul, ref. [100]. See J. I. Pankove et al., ref. [165]. D. Engemann and R. Fischer, Proc. 5th Intern. Conf. on Amorphous and Liquid Semiconductors, Garmisch-Partenkirchen, 1973, eds. J. Stuke and W. Brenig (Taylor and Francis, London, 1974) p. 947; Structure and Excitations of Amorphous Solids, A.I.P. Conf. Proc. 31 (1977) 37; Phys. Stat. Sol. (b) 79 (1977) 195. T. S. Nashashibi, T. M. Searle, I. G. Austin, K. Richards, M. J. Thompson and J. Allison, J. Non-Crystalline. Solids 35/36 (1980) 675.

[180] C. Tsang and R. A. Street, Phys. Rev. B19 (1979) 3027.

[181] R. W. Collins, M. A. Paesler and W. Paul, Solid State Commun. 34 (1980) 833.

[182] G. S. Higashi and M. Kastner, J. Phys. C12 (1979) L821.

[183] C. M. Gee and M. Kastner, Phys. Rev. Lett. 42 (1979) 1765.

[184] R. A. Street, Phys. Rev. B23 (1981) 861.

[185] R. A. Street, C. Tsang and J. C. Knights, Inst. Phys. Conf. Ser. 43 (1979) 1139.
T. M. Searle, T. S. Nashashibi, I. G. Austin, R. Devonshire and G. Lockwood, Phil. Mag. 39 (1979) 389.
S. Kurita, W. Czaja and S. Kinmond, Solid State Commun. 32 (1979) 879.
T. S. Nashashibi et al., ref. [179].

[186] R. W. Collins and W. Paul, Proc. 9th Intern. Conf. on Amorphous and Liquid Semiconductors, Grenoble, 1981, J. de Phys. (to be published).

[187] R. A. Street, Solid State Commun. 34 (1980) 157.

[188] R. W. Collins, M. A. Paesler, G. Moddel and W. Paul, J. Non-Crystalline Solids 35/36 (1980) 681.

[189] D. Engemann, R. Fischer, F. W. Richter and H. Wagner, Proc. 6th Intern. Conf. on Amorphous and Liquid Semiconductors, ed. B. T. Kolomiets (Nanka, Leningrad, 1975) p. 217.

[190] T. S. Nashashibi, I. G. Austin and T. M. Searle, Phil. Mag. 35 (1977) 831.
R. A. Street, D. Biegelson and J. Stuke, Phil. Mag. B40 (1979) 451.
U. Voget-Grote, W. Kümmerle, R. Fischer and J. Stuke, Phil. Mag. B41 (1980) 127.

[191] W. E. Spear and P. G. LeComber, in: Photoconductivity and Related Phenomena, eds. J. Mort and D. M. Pai (Elsevier, New York, 1976) p. 216.
R. C. Enck and G. Pfister, ibid. p. 297.
T. D. Moustakas, ref. [10].

[192] M. H. Brodsky, F. Evangelisti, R. Fischer, R. W. Johnson, W. Reuter and I. Solomon, Solar Cells 2 (1980) 401.

[193] See H. Fritzsche, Solar Cells 2 (1980) 289.

[194] D. L. Staebler and C. R. Wronski, Appl. Phys. Lett. 31 (1977) 292; J. Appl. Phys. 51 (1980) 3262.

[195] There are exceptions, e.g. D. Jousse, P. Viktorovitch, L. Vieux-Rochas and A. Chenevas-Paule, J. Non-Crystalline. Solids 35/36 (1980) 767.

[196] G. Moddel, J. Blake, R. W. Collins, S. Oguz, P. Viktorovitch, D. K. Paul, B. von Roedern and W. Paul, Proc. Intern. Conf. on Tetrahedrally Bonded Amorphous Semiconductors, Carefree, Arizona March 1981, eds. R. A. Street, D. K. Biegelsen and J. C. Knights (AIP Conf. Ser. No. 73, New York, 1981) p. 25.

[197] See Solar Cells 2 (3, 4) (1980). See ref. [9].
See D. E. Carlson and C. R. Wronski, in: Amorphous Semiconductors, ref. [7].

[198] $f(R)$ depends on α and d through standard formulae for thin films. The interpretation of photoconductivity is simplest for uniform volume generation of carriers, which requires that αd be small and that reflection corrections be applied.

[199] G. Moddel, measurements to be published.

See also T. D. Moustakas, D. A. Anderson and W. Paul, Solid State Commun. 23 (1976) 155.
T. D. Moustakas, ref. [10].
T. D. Moustakas, Solid State Commun. 35 (1980) 745.

[200] W. E. Spear, R. J. Loveland and A. al-Sharbaty, J. Non-Crystalline. Solids 15 (1974) 410.
D. A. Anderson and W. E. Spear, Phil. Mag. 36 (1977) 695.

[201] This is the classic mode of interpretation. See, for example, A. Rose, in: Concepts in Photoconductivity and Allied Phenomena (Interscience, New York, 1963).
The interpretation of the meaning of the β-value found may apparently be different when the mobility is time-dependent as in dispersive transport. See Street, to be published.

[202] P. E. Vanier and R. W. Griffith, to be published. Part of an extensive program at Brookhaven also involving A. E. Delahoy.
P. D. Persans, Solid State Commun. 36 (1980) 851.
P. D. Persans and H. Fritzsche, to be published.

[203] In particular, care should be taken in interpreting experiments on samples of different doping density, on the basis that doping shifts the Fermi level without much altering the gap state densities. As we stressed in section 7.3, there is now convincing evidence that n-type doping (say with P or As) may produce large changes in the density of states in the lower half of the band gap [43, 118, 121].

[204] D. E. Ackley, J. Tauc and W. Paul, Phys. Rev. Lett.43 (1979) 715.
Z. Vardeny, J. Tauc and C. J. Fang, Proc. Intern. Conf. on Tetrahedrally Bonded Amorphous Semiconductors, Carefree, Arizona, March 1981, eds. R. A. Street, D. K. Biegelsen and J. C. Knights (AIP Conf. Ser. No. 73, New York, 1981) p. 243.

[205] A. M. Johnson, D. H. Auston, P. R. Smith, J. C. Bean, J. P. Harbison and D. Kaplan, in: Picosecond Phenomena II, eds. R. M. Hochstrasser et al. (Springer, New York, 1980) p. 71, 285.

[206] P. G. LeComber, A. Madan and W. E. Spear, J. Non-Crystalline Solids 11 (1972) 219.
A. R. Moore, Appl. Phys. Lett. 31 (1977) 762.
D. Allan, P. G. LeComber and W. E. Spear, Proc. 7th Intern. Conf. on Amorphous and Liquid Semiconductors, Edinburgh, 1977 ed. W. E. Spear (CICL, Edinburgh, 1977) p. 323.
T. Tiedje, C. R. Wronski, B. Abeles and J. M. Cebulka, Solar Cells 2 (1980) 301.
P. B. Kirby, W. Paul, P. Jacques and J. Brebner, Proc. Intern. Conf. on Tetrahedrally Bonded Amorphous Semiconductors, Carefree, Arizona, March 1981, eds. R. A. Street, D. K. Biegelsen and J. C. Knights (AIP Conf. Ser. No. 73, New York, 1981) p. 207.

[207] J. M. Hvam and M. H. Brodsky, Phys. Rev. Lett. 46 (1981) 371.
R. A. Street, to be published.
P. B. Kirby and W. Paul, to be published.

[208] Z. Vardeny, J. Tauc and C. J. Fang, ref. [204].
Z. Vardeny and J. Tauc, preprint.

[209] G. Pfister and H. Scher, Advan. Phys. 27 (1978) 747.

[210] M. Pollak, Phil. Mag. 36 (1977) 1157.

[211] J. M. Marshall, Phil. Mag. 36 (1977) 959.
J. Noolandi, Phys. Rev. B16 (1977) 4466.
F. W. Schmidlin, Phys. Rev. B16 (1977) 2362.

[212] T. Tiedje and A. Rose, Solid State Commun. 37 (1980) 49.
T. Tiedje, A. Rose and J. M. Cebulka, Proc. Intern. Conf. on Tetrahedrally Bonded Amorphous Semiconductors, Carefree, Arizona, March 1981, eds. R. A. Street, D. K. Biegelsen and J. C. Knights (AIP Conf. Ser. No. 73, New York, 1981) p. 197.

[213] J. Orenstein and M. Kastner, preprint.

[214] M. Silver and L. Cohen, Phys. Rev. B15 (1977) 3276.

[215] See the references in: Proc. 8th Intern. Conf. on Amorphous and Liquid Semiconductors, Cambridge, MA, 1979, J. Non-Crystalline. Solids 35/36 (1980).

[216] T. Tiedje, B. Abeles, D. L. Morel, T. D. Moustakas and C. R. Wronski, Appl. Phys. Lett. 36 (1980) 695.

[217] T. Tiedje, A. Rose and J. M. Cebulka, ref. [212]. P. B. Kirby and W. Paul, SERI Contractors meeting, Denver, Colorado (February 1981); and to be published.

[218] P. B. Kirby and W. Paul, unpublished results.
[219] R. A. Street, preprint (1980).
[220] J. M. Hvam and M. H. Brodsky, Phys. Rev. Lett. 46 (1981) 371.
[221] This was also the case, although unremarked, in the data of Hvam and Brodsky.
[222] Although this review concentrates on a-Si:H, similar observations on chalcogenides need to be studied. See Orenstein and Kastner, ref. [213].
[223] C. R. Wronski, B. Abeles and G. D. Cody, Solar Cells 2 (1980) 245.
[224] J. Dresner, D. J. Szostak and B. Goldstein, Appl. Phys. Lett. 38 (1981) 998.
[225] J. Mort, S. Grammatica, J. C. Knights and R. Lujan, Solar Cells 2 (1980) 451.
I. Shimizu, T. Komatsu, K. Santo and E. Inoue, J. Non-Crystalline. Solids 35/36 (1980) 773.
[226] W. Paul, Warsaw Conf. ref. [1].